

**NUMERICAL SIMULATION OF HEAT TRANSFER
CHARACTERISTICS UNDER SEMI-CONFINED IMPINGING SLOT
JETS**

SHI YULING

NATIONAL UNIVERSITY OF SINGAPORE

2004

**NUMERICAL SIMULATION OF HEAT TRANSFER
CHARACTERISTICS UNDER SEMI-CONFINED IMPINGING SLOT
JETS**

SHI YULING
(M. Eng, Xi'an Jiaotong University, PRC)

A THESIS

FOR THE DEGREE OF DOCTOR OF PHILOSOPHY
DEPARTMENT OF CHEMICAL AND BIOMOLECULAR
ENGINEERING

NATIONAL UNIVERSITY OF SINGAPORE

2004

ACKNOWLEDGEMENT

This research would not have been possible without the time, effort, and encouragement of a number of people. First and foremost, I would like to thank my supervisors, Dr. M.B. Ray and Prof. A.S. Mujumdar, for their guidance throughout the past three years. They have provided insight and expertise to overcome both large and minor problems during this research. Despite his busy schedule, Prof. Mujumdar tirelessly gave his precious time and knowledge to ensure the successful completion of this thesis. I also greatly appreciate the kindness, understanding, and care of Dr. Ray from the bottom of my heart.

Special thanks should also go to my husband, Huang Yueyuan, and my parents. They have had to endure with my ups and downs, but have supported and sustained me throughout. They are the persons to whom I have turned to for comfort and relief. Thank you for your patience, understanding and support.

Last but not least, I wish to thank my son, Ze An, for his persistence and intelligence. I am proud of you.

TABLE OF CONTENTS

ACKNOWLEDGEMENT	i
TABLE OF CONTENTS	ii
SUMMARY	vi
NOTATION	viii
LIST OF FIGURES	xi
LIST OF TABLES	xvi
CHAPTER 1: INTRODUCTION	1
1.1 Background information and industrial motivation	
1.2 Research objectives and scope	
CHAPTER 2: LITERATURE REVIEW	10
2.1 Introduction	
2.2 Numerical studies of impinging jets heat transfer	
2.2.1 Studies by various k- ϵ models and Reynolds Stress Model	
2.2.1.1 Single slot impinging jet	
2.2.1.2 Multiple slot impinging jets	
2.2.1.3 Impinging round jets	
2.2.1.4 Impinging jet with cross-flow	
2.2.2 Studies with LES and DNS approaches	
2.2.3 Studies using others models	
2.3 Studies using both experimental and numerical methods	
2.4 Heat transfer in turbulent gas-particle suspension flow	
CHAPTER 3: NUMERICAL SIMULATION	36
3.1 Single phase laminar flow	
3.2 Single phase turbulent flow	

- 3.2.1 The governing equations
- 3.2.2 Models of turbulence
 - 3.2.2.1 The standard k- ϵ model
 - 3.2.2.2 RSM model
- 3.3 Multiphase flow
 - 3.3.1 Governing equations
 - 3.3.2 Gas particle interaction
 - 3.3.3 Particle-wall conduction heat transfer
- 3.4 Near wall treatment
- 3.5 Numerical techniques of turbulent impinging jet simulations
 - 3.5.1 Boundary conditions
 - 3.5.2 Numerical parameters
 - 3.5.2.1 Relaxation factors
 - 3.5.2.2 Convergence criteria
 - 3.5.2.3 Grid independence tests

**CHAPTER 4: HEAT TRANSFER UNDER A TURBULENT IMPINGING SLOT
JET** **56**

- 4.1 Introduction
- 4.2 Results and discussion
 - 4.2.1 Comparison of results from various turbulence models
 - 4.2.2 Effect of turbulent Prandtl Number
 - 4.2.3 Effect of Reynolds Number
 - 4.2.4 Effect of turbulence level at the nozzle exit on heat transfer
 - 4.2.5 Effect of the near wall function on the predicted Nusselt number
 - 4.2.6 Effect of the magnitude of the heat flux
- 4.3 Conclusions

**CHAPTER 5: EFFECT OF TEMPERATURE DIFFERENCE BETWEEN THE
JET AND IMPINGEMENT SURFACE ON HEAT TRANSFER** **74**

- 5.1 Introduction
- 5.2 Results and discussion

5.2.1 Small temperature difference case	
5.2.2 Large temperature difference case	
5.2.3 Effect of jet Reynolds number on the Nu_{jave} and Nu_{jo}	
5.3 Conclusions	

**CHAPTER 6: EFFECTS OF Pr ON IMPINGING JET HEAT TRANSFER
UNDER A SLOT JET** **101**

6.1 Introduction	
6.2 Results and discussion	
6.2.1 Laminar flow	
6.2.1.1 Effect of fluid Prandtl number on heat transfer rates	
6.2.1.2 Correlations between Prandtl number and Nusselt number	
6.2.2 Turbulent flow	
6.2.2.1 Effect of fluid Prandtl number on heat transfer rates	
6.2.2.2 Correlations between Prandtl number and Nusselt number	
6.3 Conclusions	

**CHAPTER 7: EFFECT OF CROSS FLOW ON TURBULENT FLOW AND
HEAT TRANSFER CHARACTERISTICS UNDER NORMAL AND
OBLIQUE SEMI-CONFINED IMPINGING SLOT JETS** **115**

7.1 Introduction	
7.2 Results and discussion	
7.2.1 Effect of cross flow and jet angles on flow pattern	
7.2.2 Effect of cross-flow on normal impinging jet heat transfer rate	
7.2.3 Effect of jet angle on local heat transfer rate distribution	
7.2.4 Effect of crossflow and jet angles on the average Nusselt number	
7.2.5 Effect of temperature difference between the jet and cross-flow	
7.3 Conclusions	

**CHAPTER 8: HEAT TRANSFER UNDER TURBULENT MULTIPLE SLOT
IMPINGING JETS OF GAS-PARTICLE SUSPENSION** **128**

8.1	Introduction	
8.2	Results and discussion	
8.2.1	Comparison between experiment and simulation	
8.2.2	Effect of the conduction heat transfer	
8.2.3	Effects of wall factors	
8.2.3.1	Effect of wall material	
8.2.3.2	Effect of reflection coefficient on heat transfer	
8.2.3.3	Effect of impingement wall temperature	
8.2.4	Effect of particle factors on heat transfer	
8.2.4.1	Effect of constant C and loading ratio	
8.2.4.2	Effect of particle diameter	
8.2.4.3	Effect of particle material	
8.2.5	Effect of inlet conditions	
8.2.5.1	Effect of inlet Reynolds number	
8.2.5.2	Effect of gravity direction on heat transfer	
8.3	Conclusions	

CHAPTER 9: CONCLUSIONS **148**

9.1	General conclusions	
9.2	Major contributions to knowledge	
9.3	Recommendations and for future work	

REFERENCES **153**
PUBLICATIONS

SUMMARY

In this thesis, results of computational fluid dynamic simulation of impinging jet heat transfer under semi-confined slot jets with and without cross-flow are reported. While most of the results focus on both laminar and turbulent single jets, simulation results for heat transfer in gas-particle suspension flow for multiple jets are also presented. Initially, the simulation results for a single semi-confined turbulent slot jet impinging normally on a flat plate were compared with selected experimental data from the open literature. The standard $k-\varepsilon$ and Reynolds stress turbulence models were used. Effects of turbulence models, near wall functions, turbulent Prandtl number, jet turbulence, jet Reynolds number, the type of thermal boundary condition at the target surface, as well as temperature differences between the jet and impingement surface are discussed in the light of available experimental data. Results indicate the advantages and shortcomings of the two turbulence models and the important parameters that affect the heat transfer characteristics of the impinging jet flow, specifically the jet Reynolds number, turbulent Prandtl number, jet turbulence, and near wall treatments. Further, for impinging jet heat transfer with large temperature difference between the jet and the target surface, an attempt is made to identify the optimal definitions of the Nusselt number.

While most of the numerical experiments were carried out for air jets, some simulations were performed for a variety of fluids including both liquids and gases. The results show that H_2 and He yield much higher heat transfer coefficients than air, Ar, N_2 and NH_3 under the same flow and boundary conditions. Also, the surface heat

transfer coefficient for the water jet is much higher than those for the other fluids studied here.

The simulation of the flow and heat transfer characteristics for an oblique single semi-confined turbulent slot jet impinging into an imposed cross-flow of air of the same or different temperature was also performed. Effects of the various flow and geometric parameters (e.g. jet-to-cross-flow mass ratio, nozzle-to-target spacing, jet angle and the temperature difference between the jet and the cross-flow) were evaluated.

The heat transfer rate in impinging jet flows has been observed to increase due to the presence of suspended inert particles in the air. Accurate predictions of the heat transfer characteristics of impinging jets of gas-particle suspension remain a major challenge. In the final phase of this work, heat transfer under multiple impinging jets of gas-particle suspension flow was numerically predicted by the Eulerian-Lagrangian model including the conductive heat transfer due to particle-wall collisions. The numerical results were compared with available experimental data. Finally, a parametric study characterizing the effect of geometric and particle parameters, and boundary conditions on impinging jet heat transfer in gas-particle flow was conducted.

The above studies indicate that CFD simulations provide a useful design tool for impinging slot jets under different conditions once an optimum simulation scheme is identified.

NOTATION

A	contact area
C	conduction heat source due to particle wall collision
C_p	specific heat
D	hydraulic diameter
D_p	graphite powder diameter
e	energy
E_{pw}	equivalent elastic modulus of particle and impingement wall
F_D	drag force
G_k	production of kinetic energy
h	surface heat transfer coefficient
H	nozzle-to-plate spacing
I	turbulence intensity
k	turbulent kinetic energy
k_B	turbulent kinetic energy at point B
k_p, k_w	thermal conductivity of particle and wall
k_v	von Karman's constant (=0.42)
l	turbulence length scale
L	length of the impingement surface
Lo	particle loading ratio
M	cross-flow parameter (cross-flow mass flow rate / jet mass flow rate)
m_{pw}	equivalent mass particle and impingement wall
$\overline{m_p}$	average mass of the particle in control volume

\dot{m}_{p0}	initial mass flow rate of the particle injection tracked
Nu	Nusselt number, hW/λ
P	pressure
Pr	Prandtl number $C_p\mu/\lambda$
Q,q	heat flux
R	equivalent radius of particle and impingement wall
R^2	determination factor of curve-fitting line
Re	Reynolds number, $\rho UW/\mu$
S_p	surface area of the particle
t_c	contact duration
T	temperature
T_{ig}, T_{ip}	jet inlet temperature of gas and particle
u_i, u_j	fluctuating velocities in x, y direction, respectively
U_i, U_j	velocity in x and y direction respectively
U	average velocity
U_B	mean velocity of the fluid at point B
v_p	particle normal impact velocity
W	nozzle width
WS	with conduction heat transfer condition
WOS	without conduction heat transfer condition
y^+	dimensionless distance
Y	distance from wall
y_B	distance from point B to wall
ε	rate of dissipation of turbulence energy
ε_B	production of dissipation rate

μ	dynamic viscosity
ν	kinematic viscosity or poisson ratio
ρ	density
τ	shear stress
λ	thermal conductivity
σ	constant
ζ	reflection coefficient
θ	jet angle

Subscripts

0	stagnation point
avg	average
cf	cross-flow
f	film
g	gas
in	inlet
j	jet at inlet
out	outlet
p	particle
R	radiation
ref	reference
w	impingement surface
wi	impingement surface near the inlet area
wo	impingement surface near the exit
t	turbulent

LIST OF FIGURES

Figure 1.1:	Flow regions of semi-confined impinging slot jet	2
Figure 1.2:	Flow geometry of the slot impinging jet without cross flow	8
Figure 3.1:	Near wall treatments	47
Figure 3.2:	Effect of simulation region on results	53
Figure 3.3:	Definition of different regions in the computational domain	54
Figure 3.4:	Examples of typical grid structure	54
Figure 3.5:	Effect of grid size on surface heat transfer coefficient	55
Figure 4.1:	Comparison of simulated Nusselt number to the experimental data from literature for case 1	58
Figure 4.2:	Comparison of simulated Nusselt number to the experimental data from van Heiningen for case 2	58
Figure 4.3:	Comparison of Nusselt number predicted by standard k- ϵ model with increasing turbulent Pr no. to the experimental data	61
Figure 4.4:	Comparison of Nusselt number predicted by the RSM model with increasing turbulent Pr no. to the experimental data	61
Figure 4.5:	Effect of the jet Reynolds number on the surface heat transfer coefficients	63
Figure 4.6:	Streamline contour predicted by the standard k- ϵ model for different turbulence intensities and length scales a: I = 2% (0~0.1448 kg/s), l = D; b: I = 10% (0~0.1446 kg/s), l = D; c: I = 2% (0 ~ 0.129 kg/s), l = 0.07D; d: I = 10% (0 ~ 0.1446 kg/s), l = 0.07 D	65
Figure 4.7:	Effects of turbulence intensity and length scale on Nusselt number and kinetic energy predicted by the standard k- ϵ model	65
Figure 4.8:	Streamline contour predicted by RSM model for different turbulence intensities and length scales a: I = 2% (0~0.1364 kg/s), l = D; b: I = 10% (0~0.1397 kg/s), l = D; c: I = 2% (0 ~ 0.121 kg/s), l = 0.07D d: I = 10% (0 ~ 0.125 kg/s), l = 0.07 D	66
Figure 4.9:	Effect of turbulence intensity and turbulence length scales on turbulent kinetic energy predicted by RSM model	66

Figure 4.10:	Effect of turbulence intensities and turbulent length scales on Nusselt number predicted by RSM model	67
Figure 4.11:	Effect of wall functions on Nusselt number distributions	69
Figure 4.12:	Comparison of Nusselt number at different thermal boundary conditions	70
Figure 5.1:	Effect of small ΔT between the jet and the impingement surface on Nu_j for cooling and heating. a: standard k- ϵ model; b: RSM model	76
Figure 5.2:	Effect of small ΔT between the jet and the impingement surface on Nu_f for cooling and heating. a: standard k- ϵ model; b: RSM model	77
Figure 5.3:	Effect of small ΔT between the jet and the impingement surface on Nu_w for cooling and heating. a: standard k- ϵ model; b: RSM model	78
Figure 5.4:	Effect of large ΔT between the jet and the impingement surface on Nu_j for cooling and heating. a: standard k- ϵ model; b: RSM model	80
Figure 5.5:	Effect of large ΔT between the jet and the impingement surface on Nu_f for cooling and heating. a: standard k- ϵ model; b: RSM model	81
Figure 5.6:	Effect of large ΔT between the jet and the impingement surface on Nu_w for cooling and heating. a: standard k- ϵ model; b: RSM model	82
Figure 5.7:	Effect of temperature difference between the jet and impingement surface on jet Nusselt number for heating condition by the standard k- ϵ model (Re=1500)	85
Figure 5.8:	Effect of temperature difference between the jet and impingement surface on jet Nusselt number for heating condition by the standard k- ϵ model (Re=3000)	86
Figure 5.9:	Effect of temperature difference between the jet and impingement surface on jet Nusselt number for heating condition by the standard k- ϵ model (Re=6000)	87
Figure 5.10:	Effect of temperature difference between the jet and impingement surface on jet Nusselt number for heating condition by the standard k- ϵ model (Re=12000)	88
Figure 5.11:	Effect of temperature difference between the jet and impingement surface on film Nusselt number for heating condition by the standard k- ϵ model (Re=1500)	89
Figure 5.12:	Effect of temperature difference between the jet and impingement surface on film Nusselt number for heating condition by the standard k- ϵ model (Re=3000)	90

Figure 5.13:	Effect of temperature difference between the jet and impingement surface on film Nusselt number for heating condition by the standard k- ϵ model (Re=6000)	91
Figure 5.14:	Effect of temperature difference between the jet and impingement surface on film Nusselt number for heating condition by the standard k- ϵ model (Re=12000)	92
Figure 5.15:	Effect of temperature difference between the jet and impingement surface on wall Nusselt number for heating condition by the standard k- ϵ model (Re=1500)	93
Figure 5.16:	Effect of temperature difference between the jet and impingement surface on wall Nusselt number for heating condition by the standard k- ϵ model (Re=3000)	94
Figure 5.17:	Effect of temperature difference between the jet and impingement surface on wall Nusselt number for heating condition by the standard k- ϵ model (Re=6000)	95
Figure 5.18:	Effect of temperature difference between the jet and impingement surface on wall Nusselt number for heating condition by the standard k- ϵ model (Re=12000)	96
Figure 5.19:	Effect of jet Reynolds number on average jet Nusselt number for heating predicted by the standard k- ϵ model	98
Figure 5.20:	Effect of jet Reynolds number on stagnation jet Nusselt number for heating predicted by the standard k- ϵ model	98
Figure 6.1:	Effect of Pr number on the local Nusselt number distributions for laminar flow	103
Figure 6.2:	Effect of Pr number on surface heat transfer coefficient distributions for laminar flow	104
Figure 6.3:	Local Nu distributions for gases with similar fluid Pr number for laminar flow	105
Figure 6.4:	Heat transfer coefficient distributions for gases with similar fluid Pr number for laminar flow	105
Figure 6.5:	Effect of Pr number on stagnation and average Nusselt numbers for laminar flow	107
Figure 6.6:	Effect of Pr number on the Nusselt number distributions for turbulent flow	109

Figure 6.7:	Effect of Pr number on surface heat transfer coefficient distributions for turbulent flow	109
Figure 6.8:	Local Nusselt number distributions of different gases with similar fluid Prandtl number predicted by the standard k- ϵ model	110
Figure 6.9:	Surface heat transfer coefficient distributions of different gases with similar fluid Prandtl number for turbulent flow	111
Figure 6.10:	Effect of Prandtl number on stagnation and average Nusselt numbers for turbulent flow	113
Figure 7.1:	Flow geometry of the impinging slot jet with cross-flow	116
Figure 7.2:	Streamline contours for $\theta = -30^\circ$ for two structures under small cross flow value, $M = 0.05$	117
Figure 7.3:	Streamline contours for $\theta = -30^\circ$ for two structures under large cross flow value, $M = 1$	118
Figure 7.4:	Streamline contours for $\theta = 30^\circ$ for two structures under small cross flow value, $M = 0.05$	118
Figure 7.5:	Streamline contours for $\theta = 30^\circ$ for two structures under large cross flow value, $M = 1$	119
Figure 7.6:	Effect of cross-flow on Nusselt number distributions predicted by the standard k- ϵ model	121
Figure 7.7:	Effect of θ on Nusselt number predicted by the standard k- ϵ and RSM models for $M=0$ (The values of H/W , Re , M , θ , T_j , T_{cf} , T_w and W are same for both sides)	122
Figure 7.8:	Effect of θ on Nusselt number predicted by the standard k- ϵ and RSM models for $M=0.05$ (The values of H/W , Re , M , θ , T_j , T_{cf} , T_w and W are same for both sides)	122
Figure 7.9:	Effect of θ on Nusselt number predicted by the standard k- ϵ and RSM models for $M=0.25$ (The values of H/W , Re , M , θ , T_j , T_{cf} , T_w and W are same for both sides)	123
Figure 7.10:	Effect of θ on Nusselt number predicted by the standard k- ϵ and RSM models for $M=1$ (The values of H/W , Re , M , θ , T_j , T_{cf} , T_w and W are same for both sides)	123
Figure 7.11:	Effect of M on average Nusselt number predicted by the standard k- ϵ and RSM models for $H/W=2.6$	125

Figure 7.12:	Effect of M on average Nusselt number predicted by the standard $k-\epsilon$ and RSM models for $H/W=8$	125
Figure 7.13:	Effect of temperature difference between the jet and cross-flow on the Nusselt number predicted by the standard $k-\epsilon$ model	126
Figure 8.1:	Flow configuration of the multiple impinging slot jets	129
Figure 8.2:	Comparison between the experimental results and the numerical results for WOS condition	130
Figure 8.3:	Effect of conduction heat transfer between particles and wall on heat transfer for both WOS and WS conditions	132
Figure 8.4:	Effect of wall materials on heat transfer for both WOS and WS conditions	133
Figure 8.5:	Effect of reflection coefficient on heat transfer for both WOS and WS conditions	134
Figure 8.6:	Effect of impingement wall temperature on heat transfer	135
Figure 8.7:	Effect of loading ratio on heat transfer for both WOS and WS conditions	136
Figure 8.8:	Effect of constant C in heat source term on computed heat transfer for both WOS and WS conditions	137
Figure 8.9a:	Effect of particle loading ratio on heat transfer for $L/W=5$, $C=1.0$	139
Figure 8.9b:	Effect of particle loading ratio on heat transfer for $L/W=5$, $C=1.5$	139
Figure 8.10a:	Effect of particle loading ratio on heat transfer for $L/W=7$, $C=1.0$	140
Figure 8.10b:	Effect of particle loading ratio on heat transfer for $L/W=7$, $C=1.5$	140
Figure 8.11:	Effect of loading ratio on outlet gas temperature distributions for WOS and WS conditions	141
Figure 8.12:	Effect of particle diameter on heat transfer for $L/W=5$	142
Figure 8.13:	Effect of particle diameter on heat transfer for $L/W=7$	142
Figure 8.14:	Effect of particle materials on heat transfer	144
Figure 8.15:	Effect of inlet Reynolds number on heat transfer	145
Figure 8.16:	Effect of gravity direction on heat transfer	146

LIST OF TABLES

Table 1.1:	Summary of parameters studied in this work	8
Table 2.1:	Summary of the configurations studied in literature	10
Table 2.2:	List of general reviews on jet impingement	11
Table 2.3:	A literature summary on the experimental studies of impinging jet flow and heat transfer	27
Table 2.4:	Studies on gas-particle flow	33
Table 4.1:	Geometric parameters and boundary conditions for the two cases tested for turbulence models	57
Table 4.2:	Geometric parameters, boundary conditions and maximum surface heat transfer coefficient for the test cases for different Reynolds numbers	63
Table 4.3:	Geometric parameters and boundary conditions for the test cases	64
Table 4.4:	Geometric parameters and boundary conditions for the test cases	70
Table 6.1:	Thermal properties of fluids studied here at $T = 300$ K	102
Table 6.2:	Stagnation and average Nusselt number correlations	112
Table 8.1:	Structure and operating parameters	131
Table 8.2:	Material properties of graphite, glass, copper, aluminum and steel	132
Table 8.3:	Correlations between heat transfer and loading ratio	138

Chapter 1

Introduction

1.1 Background information and industrial motivation

Impinging jets of various configurations are used in numerous industrial processes because of their highly favorable heat and mass transfer characteristics. Impinging jets provide much higher convective heat and mass transfer rates than those with the same amount of gas flowing parallel to the target surface. The heat transfer coefficient for the typical application of impinging jets including many heating, cooling and drying processes is a few times (typically, 2-10 times) higher than that of a cross circulation dryer (Seyedein et al.) (1995). Moreover, impinging jets provide the potential of fine and fast control of local transfer rates by varying operating parameters such as the jet velocity and size of the nozzle opening. Depending upon the application, either slot or round jets, single or multiple jets and single phase or gas-particle two phases can be selected in impinging jets. The major applications of impinging jets include photographic films and paper, annealing of nonferrous metal sheet and glass, internal cooling of the leading edge of turbine blades, etc. Polat et al. (1989) provided detailed descriptions of the different flow regions in impinging jet. Figure 1.1 shows the flow regions of a single semi-confined impinging jet. In the potential core region, the axial velocity remains almost the same as the nozzle exit velocity. In the impingement region, the static pressure increases as a result of the sharp decrease in mean axial velocity. Upon impingement, the flow deflects and starts to accelerate along the impingement surface. In the wall jet region, the boundary layer grows along the

impingement surface. The free jet region is characterized by the associated processes of decrease of centerline velocity and spreading of the jet in the transverse direction.

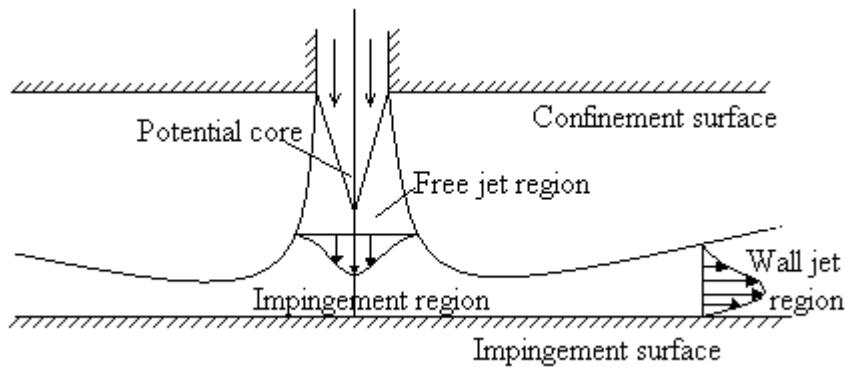


Figure 1.1 Flow regions of semi-confined impinging slot jet

Although the basic heat and mass transfer in impinging slot jets can be shaped by the flow field, the effects of numerous parameters, such as nozzle geometry and size, nozzle configuration, location of exhaust ports, nozzle-to-target spacing, surface motion, and operating variables such as cross flow and jet axis velocity, complicate the analysis.

At present, complete understanding of the influence of all the design and operating parameters is lacking. With the advent of high performance computing, numerical experimentation is gradually replacing expensive and tedious laboratory and pilot-scale studies wherever possible. Many researchers simulated the turbulent impinging jet using different turbulence models (Amano and Brandt (1984) and Seyedein et al. (1994)). However, with the recent development of the numerous powerful computational fluid dynamics (CFD) programs, use of the commercial CFD programs has been proven to be a useful tool in numerically experimenting with complex fluid flow problems. Morris et al. (1996, 1999) used the commercial CFD package FLUENT to calculate the flow-field and local heat transfer coefficient distribution in

submerged and confined liquid jet impingement. However, their studies show significant deviation from the experimental data. Both the turbulence and near wall models were suspected to be responsible for the difference.

Most experimental and computational studies of impingement heat transfer, which form the basis for design of impingement heat transfer equipment, have been made with small temperature differences between the jet and the target surface. Heat transfer rate can be further enhanced by increasing the temperature difference between the inlet and the impingement surface. Under small temperature differences, all fluid properties can be taken as constant (i.e. temperature-independent). However, many industrial applications for impinging jets involve processes at large temperature differences, for example, paper drying and turbine blade cooling. Under such large temperature difference conditions, the thermo-physical properties of the fluid change with local temperature. Few experimental studies exist for high impingement temperature difference between the jet and impingement surface. Das (1982) analyzed these studies and indicated that due to the shortcomings of the experimental techniques and large differences in their data, these studies did not provide a reliable basis for design and optimization of industrial processes using impinging jet. Das et al. (1985) also presented data on the effect of large temperature differences on the local and average heat transfer rates under a confined single slot jet by experiments over a range of temperature differences, from 50 to 300 °C. More recently Heikkila and Milosavljevic (2002) presented an overview of experimental investigation of impingement heat transfer rate at high air impingement temperatures from 100 to 700 °C, under arrays of round jets, a problem of considerable industrial interest in the design of Yankee dryers for tissue paper in particular. However, the studies on heat transfer under large

temperature differences are not adequate for the design and optimization of impinging jet used in industrial processes.

Generally, the dimensionless heat transfer rate, the Nusselt number is used to report the heat transfer behavior. The local Nusselt number for an isothermal impingement

surface can be defined as $Nu_x = \frac{h_x W}{\lambda}$, where λ is the fluid thermal conductivity,

$h_x = q / \Delta T$ and ΔT is the temperature difference between the jet and impingement

surface. The fluid conductivity can be calculated according to different reference temperatures. The most popular method is to calculate the λ by film temperature,

$T_f = \frac{(T_w + T_j)}{2}$. It is well known that the film Nusselt number changes significantly

under large temperature difference. For a Nusselt number defined at a certain reference temperature by which the spread in Nusselt number under large ΔT is less, that will be able to furnish heat transfer data under large ΔT .

Although jet impingement has been extensively studied and several excellent reviews of the contemporary research are available, the influence of fluid thermo-physical properties has received little attention. Only a few studies have reported the effect of fluid Prandtl number on heat transfer rate. Many researchers have reported experimental or numerical studies on impingement heat transfer for air. The heat transfer rates of some liquids, such as FC-77 have also been investigated. Garimella and Rice (1995) developed heat transfer correlations for the effect of fluid Prandtl number by employing a fixed Prandtl number exponent of 0.4. More recently, Li and Garimella (2001) experimentally determined the effect of Prandtl number on heat

transfer of round jet and accounted for fluid properties in their correlations of stagnation and average Nusselt number by deducing these exponents based on regression of their experimental data. Proper understanding of the effect of fluid properties on the flow and heat transfer characteristics is very important especially in the design of liquid impinging jet in industrial applications such as the cooling of combustion engines, and high-performance electrical circuits.

It is well-established that single jets provide the best convective heat transfer rate in the impingement and the adjoining wall jet region of the impinged surface. However, due to high heat load, in industrial practice it is necessary to use multiple jets. There, the interaction between jets can have crucial effects on their heat transfer performance. Saad (1981) has shown that if the jets interact with each other before impingement, the average heat transfer rate under the jets is reduced. If the spent flow from each jet is not allowed to exit the enclosure without interaction with the neighboring jets, it is forced to cross the normal jet flow and deflect it towards the exhaust, thereby reducing its thermal performance. The influence of cross flow together with the inclined jet on impingement heat transfer has received little attention in literature. This cross-flow effect is obviously more significant for two dimensional slot jets and less so for arrays of round jets which provide opportunity for the spent flow from upstream jets to negotiate their way around the downstream jet towards the exhaust port without significant interaction. Cross-flow in industrial equipment is therefore undesirable but also unavoidable since it is practically not feasible to design the equipment with a large number of jets that exhaust individually. Cross-flow due to neighboring jets is often termed “induced cross-flow” in the literature.

Induced cross-flow can also result from the motion of the target surface as in the case of paper dryers where the high-speed sheet entrains significant amount of air as a boundary layer upon which the jets impinge in the drying chamber. Mujumdar et al. (1985) investigated turbulent jets impinging on a moving surface in the presence of a cross-flowing stream using the high-Reynolds-number $k-\epsilon$ model. The results showed that the cross-flow and wall motion had significant effects on Nusselt number and wall shear stress distributions. Saad (1981) investigated heat transfer under a row of slot jets and showed the negative effects of the induced cross-flow from upstream jets on heat transfer. Oblique impinging jet plays an important role in electronic chip cooling because inclined jets not only offer localized cooling but also serve to guide the spent air away from the hot spots. Goldstein and Franchett (1988) studied the local heat transfer for a jet issuing from a square-edge orifice and impinging at different angles ($40-90^\circ$) onto a flat surface using naphthalene sublimation method. The results showed that the displacement of the peak heat transfer location was mainly due to the angle of inclination. Ward et al. (1991) investigated the heat transfer between a circular air jet impinging onto a uniform cross-flow of air over a flat surface coated with naphthalene. The maximum value of heat transfer was found to depend on the impinging jet angle and the velocity ratio between the impinging jet and the cross flow. Despite their obvious practical implications, the normal and oblique impinging jets in cross flow have received very little attention both experimentally and numerically. Few researchers have studied the effect of cross-flow as well as jet inclination angles on slot jet impingement flow and heat transfer behavior.

Heat transfer in turbulent gas-particle flow is an essential part of many industrial processes. Addition of inert particles in impinging jet turbulent flow is expected to

have an important influence on the dynamic flow characteristics and on the heat transfer between the wall and the suspended particles (Mujumdar and Huang (1995)). Numerous numerical studies on the influence of particles on turbulent flow and heat transfer characteristics have been performed for channel flows. However, very little research has been reported on impingement flows of gas-particle suspensions. Yoshida et al. (1990) investigated the turbulence structure and heat transfer mechanism for a two-dimensional impinging jet with gas-particle suspensions using laser-Doppler anemometry. The results showed that with increase of loading ratio, the Nusselt number markedly increased in the vicinity of the stagnation point. Hosseinalipour and Mujumdar (1995) numerically studied the flow and heat transfer in confined opposing jets of particle suspensions using Eulerian-Lagrangian models. More recently, Yokomine et al. (2002) experimentally and numerically investigated the heat transfer mechanism of multiple impinging jets of gas-particle suspensions and evaluated the effects of nozzle Reynolds number, solid loading ratio, distance from jet exit to impingement surface, spacing between jets and solid particle characteristics on the heat transfer coefficient. However, the predicted Nusselt number did not agree well with their experimental data; the results matched only qualitatively. Optimum design and scale-up of such systems need a thorough understanding of impinging jet gas-solid flow and heat transfer behavior.

1.2 Research objectives and scope

In light of the above studies, comprehensive numerical experiments on impinging jet heat transfer including all of the above aspects have been conducted in this study. The objectives of this work are to predict the flows and heat transfer rates between the semi-confined impinging slot jets for both single phase and gas-particle two phases

using the commercial CFD software, FLUENT. The numerical results were compared with selected experimental data, followed by detailed parametric studies. Numerical simulations were conducted to characterize impinging jet heat transfer varying the following parameters:

- Geometric parameters (H/W and W) and boundary conditions (Re , turbulence intensity of inlet, T_w , and q_w).
- Fluid properties under various thermal boundary conditions.
- Thermal properties of fluid and the Prandtl number
- Jet-to-cross-flow mass ratio and jet angles
- Inclusion of inert particles

Figure 1.2 illustrates the basic flow geometry of the slot impinging jet simulated in this work. The commercial CFD software, FLUENT is used to solve the governing equations involved in impinging jet heat transfer. The matrices of parameters studied in this work are summarized in Table 1.1.

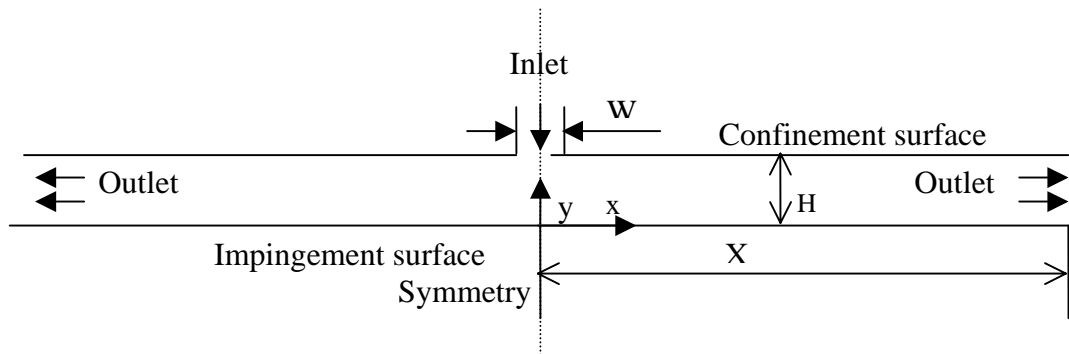


Figure 1.2 Flow geometry of the slot impinging jet without cross flow

Table 1.1 Summary of parameters studied in this work

Boundary condition	Jet Configuration	Fluids
✓ Re	✓ Single jet	✓ Gas: Air, Ar,
✓ ΔT	✓ Cross-flow	NH ₃ , H ₂ , He,
✓ q_w	✓ Inclined jet	C ₂ H ₂
✓ Turbulence intensity	✓ Multiple jets	✓ High Prandtl fluids (Liquid)
	✓ Nozzle to target spacing	✓ Inert particles

In what follows is a brief overview of the chapters included in this thesis. Chapter 2 presents a short literature review on impinging jet heat transfer. The model and the numerical simulation scheme adopted in this work are presented in Chapter 3. Chapters 4-6 deal with single impinging slot jets, while Chapter 7 investigates single slot impinging jet with cross-flow and Chapter 8 presents the results on multiple impinging slot jets flow with gas particle suspensions. Finally, conclusions of this work are presented in Chapter 9.

Chapter 2

Literature review

2.1 Introduction

Numerous studies on the hydrodynamics and the heat and mass transfer characteristics of jet impingement in various configurations have been reported in the literature. A review of the flow, heat and mass transfer characteristics under impinging jets is presented in this chapter. A summary of the different configurations of impinging jet factors studied in literature is presented in Table 2.1, while several available review articles are summarized in Table 2.2. Initially, a review of the numerical studies on impinging jet flow and heat transfer is presented in section 2.2, followed by the studies which cover both the experimental and numerical analysis of flow and heat transfer behavior of impinging jet in section 2.3. The literature on the heat transfer characteristics of the gas-particle suspension flow is discussed in section 2.4.

Table 2.1 Summary of the configurations studied in literature (see pages 32-33 for nomenclature)

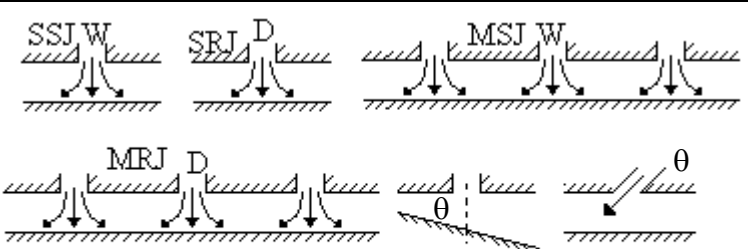
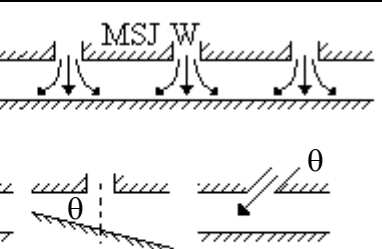

Types of Study	Numerical	Experimental
Configuration		
Jets		
Data collected	Steady or pulse jets; Newtonian fluids (low and high Prandtl number); non-Newtonian fluid; Single phase or multiphase V ; Nu ; Sh ; turbulence; pressure; k ; Recovery factor	

Table 2.2 List of general reviews on jet impingement

Year	Authors	General Review on the Topic
1987	Downs, S.J. and E.H.James	Heat transfer under round jet impingement
1989	Polat, S. et al.	Numerical flow and heat transfer under impinging jets
1992	Jambunathan, K. et al.	Heat transfer under single circular jet impingement
1993	Viskanta, R.	Heat transfer under single and multiple isothermal turbulent air and flame jets impinging on surfaces
1995	Webb, B.W. and C.F. Ma	Single phase liquid jet impingement heat transfer
1995	Mujumdar, A.S. and B. Huang	Impingement drying

2.2 Numerical studies of impinging jets heat transfer

Many researchers simulated the turbulent impinging jet using different turbulent models, e.g. one-equation models, two-equation models, Reynolds Stress Model (RSM), Large Eddy Simulation (LES) and Direct Numerical Simulation (DNS). However, these studies show significant deviations among themselves and also from the relevant experiments.

2.2.1 Studies by various k- ϵ models and Reynolds Stress Model

The k- ϵ model is most widely used in various flow and heat transfer problems. The standard k- ϵ model is not applicable in the vicinity of the solid walls in which the viscous effect is neglected. To handle the near wall flows, the following two procedures have been used.

1. Use the low-Re model instead of the high-Re k- ϵ model;
2. Use high-Re k- ϵ model together with a separate model to treat the near-wall boundary.

In the low-Re k - ε model, some additional terms are included in the k and ε equations to account for the effects of viscous diffusion of k and ε and nonisotropy due to the wall. Patel et al. (1985) gave a review of the comparison of 8 low-Re k - ε models. The frequently used low-Re k - ε models in impinging jet flow problems are Launder-Sharma (referred to as LS)(1974); Lam-Bremhorst (referred to as LB)(1981), Abid (referred to as AB) (1993), Fan et al. (referred to as FLB) (1993) and Abe et al. (referred to as AKN)(1994).

2.2.1.1 Single slot impinging jet

Seyedein et al. (1994) carried out a numerical investigation of single confined impinging slot jets using various low-Re and high-Re turbulence k - ε models. The parameters studied were jet Reynolds number and nozzle-to-target spacing, the values of which ranged from $5000 < Re < 20,000$ and $2.5 < H/W < 7.5$, respectively. The results of simulation using low-Re number turbulence models presented by LB (1981) and LS (1974) exhibited very good agreement with the available experimental data. However, the standard k - ε model underestimated the Nusselt number. The accuracy of the results of the standard k - ε model depended on both the model parameters and near-wall treatment. Hosseinalipour and Mujumdar (1995) numerically investigated the flow and heat transfer characteristics of two-dimensional turbulent confined impinging slot jet flow. Five low-Reynolds k - ε models and standard high-Reynolds numbers k - ε model were used. A proposed Yap correction with low-Re model was tested and it was found that this correction improved the heat transfer predictions in some models.

2.2.1.2 Multiple slot impinging jets

The flow and heat transfer characteristics of multiple slot impinging jets were also investigated by various low Reynolds number k - ϵ models and high Reynolds numbers k - ϵ model (Shiravi et al. (1995), Seyedein et al. (1995) and Tzeng et al. (1999)). Shiravi et al. (1995) found that high Reynolds number turbulence models failed to predict heat transfer accurately although they predicted flow field reasonably well. On the other hand, the low Reynolds number models predicted considerably better results for both fluid flow and heat transfer. While Seyedein et al. (1995) found that the LB model over-predicted the normalized heat transfer coefficient Nu_x , the standard high Reynolds number model under-predicted it. The ranges of Re and H/W used in this work were the same as those in their previous work on single slot impinging jet (see 2.2.1.1) (Seyedein et al. (1994)). However, it was noted that there was a difference in performance of the LB low Re k - ϵ for single slot jet and multiple slot jets. More recently, Tzeng et al. (1999) pointed out that the prediction by each turbulence model depended on grid distribution and numerical scheme adopted in the work.

2.2.1.3 Impinging round jets

Knowles (1996) numerically studied the single and multiple impinging round jets flow by the k - ϵ turbulence model with Rodi and Malin corrections. It was found that both the Rodi and Malin corrections tended to improve the prediction of the hydrodynamic field of free and impinging jets but there were still significant errors in the predicted wall jet growth. Dianat et al. (1996) predicted the axisymmetric impinging jet flow using the standard k - ϵ turbulence model and RSM turbulence model, which included the effect of pressure reflections from a solid surface. Comparison of the predictions with the experimental data demonstrated the superiority of the RSM model where

observed mean velocities and shear and normal stresses were reproduced accurately. On the contrary, the standard k - ϵ model did not predict the experimental observations accurately.

Craft et al. (1993) studied an axisymmetric turbulent impinging jet flow and heat transfer by a k - ϵ eddy viscosity model and three second-moment closures (RSM). It was found that the k - ϵ model and one of the Reynolds stress models predicted large levels of turbulence near the stagnation point. This excessive energy in turn resulted in much too high heat transfer coefficients and turbulent mixing with the ambient fluid. The other two second-moment closures accounted for the wall's effect on pressure fluctuations and performed better. But none of the methods was entirely successful in predicting the effects of Reynolds number, which varied from 23,000 to 70,000. More recently, Shuja et al. (1999) investigated an axisymmetric impinging jet by four turbulence models, which were low Reynolds number k - ϵ model, high Reynolds number k - ϵ model and two Reynolds stress models. The agreement between the temperature profiles predicted by both the low Reynolds number k - ϵ model and RSM turbulence models was better than that obtained from the standard k - ϵ model. The reason was that the standard k - ϵ model predicted excessive kinetic energy generation in the vicinity of the stagnation region, which in turn, resulted in excessive heat transfer and the lowering of the temperature in this region.

Park and Sung (2001) developed a near-wall turbulence model called k - ϵ - f_μ to study the fluid flow and heat transfer for an axisymmetric impinging jet flow. The f_μ^2 function was newly formulated to derive a realizable eddy viscosity. The model performance was validated by available experimental data and compared with those by

the $k-\varepsilon$ and $k-\varepsilon-v^2$ models. It was found that the predicted results from $k-\varepsilon-f_\mu$ model agreed well with the available experimental data, while the $k-\varepsilon$ model over-predicted heat transfer and the $k-\varepsilon-v^2$ model slightly over predicted the Nusselt number. Behnia et al. (1997 and 1999) numerically investigated heat transfer in an axisymmetric turbulent jet impinging on a flat plate by the normal-velocity relaxation turbulence model (V2F model). Local heat transfer coefficient predictions were compared to the available experimental data and also to the predicted results by the standard $k-\varepsilon$ model. It was found that the V2F heat transfer predictions were in excellent agreement with the experiments while the $k-\varepsilon$ model greatly over-predicted the heat transfer rate. Results also indicate the effect of confinement is limited to very low nozzle-to-plate distances and confinement leads to a decrease in the average heat transfer rates, but the local stagnation heat transfer coefficient is unchanged.

Morris et al. (1996) numerically predicted the local heat transfer coefficient distribution on a square heat source due to an axisymmetric, confined and submerged liquid impinging jet using the standard $k-\varepsilon$ model with different turbulent Prandtl number functions. The predicted heat transfer coefficients were compared with available experimental data and it was found that the predicted stagnation and average heat transfer coefficients agreed well with the experimental data within a deviation of 16 to 20%, respectively. Morris et al. (1999) investigated the flow field of a normally impinging, axisymmetric, confined and submerged liquid jet by Reynolds stress model (RSM) using FLUENT. The computed flow patterns were in good agreement with the experimental measurements. The predictions of the flow field using the standard $k-\varepsilon$ and RNG $k-\varepsilon$ models were shown to be inferior to the predictions of Reynolds stress model.

2.2.1.4 Impinging jet with cross-flow

Mujumdar et al. (1985) predicted heat transfer under an axisymmetric plane turbulent impinging jet including the effect of cross-flow and wall motion by k - ϵ model. It was found that the effects of cross-flow and wall motion on the local Nussult number and wall shear stress distributions were significant. The local wall shear stress and Nussult number in impingement region decreased with the increase of the cross flow. Chuang et al. (1992) simulated twin-jet impingement with cross flow by Jones-Launder (1972) k - ϵ model. The computed velocity without cross-flow was compared with the published data and good agreement was observed. The simulations showed that the strength of cross-flow had a strong influence on the pressure distributions of the lower and upper plates and on the lift of the flow. Kim and Benson (1992) calculated a three-dimensional turbulent flow of a jet in a cross flow using a multiple-time-scale turbulence model (MS turbulence model). It was found that the turbulent transport of mass, concentration and momentum was strongly governed by the non-equilibrium turbulence in which the turbulent transport of mass and momentum was described using the time scale of large eddies and the dissipation rate was described using the time scale of fine-scale eddies. The calculated flow and concentration fields were in good agreement with the measurement.

Sarkar and Bose (1995) presented a comparison of performance of different turbulence models for the predictions of flow and temperature fields created by the interactions of jet and cross flow for film cooling. The low Reynolds number k - ϵ model and k - ω models, the algebraic Baldwin-Lomax (1978) model and also a relaxation eddy viscosity model were used to simulate the fine-scale turbulence. Low Reynolds number k - ϵ model seemed to perform better compared to others in view of both the

predicted surface temperature distribution and the relaxation behavior of the velocity. He et al. (1999) discussed the effect of Schmidt number on turbulent scalar mixing in a jet-in-cross-flow using the standard k - ϵ turbulence model. It was noted that the turbulent Schmidt number had a significant effect on the spreading rate of the species in jet-in-cross-flow, especially for the cases where the jet-to-cross-flow momentum flux ratios were relatively small. A turbulent Schmidt number of 0.2 was recommended for best agreement with the experimental data. More recently Kalita et al. (2002) numerically predicted the flow field of turbulent plane jets discharged normal to a weak or moderate stream by the standard k - ϵ model. The agreement between the predicted results and available experimental data was found to be satisfactory.

2.2.2 Studies with LES and DNS approaches

The large-eddy simulation (LES) method integrates the three-dimensional (3-D) time-dependent Navier-Stokes equations directly to resolve the large eddies, while the small eddies that cannot be resolved on the grid are represented by a sub-grid model. Direct numerical simulation (DNS) does not rely on any empirical model and is able to solve all the physical scales of flows. As both direct and large-eddy simulations contain time-dependent information, they can give a much more realistic picture of the turbulence than traditional methods. However both LES and DNS are limited by the computational resource because both of them are time-consuming methods. Recently, with the development of high speed computer, a growing number of researchers are using LES and DNS models.

Gao and Voke (1995) presented the results of large-eddy simulation (LES) of thermally inhomogeneous jets issuing into an enclosed pool and impinging on a plate. The LES predictions of mean quantities and low-order statistics were in sufficient agreement with the experimental data. Voke and Gao (1998) numerically studied the heat transfer from an impinging jet using LES. It was found that the lateral heat conduction within the plate did not have any significant effect on the transmission of thermal fluctuations from the fluid in the plate and by this means a simple one-dimensional model of the thermal, interaction between the media can be justified. Chattopadhyay et al. (1999, 2000 and 2001) reported turbulent flow field and heat transfer from an array of impinging slot jets on a moving surface by large-eddy simulation (LES). The performance of a horizontal knife jet with an exit angle of 60° was compared with standard jet (Chattopadhyay et al. (2000 and 2001)). Nusselt number distributions for varying surface velocity were presented and it was found that increasing velocity of the impingement plate reduced the heat transfer for both types of jets and distribution of Nusselt number over the impingement surface became more uniform with the increasing velocity of the impingement surface. Cziesla et al. (2001) also simulated the flow field due to an impinging jet from a rectangular slot nozzle using LES technique. The computed results compared favorably with the experimental observation, especially in the stagnation zone.

To understand the detail flow feature of the impinging round jet, Satake and Kunugi (1998) carried out numerical simulation on a round turbulent impinging jet using the DNS approach for Reynolds number of 10,000. The results in the downstream region were in fairly good agreement with the available experimental data. It was also found that the wall-layer streaks were extended in the radial direction. More recently, Chung

et al. (2002) used direct numerical simulations (DNS) to study momentum and heat transfer characteristics in an unsteady impinging jet. Detailed analysis of the instantaneous flow and temperature fields were performed and showed that the impingement heat transfer was very unsteady, and the unsteadiness was caused by the primary vortices emanating from the jet nozzle. The correlation between the local heat transfer and the flow field was examined.

Some studies on the impinging jet flow and heat transfer with high Prandtl number fluids were conducted numerically. Generally, the flow with high Prandtl number is in the laminar region, thus, the laminar model is always applied. Rahman et al. (1999) presented the numerical simulation results of a free impinging jet with high Prandtl number fluids. The solid and fluid regions were solved as a conjugate problem. The influence of different operating parameters such as jet velocity, heat flux, plate thickness, nozzle height, and plate material was investigated. Similarly, Bula et al. (2000) numerically investigated the conjugate heat transfer from discrete heat sources to a two-dimensional jet of a high Prandtl number fluid discharging from a slot nozzle. The effects of the heat flux, jet Reynolds, physical properties of the substrate material, location and power of the discrete heat sources on the maximum substrate temperature, temperature variation at the solid-fluid interface, local and average heat transfer coefficients and local and average Nusselt numbers were studied. It was found that besides jet Reynolds number, plate thickness and its thermal conductivity had significant effect on temperature distribution and average Nusselt number. Tan (2001) developed the heat transfer coefficient correlations for low viscosity fluids based on his simulated data by CFD software, FLUENT. Chatterjee et al. (2002) numerically studied a confined axisymmetric impinging flow heat transfer with a purely viscous

inelastic fluid. Important features of the non-Newtonian developing flow field were described and contrasted with the Newtonian flow field. The effects of nozzle-to-target spacing, the rheological parameters, jet Reynolds number and Prandtl number on the off-stagnation point peak heat transfer rate were discussed.

2.2.3 Studies using other models

Gibson and Harper (1997) studied an axisymmetric turbulent impinging jet heat transfer with the low-Reynolds-number q - ξ turbulence model. The new variables were the square root of the temperature variance and its dissipation rate and these variables were attractive for eddy-diffusivity calculations. It was found that the results by the q - ξ low-Reynolds number eddy-viscosity model were better than those by the corresponding k - ϵ model. However, q - ξ low-Reynolds number eddy-viscosity model still has some deficiencies. This model predicted high levels of kinetic energy and square root of the temperature q . It was shown that the use of the equivalent q_0 - ξ_0 model for heat transfer produced dramatic improvements in the stagnation Nusselt number. Fujumots et al. (1999) investigated the convective heat transfer between a circular free surface impinging jet and a solid surface numerically. The effects of surface tension, viscosity, gravity and heat transfer between the film flow and the solid surface were taken into account, but the turbulence was neglected. The steady-state flow on non-heated surface was examined first with experimental data and it was found that the predicted flow structure agreed reasonably well with the experimental data. Then the simultaneous flow and heat transfer were studied. It was shown that although the local Nusselt numbers were over-predicted in the stagnation region, the calculated Nusselt number agreed well with the experimental data in the downstream region.

Careful analysis of boundary layer at impingement surface was necessary for accurate determination of wall shear stress and heat and mass transfer rates under an impinging jet due to the large pressure gradients near the stagnation point. In order to provide the boundary conditions, Phares et al. (2000) modeled the inviscid impingement of a jet with arbitrary velocity profile. Expressions for the stream function were derived in terms of the vorticity function distribution. The method was applied to flow calculations for various two-dimensional and axisymmetric impinging jet configurations. The calculations showed excellent agreement with previous experimental and numerical results. Abdon and Sunden (2001) numerically investigated heat transfer of a single round unconfined impinging air jet under different flow and geometrical conditions using linear and nonlinear two-equation turbulence models, which are the various k - ϵ and k - ω turbulence models. The results by different linear and nonlinear two-equation turbulence models were compared and discussed.

2.3 Studies using both experimental and numerical methods

Catalano et al. (1989) investigated the flow of a turbulent impinging round jet with cross flow by both measurement using Laser-Doppler anemometry and simulation employing two-equation k - ϵ turbulence model. Good agreement between experimental data and simulated results was obtained in the downstream region, but only fair agreement occurred in the initial region. It was found that the jet trajectory and the existence of impingement were strongly dependent on the velocity ratio. Liu et al. (1991) analytically and experimentally investigated the impingement cooling of unsubmerged, circular liquid jet. The predictions were found to agree well with the measurements for both laminar and turbulent flows. The effects of Prandtl number

were investigated and predictive correlations for Nu were developed for the entire range of the radii of the jet.

Barata et al. (1992) characterized the effect of jet-to-crossflow velocity ratio on the mean and turbulent velocities by Laser-Doppler anemometry for single round impinging jet. The experimental data were used to examine the predictive capability of standard k- ϵ model, particularly in the immediate vicinity of the stagnation point. It was found that the shear stress was not predicted correctly in the impingement zone. Ashforth-Frost and Jambunathan (1996) numerically investigated the turbulent flow and heat transfer behavior under an axisymmetric impinging jet using standard k- ϵ model in conjunction with logarithmic law of the wall as well as by experimental method using Laser-Doppler anemometry and liquid crystal thermography. It was found that the stagnation point heat transfer was over-predicted by about 300%, which was due to the inapplicability of the wall function.

Chen and Chalupa's research group (2000, 2001) experimentally and numerically investigated high Schmidt-number mass transfer in impinging slot jet for laminar and turbulent flows, respectively. Both the experimental and theoretical results showed that the peak values in Nusselt number occurred at 1-1.5 times and 1 time of the nozzle width (W), for laminar and turbulent flow, respectively. Prakash et al. (2001, part I, II) reported the studies on impinging round jet in a cylindrical enclosure with and without a porous layer. The effect of a porous layer on flow patterns was investigated. The part I of their work presented the flow visualization experiments and comparisons with CFD simulations. Part II presented laser Doppler velocimetry measurements for the same system and comparisons of these measurements with the CFD simulations to

evaluate the mathematical model. Two low-Reynolds number k - ϵ turbulence models and a laminar model for the porous medium were used. The turbulent kinetic energy profiles in the fluid layer showed good agreement with predictions by all three models for the porous medium.

Roy et al. (2002) experimentally and numerically studied the heat transfer between an impinging jet and an inclined surface. 3D numerical simulations by RNG k - ϵ turbulence model for heat transfer were validated by the experimental results. The effect of different turbulence levels on Nusselt number in the numerical solution was documented on six specific lines on heat pad.

2.4 Heat transfer in turbulent gas-particle suspension flow

Avila et al. (1995) numerically predicted an isothermal particulate pipe flow by a Eulerian-Lagrangian mathematical model. The turbulence of air flow was calculated by the standard k - ϵ model. The predicted average heat transfer coefficients at the inner wall of a vertical pipe with spherical glass particles were compared with the published experimental data. It was found that they over-predicted the average heat transfer coefficients for small particle size. Sharma (1997) experimentally investigated the relative contributions from particle conduction and gas convection to the heat transfer coefficient between gas-solid fluidized beds and surfaces. 18 different fluidization systems were studied including five different materials, twelve different particle sizes and two distributor plates. The proportions of the particle conductive contribution to surface heat transfer coefficient were found to be over a wide range.

Sato et al. (1998) used Eulerian-Lagrangian method to investigate the mechanism of two-phase heat and turbulent transport by small solid particle suspended in a gas flow. The DNS model was used to solve the continuous phase. The simulation of the dispersed phase was achieved using a Lagrangian model. They tested the effect of fluid mean temperature gradient on heat transfer between dispersed and gas phases. It was found that DNS model was able to simulate the heat transfer between the gas and the solid particles and also the heat and turbulent transport in the dispersed phase. Nguyen et al. (1999) numerically investigated the heat transfer process between a dilute gas-particle suspension flow and an obstruction using their novel Eulerian formulation by taking into consideration the particle incidence and reflection explicitly. It was noted that the particle size and the concentration affected the heat transfer and there was an optimum particle size for maximum enhancement of the heat transfer.

Murray (1994) studied heat transfer characteristics in a cross-flow situation. His study indicates that the main mechanisms by which the particles affected heat transfer in gas-particle flow are the increased effective thermal capacity of the suspension, conduction between impacting particles and the tube wall, thermal energy transport by rebounding particles and changes in the boundary-layer characteristics and turbulent structure of the gas flow. Li (2000) numerically studied heat transfer in gas-particle flows through pipes using a two-dimensional coupled CFD and discrete element method (DEM) model. A quantitative estimate of the proportions contributed to the total heat transfer rate by each of the above four heat transfer mechanisms was presented. It was reported that conduction heat transfer due to particle-wall collisions had negligible effect on heat transfer. Its proportion was less than 0.05% in the case of a horizontal pipe flow.

Boulet et al. (2000) used the Eulerian-Lagrangian model to numerically predict the heat transfer between a vertical pipe wall and a turbulent gas-particle suspension. A $k-\varepsilon$ model coupled with a particle tracking method was used. Heat transfer by conduction due to particle-particle interactions and particle-wall interactions was neglected. The results were compared with available experimental data, and they found that although the tests indicated encouraging results, the model became unsatisfactory as loading ratio increased. Bourloutski et al. (2002) compared two theoretical approaches (viz. Eulerian-Eulerian modeling and Eulerian-Lagrangian approach) for the numerical investigation of turbulent gas-solid flows with heat transfer in a pipe. The comparison of the theoretical approaches showed good predictive properties of the theoretical tool for research activities to study new models of turbulent gas-particle suspension flow. In very recent studies Mansoori et al. (2002a, 2002b) studied the turbulent heat transfer in vertical gas-particle flows and proposed new models allowing for the two-way and four-way interactions of two-phase flows following the Eulerian-Lagrangian approach. Their simulation results were in good agreement with the available experimental data. The simulations indicated that the levels of thermal turbulence intensity and heat transfer were strongly affected by particle collisions while the inter-particle contact conduction heat transfer during collisions had no significant effect in the range of Reynolds number and particle diameter studied. Rozenblit et al. (2000) investigated the heat transfer coefficient of solid-liquid pipe flow using an electro-resistance sensor and infra-red imaging. It was found that the local value of the heat transfer coefficient was influenced by the distribution of the solid phase in the pipe cross section and the average heat transfer increased with particle concentration.

Although there are numerous numerical studies on the influence of particles on the heat transfer for channel flows, very little research has been reported on impingement flows of gas-particle suspensions. Hosseinalipour and Mujumdar (1986) numerically studied the flow and heat transfer in confined opposing jets of particle suspensions using Eulerian-Lagrangian models. Yoshida et al. (1990) investigated the turbulence structure and heat transfer mechanism for a two-dimensional impinging jet with gas-particle suspensions using laser-Doppler anemometry. The results of Yoshida et al. (1990) showed that with increase of loading ratio, the Nusselt number markedly increased in the vicinity of the stagnation point. More recently, Yokomine et al. (2002) experimentally and numerically investigated the heat transfer mechanism of multiple impinging jets of gas-particle suspensions. They carried out heat transfer experiments and evaluated the effects of nozzle Reynolds number, solid loading ratio, distance from jet exit to impingement surface, spacing between jets, and solid particle characteristics on the heat transfer coefficient. Their experimental results showed that in the case of graphite powder, the heat transfer coefficient increased greatly compared with that obtained for a single phase gas flow. Numerical simulations were also performed using the Eulerian-Lagrangian approach; conduction heat transfer due to the particle-wall collisions was neglected. The turbulence of gas was calculated by the low-Reynolds number $k-\varepsilon$ model. The predicted Nusselt numbers did not agree well with their experimental data; the results matched only qualitatively.

Besides the numerical studies of impinging jet flow and heat transfer, many researchers investigated the impinging jet flow and heat transfer by experimental methods. Table 2.3 is a summary of experimental studies on impinging jet flow and heat transfer limited to the recent 15 years. The studies on flow behavior of gas-

particle suspension flow are fundamental to the studies of heat transfer characteristics in gas-particle suspension flow. Thus, Table 2.4 summarizes the studies on flow behavior of gas-particle suspension flow.

Table 2.3 A summary of the experimental studies of impinging jet flow and heat transfer

Author	Configurations and Range of Operation	Variables Reported	Objectives
Das et al. (1985)	SSJ; $W = 6\text{mm}$; $H/W = 5, 8, 10, 12$; $Re = 1000-20,000$; $T_j - T_w = 50-300\text{K}$	Nu_x, Nu_{ave}	Heat transfer under large ΔT ; correlation of Nu_{ave}
Polat et al. Part I (1991)	SSJ; $H/W = 2.5$; $16,400 < Re < 57,700$	$Nu_{ave}; Nu_x$	Effect of throughflow on impingement heat transfer
Polat et al. Part II (1991)	SSJ; $H/W = 2.5$; $Re = 18,100-35,400$; $Mvs = 0.03-0.35$	$Nu_x; Nu_{ave}$; position of off-stagnation maxima	Effects of surface motion and throughflow on heat transfer
Stevens and Webb (1991)	Single obliquely round free liquid jet; $D = 4.6$ and 9.3mm ; $\theta = 40-90^\circ$; $Re = 6600-52,000$	Nu_x ; correlation of Nu and Nu_{max} ; Effect of θ on upstream shift of the point of Nu_{max}	Effect of jet inclination on heat transfer for various Re
Gau and Chung (1991)	SWJ on concave and convex surfaces; $W = 0.35, 0.6, 1, 1.5$ & 2cm ; $D_c/W = 8-45.7$; $H/W = 2-12$; $Re = 6000-35,000$	Photos of flow field; $Nu_x; Nu_0$; correlation of Nu_0 and Nu_{ave}	Effects of surface curvature on impingement cooling flow and heat transfer
Saad et al. (1992)	SSJ&MSJ; $W = 2.5-13.3\text{mm}$; $H/W = 4-30$; $S/W \leq 24$; $Re \leq 21,720$	Fluctuating velocity; mean velocity; static pressure; stagnation pressure; $Nu_0; Nu_x$	Comparison turbulence, mean flow and heat transfer characteristics of SSJ and MSJ
Copper et al. (1993)	SRJ, $D = 26, 106\text{mm}$; $H/D = 2-10$; $Re = 23,000-70,000$	Mean and turbulent velocity; Nu_x ; turbulent shear stress	Data suitable for assessing the engineering models
Hansen & Webb (1993)	SRJ on modified surfaces with arrays of fin-type extensions. $H/D = 0.25-14$; $D = 6.91-13.3\text{mm}$; $Re = 4700-33,000$	Nu_{ave} vs Re for various surfaces; Nu_{ave} vs H/D for various surfaces	Evaluation of the heat transfer enhancement for various surfaces
Mohanty and	SRJ; $H/D = 4-58$;	$Nu_x; Nu_0; Nu_x/Nu_0$;	Heat transfer

Tawfek (1993)	D = 3, 5 and 7mm; Re = 4860-34,500	h_x	characteristics due to a round jet impinging on a flat surface
Lytle and Webb (1994)	SRJ; H/D = 0.1, 0.15, 0.2, 0.25, 0.5, 0.75, 1.0 and 6.0; Re = 3600-27,600	Mean velocity; Static pressure; Nu_0 ; Nu_x	Local heat transfer characteristics using an infrared thermal imaging technique.
Huber et al. (1994)	MRJ; S/D = 4, 6 and 8; H/D = 0.25, 1.0 and 6.0; Re = 3500-20,400	Nu_x ; Nu_{ave}	Effects of S/D, H/D and spent air exits locations on Nu
Lee et al. (1994)	An elliptical nozzle on a flat plate; AR = 2.14; H/D = 2, 4, 6 and 10; Re = 5000, 10,000 and 20,000	Nu_x ; Nu_0 ; Isothermal contour	Nu for an elliptical jet. Found that Nu for elliptical jet in impingement region was larger than that for a circular jet.
Gaimella et al. (1995)	SRJ; FC-77; 0.79 mm < D < 6.35 mm; 1 ≤ H/D ≤ 14; Re = 4000 to 23,000; $q_w = \text{constant}$;	h_x ; Nu_0 ; Nu_{ave} ; sketches of pathline; correlations of Nu_{of} and Nu_{avef}	Local heat transfer rate distributions and correlations of Nu_{of} and Nu_{avef}
Liu and Sullivan (1996)	SRJ; Free jet & IJ; D = 12.7mm; H/D ≤ 2; $q_w = 2756 \text{W/m}^2$ Re = 12000-15000	Nu_0 , $Nu_x(2D \& 3D)$; η ; photos of flow field	Flow structure & heat transfer.
Colucci and Viskanta (1996)	SRJ; 0.25 < H/D < 6.0; Two hyperbolic nozzles; Re = 10,000, 50,000	ΔP ; Nu_x for various H/D, Re and nozzle geometries	Effects of hyperbolic nozzle geometry on local heat transfer coefficients
Garimella and Nenaydykh (1996)	SRJ; D = 0.79-6.35mm; H/D = 1-14; Re = 4000-23,000	h_x ; h_0 ; h_{ave} ; Nu_x ; correlations of Nu_{of}	Influence of nozzle geometry on local heat transfer on a small, square heat source
Nishino et al. (1996)	SRJ, D = 40 mm; H/D = 5.86 and 5.63; Re = 13,000 and 10,400;	Flow axisymmetry mean velocity; axial mean momentum; I ; turbulent shear stresses	Various turbulence statistics properties.
Lee et al. (1997)	SRJ, D = 1.3, 2.15, 3.4cm H/D = 2-10; Re = 11,000 to 50,000	Mean velocity; I ; pressure coefficient; Nu_x ; Correlations of Nu_0 and Nu_{ave}	Effects of geometric parameters and Re on heat transfer; Correlations of Nu_0 and Nu_{ave}

Lin et al. (1997)	SSJ; H/W = 1-8; W = 5mm; Re =190-1537	Mean velocity; Nu _x ; correlations of Nu ₀ and Nu _{ave}	Parametric effects of Re, H/W on heat transfer behaviors
Yan and Saniei (1997)	Obliquely impinging round jet; $\theta = 90^\circ$ -45°; H/D = 2, 4, 7 and 10; Re = 10,000-23,000	Velocity; I ; shift of Nu _{max} ; Nu _x	Heat transfer of obliquely impinging jet. Effect of θ on heat transfer
San et al. (1997)	SRJ, D = 3, 4, 6 & 9mm H/D = 2; Re =30,000- 67,000; q _w = 500-2000W/m ²	Nu _x ; Nu ₀ ; T _j -T _w Correlation of stagnation ΔT	Effect of Re, D, q _w on heat transfer
Ashforth-Frost et al. (1997)	SSJ; H/W = 4 and 9.2; W = 30mm Re = 20,000	Nu _x /Nu ₀ ; mean velocity; surface pressure; spanwise velocity; spanwise turbulence	Velocity and turbulence characteristics under above conditions
Ma et al. Part I (1997)	SRJ; Liquid jet with high Pr number; Pr = 263-270; H/D = 2-20; Re = 220-1500	T _w ; r; Nu ₀ ; Nu _x ; Nu _x /Nu ₀ ; Nu _{ave} /Nu ₀	Heat transfer for submerged impinging jet with large Pr
Ma et al. Part II (1997)	SSJ; Liquid jet with high Pr number; Pr = 200-270; W = 0.091, 0.146 and 0.234 mm; Re = 55-415	Nu ₀ ; r; Nu _x /Nu ₀ ; Nu _x /Pr ^{1/3} ; Nu _{ave} /Nu ₀	Heat transfer for submerged impinging jet with large Pr for tiny slot nozzles
Ma et al. (1997)	Oblique round free surface jets with large Pr number liquid; H/D = 4-12; $\theta = 90^\circ$ -45°; Re = 235-1745	Nu _{max} /Pr ^{1/3} ; r; shift of Nu _{max} ; Nu/Nu _{max}	Heat transfer for submerged impinging jet with large Pr for oblique round free jet
Haneda et al. (1998)	SSJ, H/W = 3 and 5; W =15mm; A cylinder was set between the plane and jet; Dv = 2, 3, 4, 6 and 8 mm; Re = 10000	Frequent velocity; Mean pressure; Nu _x ; flow field photo	Effects of suspended cylinder; Effectively enhanced heat transfer outside the stagnation point
Fitzgerald and Garimella (1998)	SRJ confined and submerged turbulent jet FC-77, D=3.18 and 6.35 mm; H/D =2, 3, 4 Re =8500-23000	Streamlines centerline velocity; radial velocity; I ;	Flow field of a confined and submerged impinging jet

Chen et al. (1998)	SRJ on a rotating disk; $\omega=500-4000\text{rpm}$ $H/D=5$, $Re=2000-100000$	Shr	Heat (mass) transfer of a rotating disk with an impinging round jet
Cornaro et al. (1999)	SRJ on concave, convex and flat surfaces; $D=47.2, 72.6 \& 98.6 \text{ mm}$; Free jet and impinging jet; $H/D=1, 2, 3, 4$; $I=0.15-16\%$ $Re=6000-20000$	Axial velocity; I ; photos of flow visualization	Flow behavior; Effects of relative curvature, D , H/D and Re on flow structure
Yang et al. (1999)	Impingement cooling on a concave surface; 3 slot nozzles, 1 round nozzle, 1 rectangular nozzle and 1 2D contoured nozzle; $5920 \leq Re \leq 25500$	Mean velocity; Nu_0 ; Nu_{ave} ; comparison of Nu_x , Nu_0 and Nu_{ave} with other literature data	Jet impingement cooling on concave surface for different nozzle geometries. Effects of nozzle shapes, curvature, Re and H/D on heat transfer
Lee et al. (1999)	Round jet on concave surface; $D=1.3, 2.15 \text{ and } 3.4\text{cm}$; $D/D_c=0.034, 0.056 \text{ and } 0.089$; $Re=11000, 23000 \text{ and } 50000$	Nu_0 ; Nu_x	Effect of concave surface curvature on heat transfer
Failla et al. (1999)	MRJ on finned surface with controlled crossflow; $H=1, 3, 5, 7$; $W_f=3.23\text{mm}$ $Re \leq 4700$	Various dimensionless heat transfer rate vs various parameters (flow power; Re ; pressure drop) Nu correlations	Overall heat transfer under conditions: only IJ, only crossflow and combined jet with crossflow for several geometries
Sailor et al. (1999)	Pulsed SRJ on a heated surface; $D=14\text{mm}$; $L=51\text{mm}$ $DC=0.25, 0.33, 0.5$; $0.009 < St(f) < 0.042$; $Re=21000, 26000, 31000$	Radial velocity; Centerline velocity Nu_x vs frequency (Hz)	Effects of H , Re , pulse frequency and duty cycle on Nu_x
Lee et al. (1999)	A air round jet impinging perpendicularly on convex hemispherical surface; $D=2.87\text{cm}$; $H/D=2-10$, $D_c/D=10.6$; $Re=11000-87000$	Nu_x ; Nu_0 vs H/D ; Nu_0 vs Re ; Nu_0 correlations	Heat transfer from a convex hemispherical surface to a round IJ
Yapici et al. (1999)	Single submerged round jet; $H/D=2-10$; $D=8\text{mm}$; $Re=9200-73500$	Surface shear stresses	Effect of experimental parameters on shear stresses.
Lee and Lee	An elliptic impinging jet	Flow visualization;	Heat transfer

(2000)	on a heated flat plate; AR=1, 1.5, 2, 3 and 4; Equivalent diameters, $D_e=$ 25mm and 60mm; $H/D_e=2-10$; $Re=10000$ and 40000	Nu_x ; location and ratio of first and second peak Nu ; Nu_0 ; Correlation of Nu_0	characteristics for various nozzle aspect ratios
Inoue et al. (2000)	Planar jet to concave surface with high heat flux $Rc=24.8, 62.1, \infty$ mm; $V_j=5, 8, 12$ m/s; Subcooling $\Delta T_{sub}=30, 60$ and 80 K	Heat flux vs surface superheat (ΔT_{sat}); Critical heat flux (CHF); Pressure;	CHF in confined flow of 2D jet on flat and concave surfaces in various flow conditions
Choi et al. (2000)	SSJ on a semi-circular concave surface; $Rc=150$ mm; $H/W=0.2-14$; $W=5$ mm; $Re=1780-7100$	Velocity and velocity fluctuation; Nu_0 ; Nu_x	Flow and heat transfer characteristics under various flow and geometric parameters
Beitelmal et al. (2000)	Single inclined 2D slot impinging air jet; $H/2W=4-12$; $W=5.5$ mm; $\theta=90^\circ-40^\circ$; $Re=4000-$ 12000	Nu_x ; Nu_{max} ; correlations of Nu	Effect of inclination on heat transfer of an impinging 2D jet.
Li et al. (2001)	Single confined submerged impinging jet; air, FC-77 and water; $Pr=0.7-25.2$; $D=1.59-12.7$ mm; $H/D=1-$ 5; $Re=4000-23000$	Correlations of Nu_0 and Nu_{ave} for water, FC-77, air, liquids and all fluids; h_x distributions	Influence of thermophysical properties on heat transfer
Zhe and Modi (2001)	SSJ; $H/W=2-9.2$; $W=40$ mm; $Re=10000-30000$	Mean velocity and root mean square velocity; Normal stresses; skin friction coefficient	Near wall measurements
Tawfek (2002)	Single oblique round jet on a curved surface; $D=3, 5, 7$ mm; $H/D=7-30$; $Re=3800-40000$; $\theta=90^\circ-20^\circ$	Nu_x/Nu_0 ; Nu_{max}/Nu_0 ; effect of θ on upstream shift of maximum heat transfer (S/D vs θ); Nu_{max} , S/D , Nu_{ave} correlations	Effect of inclination on heat transfer
Lee et al. (2002)	A swirling round turbulent jet impinging on a flat- plate; $H/D=2-10$; $D=3.4$ cm; swirl number=0-0.77; $Re=23000$	Nu_0 ; Nu_x ; Nu_{ave}	Effects of swirl number on Nu_0 and Nu_x
Lee et al. (2002)	SRJ with perforated plate installed between the jet	Heat transfer visualization	Heat transfer enhancement by

	and target plate; D=3.4cm, H/D=2, 6, 10; z/d _h =1, 2, 3; p _h /d _h =1.5, 2, 2.5; d _h =4-12mm; Re=23000	Nu _x ; Nu _{ave}	perforated plate installed between impinging jet and target plate
Heikkila and Milosavljevic (2002)	Round jet; Nozzle geometry resembling those used in Yankee hoods T _{studied} =100°C-700°C	Various temperature distributions; Heat transfer coefficients	Impingement heat transfer under large temperature difference
Guo and Wood (2002)	SRJ, H/D=2, 4, 5	Mean velocity; stresses; pressure- containing terms; spectral densities; plate pressure; shear stress	Measurements in the vicinity of stagnation point
Ekkad and Kontrovitz (2002)	MRJ; 48 impingement holes of 0.635cm diameter H/D=3; S/D=4; Re=4800-14800	Nu _x /Nu ₀ ; Nu _{ave} /Nu ₀	Effect of dimple location, underneath the jets or between the jets
Bart et al. (2002)	Multiple jet; H/D=4 and 6; Re=10000	Nu _x	Effects of mechanical modulation of a jet assembly

D: jet diameter.

D_c: outer diameter of the hemisphere.

DC: duty cycle of flow field (ratio of on time to total cycle time).

d_h: hole diameter on perforated plate; p_h/d_h: pith-to-hole diameter.

D_v: the diameter of cylinder.

I: turbulent intensity.

MSJ: multiple slot impinging jets.

MRJ: multiple round impinging jets.

Nu_{of} and Nu_{avef}: stagnation and average Nusselt number with properties
evaluated at film temperature.

r: recovery factor, $r = \frac{(T_w - T_j)}{\sqrt{V_j^2 / 2C_p}}$.

Rc: surface curvature R; AR-elliptic nozzles ratio.

SSJ: single slot impinging jet.

SRJ: single round impinging jet.

S/D or S/W: dimensionless spacing between jets.

W_f : fin width.

η : heat transfer enhancement factor $\log(Q/Q_0)$.

ω : rotational speed of disk.

Table 2.4 Studies on gas-particle flow

Author	Configuration and Operation Parameters	Methods	Abstract
Arastoopour (2001)	gas/solid flow system	Numerical and experimental methods	A review
Sato et al. (1994)	Vertical channel flow with soft magnetic particles; $Lo=0.13, 0.7$ (downward flow) and 0.18 (upward)	Experimental and simulation by high-Re $k-\epsilon$ model and Lagrangian simulation	Turbulence modification was investigated. The turbulence attenuation or augmentation level in 2-phase dilute flows is correlated with the modified particle Re.
Arastoopour and Hea (1994)	Steady-state 2D dilute gas-particle flow	Numerical method based on kinetic theory using conservative variables, the orthogonal collocation method and the non-linear minimization technique	1. A computer code based on the kinetic theory to simulate steady state 2D gas-particle flow was developed. 2. Predicted gas and particle V , mass flux and concentration agreed reasonably well with available experimental data
Cao and Ahmadi (1995)	Gas-particle turbulent flow in a vertical duct	Simulation by a thermodynamically consistent turbulent 2-phase flow model using two-equation $k-\epsilon$ model for turbulence analysis	1. Gas-particle flows at various Lo between two vertical parallel plates. 2. The predicted V and I were compared with available experimental data. 3. The phase fluctuation energy, and its production and dissipation and interaction momentum and energy supply terms

Sato et al. (1996)	Vertical down-flow turbulent wall jet embedded in a uniform stream with interaction between particles and fluid; $Lo < 0.3$	Both experimental and numerical methods: Laser-Doppler; Eulerian-Lagrangian (with k- ϵ model)	<ol style="list-style-type: none"> 1. Motion of small particles was influenced by strong shear in the developing region; 2. Streamwise I was strongly attenuated by particles in the free shear layer region; 3. Transverse I was suppressed in the fully-developed region of both the free and wall shear regions
Levy, et al. (1997)	Gas-particle flow through an inclined section of pipe	Analytical approach and numerical model by EE simulation: k- ϵ model was used	<ol style="list-style-type: none"> 1. Flow characteristics by both analytical and numerical models were predicted. 2. The agreement between the experimental data and models was satisfactory.
Zhao and Brodkey (1998)	Particle paths in 3D opposing jet mixing system	Experimental method: PTV technique	<ol style="list-style-type: none"> 1. Mixing process was Analyzed. 2. Experimental velocity field is determined by using neutrally buoyant particles. 3. The effect of gravity can be easily studied.
Nguyen and Fletcher (1999)	Gas-particle flow	Numerical simulation by Eulerian-Lagrangian model using FLUENT	<ol style="list-style-type: none"> 1. Incidence and reflection of small particles. 2. The boundary layer theory is employed to predict the key model parameters. 3. The analytical prediction agrees well with the computational results.
Schiewe et al. (1999)	Downward vertical gas-solid flow; $D=15$ cm; $D_p=125\mu\text{m}$, glass bead; $V_g=0-6.6\text{m/s}$	Experiment by two measurement techniques: gamma-absorption tomography and capacitance sensing	<ol style="list-style-type: none"> 1. Solid concentration. 2. Good agreement was obtained between the solid concentration measurements from both measurement techniques.
Sommerfeld and Huber (1999)	Particle-laden horizontal channel flow; $D_p=100, 500\mu\text{m}$; glass bead; quartz particles;	Experimental and numerical methods	<ol style="list-style-type: none"> 1. Particle-wall collisions were studied in detail. 2. The effect of wall material on the collision process was analyzed. 3. All the parameters for the wall collision model were assumed as function of impact angle and were obtained from experiments
Tanlbee et al.	Homogeneous turbulent shear	Eulerian- Eulerian simulation:	<ol style="list-style-type: none"> 1. New RSM model for the simulation of gas-particle flow

(1999)	gas-particle flow	1. carrier phase: DNS and RSM; 2. dispersed phase: Lagrangian frame;	was developed; 2. DNS was used to determine the magnitudes of the empirical constants in RSM. 3. Final model predictions were compared with DNS data.
Cao and Ahmadi (2000)	Gas-particle turbulent flow in horizontal and inclined ducts	Simulation by two- phase flow model closed by low-Re turbulence closure	1. Predicted V and solid volume fraction were compared with experimental data. 2. Fluctuation energy; fluctuation energy production; dissipation and shear stress were discussed; effect of Dp on flow properties was presented.
Triesch and Bohnet (2001)	An upstream gas solids flow in pipes and diffusers	Measurement by PDA technique and simulation by standard k- ϵ model and Lagrangian particle tracking using FLUENT.	1. Good agreement was obtained between Exp. & Numerical data if the additional models available in FLUENT. 2. Individual influence of added model was discussed. 3. The improved version of FLUENT was applied to various Lo.
Mashaye k and Taulbee (2002)	Dilute gas- particle turbulent flow	Simulation by a four-equation model	1. The model was based on explicit algebraic relations for Reynolds stress and turbulence fluxes of the void fraction. 2. Encouraging agreements with available experimental data
Lain et al. (2002)	Particle-laden horizontal channel flow	Measurement using phase-Doppler anemometry; numerical calculations based on Eulerian- Lagrange approach	1. Comparison of experiment and numerical data was presented for different Dp and Lo; 2. The agreement was found to be reasonable for both mean and fluctuating velocities.

Chapter 3

Numerical simulation

The focus of this study is the investigation of the flow and heat transfer characteristics of two-dimensional, steady state semi-confined turbulent impinging slot jets. The commercial CFD software, FLUENT, was used in conjunction with its user defined function option to solve the governing conservation equations and turbulence models as required. In most of the simulations, the default options of FLUENT have been used, except for the cases with gas-solid heat transfer where a user-defined subroutine was deployed to introduce a new heat transfer model to account for conductive heat transfer due to particle collisions with the impingement wall. The governing equations describing the flow and heat transfer along with the appropriate boundary conditions in such systems are described below.

3.1 Single phase laminar flow

The two-dimensional, laminar incompressible steady flow and heat transfer in semi-confined impinging slot jets can be described by the following continuity, momentum and energy equations. Under the assumptions that all properties of the working fluids remain constant, viscous dissipation and buoyancy are neglected; the continuity, momentum and energy equations for a Newtonian fluid in the dimensionless form can be written as follows:

$$\frac{\partial U}{\partial X} + \frac{\partial V}{\partial Y} = 0 \quad (3.1)$$

$$U \frac{\partial U}{\partial X} + V \frac{\partial U}{\partial Y} = -\frac{\partial P}{\partial X} + \frac{1}{\text{Re}} \nabla^2 U \quad (3.2a)$$

$$U \frac{\partial V}{\partial X} + V \frac{\partial V}{\partial Y} = -\frac{\partial P}{\partial Y} + \frac{1}{\text{Re}} \nabla^2 V \quad (3.2b)$$

$$U \frac{\partial T}{\partial X} + V \frac{\partial T}{\partial Y} = -\frac{1}{\text{Re Pr}} \nabla^2 T \quad (3.3)$$

In these equations, for a slot jet, $\text{Re} = \frac{UW}{\nu}$ and $\text{Pr} = \frac{\mu C_p}{\lambda}$, where ν is the kinematic

viscosity and μ is the dynamic viscosity.

3.2 Single phase turbulent flow

3.2.1 The governing equations

The partial differential equations, including conservation of mass, momentum, and energy for a time-dependent three dimensional fluid flow and heat transfer of a compressible Newtonian fluid are expressed in the following form.

$$\text{Mass} \quad \frac{\partial \rho}{\partial t} + \frac{\partial}{\partial x_i} (\rho u_i) = 0 \quad (3.4)$$

$$\text{Momentum} \quad \frac{\partial}{\partial t} (\rho u_i) + \frac{\partial}{\partial x_j} (\rho u_i u_j) = -\frac{\partial p}{\partial x_i} + \frac{\partial \tau_{ij}}{\partial x_j} + \rho g_i + F_i \quad (3.5)$$

$$\text{Internal energy} \quad \frac{\partial (\rho \cdot e)}{\partial t} + u_i \frac{\partial (\rho \cdot e)}{\partial x_i} = -p \frac{\partial u_i}{\partial x_i} + \frac{\partial}{\partial x_i} \left(\lambda \frac{\partial T}{\partial x_i} \right) + \mu \cdot \Phi \quad (3.6)$$

Modeling of turbulent flows requires describing the effect of turbulent fluctuations of velocity and scalar quantities on mean flow and energy quantities. In turbulent flows, the velocity, pressure and temperature at a point are considered as a sum of the mean and fluctuating components.

$$u_i = U_i + u_i'; \quad p = P + p' \quad \text{and} \quad t = T + T' \quad (3.7)$$

Substituting equation (3.7) into equations (3.4), (3.5) and (3.6) and taking the assembly averages of resulting equations for an incompressible Newtonian fluid, the governing equations become:

$$\text{Continuity:} \quad \frac{\partial U_i}{\partial x_i} = 0 \quad (3.8)$$

$$\text{Momentum balance:} \quad -\frac{\partial P}{\partial x_i} + \frac{\partial}{\partial x_j} \left[\mu \left(\frac{\partial U_i}{\partial x_j} + \frac{\partial U_j}{\partial x_i} \right) - \overline{\rho u_i u_j} \right] = 0 \quad (3.9)$$

$$\text{Energy balance:} \quad \frac{\partial}{\partial x_j} \left(\frac{\mu}{Pr} \frac{\partial T}{\partial x_j} - \overline{\rho u_j T'} \right) = 0 \quad (3.10)$$

In the averaged equations, Reynolds stresses, $\overline{u_i u_j}$, and the turbulent heat fluxes, $\overline{u_i T'}$ are required to be determined to address the effects of them on mean flow and energy quantities.

3.2.2 Models of turbulence

In order to characterize $\overline{u_i u_j}$ and $\overline{u_i T'}$, many turbulence models have been proposed in the literature. In this work, we use the standard k- ϵ model and Reynolds stress model to close the above governing equations (3.8 to 3.10). These models are selected mainly due to their frequent successful applications in this field, and also in the light of the past experience of our research group.

3.2.2.1 The standard k-ε model

In k-ε model, the turbulence kinetic energy, k , and the dissipation rate of the turbulence kinetic energy, ε , can be determined by using the Boussinesq approximation, which states that the Reynolds stresses are directly proportional to the velocity gradients with an eddy turbulent viscosity, μ_t , which is correlated with k and ε via the expression $\mu_t = \rho C_\mu k^2 / \varepsilon$, where C_μ is the constant of k-ε model. The turbulent kinetic energy, k , and its dissipation rate, ε , are obtained from the following transport equations:

$$\rho \frac{Dk}{Dt} = \frac{\partial}{\partial x_i} \left[\left(\mu + \frac{\mu_t}{\mu_k} \right) \frac{\partial k}{\partial x_i} \right] + G_k + G_b - \rho \varepsilon - Y_M \quad (3.11)$$

$$\text{and } \rho \frac{D\varepsilon}{Dt} = \frac{\partial}{\partial x_i} \left[\left(\mu + \frac{\mu_t}{\sigma_\varepsilon} \right) \frac{\partial \varepsilon}{\partial x_i} \right] + C_{1\varepsilon} \frac{\varepsilon}{k} (G_k + C_{3\varepsilon} G_b) - C_{2\varepsilon} \rho \frac{\varepsilon^2}{k} \quad (3.12)$$

In these equations, G_k and G_b are the generations of turbulent kinetic energy due to the mean velocity gradients and buoyancy, respectively. Y_M represents the contribution of the fluctuating dilatation in compressible turbulence to the overall dissipation rate. $C_{1\varepsilon}$, $C_{2\varepsilon}$ and $C_{3\varepsilon}$ are constants and equal to 1.44, 1.92 and 0.09, respectively. $\sigma_k = 1.0$ and $\sigma_\varepsilon = 1.3$ are the turbulent Prandtl numbers for k and ε , respectively.

3.2.2.2 RSM model

The Reynolds stress model uses the exact transport equations for the transport of the individual Reynolds stresses and turbulent fluxes. A particular advantage of deriving the exact equations is that these terms overcome some of the limitations of the k-ε model and account for buoyancy, rotation and other effects inherently present in turbulent flows. The RSM model may be written as follows:

$$\begin{aligned}
 & \underbrace{\frac{\partial}{\partial t}(\overline{\rho u_i u_j})}_{\text{Local Time Derivative}} + \underbrace{\frac{\partial}{\partial x_k}(\overline{\rho U_k u_i u_j})}_{C_{ij} \equiv \text{Convection}} = - \underbrace{\frac{\partial}{\partial x_k}[\overline{\rho u_i u_j u_k} + p(\delta_{kj} u_i + \delta_{ik} u_j)]}_{D_{ij}^T \equiv \text{Turbulent Diffusion}} + \underbrace{\frac{\partial}{\partial x_k} \left[\mu \frac{\partial}{\partial x_k} (\overline{u_i u_j}) \right]}_{D_{ij}^L \equiv \text{Molecular Diffusion}} \\
 & - \underbrace{\rho \left(\overline{u_i u_k} \frac{\partial U_j}{\partial x_k} + \overline{u_j u_k} \frac{\partial U_i}{\partial x_k} \right)}_{P_{ij} \equiv \text{Stress Production}} - \underbrace{\rho \beta (g_i \overline{u_i \theta} + g_j \overline{u_j \theta})}_{G_{ij} \equiv \text{Buoyancy Production}} + p \underbrace{\left(\frac{\partial u_i}{\partial x_j} + \frac{\partial u_j}{\partial x_i} \right)}_{\phi_{ij} \equiv \text{Pressure Strain}} + 2\mu \underbrace{\frac{\partial u_i}{\partial x_k} \frac{\partial u_j}{\partial x_k}}_{\varepsilon_{ij} \equiv \text{Dissipation}} \\
 & - 2\rho \Omega_k \underbrace{\left(\overline{u_j u_m} \varepsilon_{ikm} + \overline{u_i u_m} \varepsilon_{jkm} \right)}_{F_{ij} \equiv \text{Production by System Rotation}}
 \end{aligned} \tag{3.13}$$

The detailed descriptions of the transport equations for individual Reynolds stresses and turbulent fluxes appearing in eq. 3.13 are provided following the models of Gibson and Launder (1978), Launder (1989) and Launder et al. (1975).

Both of the above two turbulence models are only valid at high local turbulence Reynolds number; therefore they cannot be used in the viscous sub-layer. Hence this region has to be bridged by so-called wall functions to the main flow, as described in section 3.4.

3.3 Multiphase flow

The multiphase (gas-solid) flow can be described by two possible theoretical approaches. One is called Eulerian-Eulerian modeling, which is based on two-fluid assumptions. The other is Eulerian-Lagrangian approach, in which the particles are regarded as the discrete phase and the fluid as the continuous one. In this work, we use the Eulerian-Lagrangian approach to solve the multiphase flow. The mathematical model for the two-way interaction of gas-particle flow in a Eulerian-Lagrangian approach is presented in the following section. The basic assumptions used in our mathematical formulation for the gas-solid flow are the following:

1. The flow is steady

2. The gas is incompressible
3. Each particle has uniform temperature and constant characteristics
4. Particles are solid, spherical, with fixed diameter
5. The heat transfer by conduction due to particle-particle interactions is negligible

Under above assumptions, the conservation equations for the flow and heat transfer in gas and suspended particles can be modeled as follows:

3.3.1 Governing equations

The turbulent gas flow is governed by the mass, momentum and energy equations, which are described in the previous section by equations (3.8), (3.9) and (3.10). In the simulation of gas-solid flow, we used the standard k- ϵ model (equations (3.11) and (3.12)) to close the governing equations.

The solid phase is described by a Lagrangian particle tracking approach in the simulation. The trajectory of the suspended particle can be determined by integrating the differential force balance equation for the particle. The suspended particle in a gas flow is subjected to aerodynamic, gravitational, buoyancy, contact, thermophoretic, Brownian as well as the Saffman's lift forces. These forces can be calculated simultaneously with the particle motion using the local parameters of the gas and the particles. In this work, the thermophoretic force, Brownian force and Saffman's lift force are assumed to be negligible. The force balance on single particle can be written as,

$$\frac{dU_p}{dt} = F_D(U_g - U_p) + g(\rho_p - \rho_g)/\rho_p \quad (3.14)$$

where $F_D (U_g - U_p)$ is the drag force per unit particle mass, and

$$F_D = \frac{18\mu_g C_D \text{Re}}{\rho_p D_p^2 24} \quad (3.15)$$

Re is the relative Reynolds number, which is defined as

$$\text{Re} = \frac{\rho_g D_p |U_p - U_g|}{\mu_g} \quad (3.16)$$

where C_D is the drag coefficient. When a particle strikes a wall, it is assumed that it will bounce from the surface. The rebound velocity of the particle from the wall is evaluated using the classical inelastic collision equations. The thermal energy equation of the particles is given as:

$$m_p c_p \frac{dT_p}{dt} = hA_p (T_g - T_p) + \varepsilon_p S_p \sigma (T_R^4 - T_p^4) \quad (3.17)$$

3.3.2 Gas-particle interaction

The influence of particles on the flow and heat transfer field of the continuous phase is considered by the momentum and heat transfer for each particle. The momentum transfer is computed by examining the change in momentum of a particle as it passes through each control volume. Similarly, the heat transfer rate is also computed by examining the change in thermal energy of a particle as it passes through each control volume. The momentum change and heat exchange are computed by equations 3.18 and 3.19, respectively.

$$F = \sum \left(\frac{18\mu C_D \text{Re}}{\rho_p D_p^2 24} (U_p - U_g) \right) \dot{m}_p \Delta t \quad (3.18)$$

$$Q = \left[\frac{\overline{m}_p}{m_{p0}} c_p \Delta T_p + \frac{\Delta m_p}{m_{p0}} \left(\int_{T_{ref}}^{T_p} c_{p,i} dT \right) \right] \dot{m}_{p0} + S \quad (3.19)$$

The source term S , which represents the conductive heat transfer when particle and impingement wall impact, will be discussed in the following section. These momentum and heat exchange terms appear as source or sink in the continuous phase momentum balance and energy balance during any subsequent calculations of the continuous phase flow field.

3.3.3 Particle-wall conduction heat transfer

When moving particles impact on the impingement surface, heat conduction occurs. Sun and Chen (1988) theoretically analyzed the heat transfer due to particle-wall impact. They modelled the conduction heat transfer due to particle-wall collisions from the elastic collision equation. From the elastic collision theory, the rate of the area change for the compression process is

$$\frac{dA}{dt} = \left[\left(\pi \cdot v_p R_{pw} \right)^2 - \frac{4}{5\sqrt{\pi}} \frac{E_{pw}}{m_{pw}} A^{5/2} \right]^{1/2} \quad (3.20)$$

$$\text{where } R_{pw} = \frac{R_p R_w}{R_p + R_w} \quad (3.21)$$

$$E_{pw} = \frac{4/3}{\frac{1 - \mathcal{G}_p^2}{E_p} + \frac{1 - \mathcal{G}_w^2}{E_w}} \quad (3.22)$$

$$\text{and } m_{pw} = \frac{m_p m_w}{m_p + m_w} \quad (3.23)$$

The decompression process is exactly the inverse of the compression process. The maximum contact area A_c and its radius r_c are found by setting the derivative to zero.

$$A_c = \pi \cdot r_c^2 = \pi \left(\frac{5m_{pw} R_{pw}^2}{4E_{pw}} \right)^{2/5} v_p^{4/5} \quad (3.24)$$

The dependence of contact area A on time can best be seen with the following dimensionless variables:

$$A^* \equiv \frac{A}{A_c} \equiv \frac{r^2}{r_c^2} \quad (3.25)$$

$$\tau \equiv \left(\frac{4E_{pw}}{5m_{pw}} \right)^{2/5} (R_{pw} v_p)^{1/5} t \quad (3.26)$$

where r and r_c are radii of A and A_c , respectively. Equation (3.20) can then be integrated for the compression to yield

$$\tau = \int_0^{A^*} \frac{dx}{\left(1 - x^{5/2}\right)^{1/2}} \quad (3.27)$$

The total contact duration is then found to be

$$t_c = 2.94 \left(\frac{5m_{pw}}{4E_{pw}} \right)^{2/5} (R_{pw} v_p)^{-1/5} \quad (3.28)$$

The heat conduction between the two particles is treated as that between two semi-infinite media. Within the contact area, perfect thermal contact is assumed, that is, there is no thermal resistance between the contact surfaces. Therefore, the problem is governed by two axi-symmetric heat conduction equations with appropriate boundary and initial conditions.

When the contact duration t_c is very small, the heat conduction in the two media will not penetrate too deeply from the surfaces. This suggests that one-dimensional heat transfer between the two media may be a good approximation for this situation. Under the above condition, the solution of above equation is

$$q_w = \frac{(T_w - T_p)(\pi \cdot t)^{-1/2}}{(\rho_p c_{pp} k_p)^{-1/2} + (\rho_w c_{pw} k_w)^{-1/2}} \quad (3.29)$$

where t is elapsed time measured from the moment of initial contact, which is a function of r . The total energy exchange per unit contact area is thus a function of the local duration of contact, which is also a function of r . Hence the total energy exchange per impact is

$$e = 2\pi \int_0^{r_c} \int_0^{t_{1c}(r)} q_w dt r dr \quad (3.30)$$

where the local contact duration $t_{1c}(r)$ can be computed from

$$t_{1c}(r) = t - 2t(r) \quad (3.31)$$

where $t(r)$ is determined from equations (3.25)-(3.27). Integrating (3.30), the following was obtained

$$e_{pw} = \frac{0.87(T_w - T_p)A_c t_c^{1/2}}{(\rho_p c_{pp} k_p)^{-1/2} + (\rho_w c_{pw} k_w)^{-1/2}} \quad (3.32)$$

In each trajectory, the heat transferred per second is:

$$S = Cn \frac{0.87(T_w - T_p)A_c t_c^{1/2}}{(\rho_p c_{pp} k_p)^{-1/2} + (\rho_w c_{pw} k_w)^{-1/2}} \quad (3.33)$$

where n is the number of the particles impacted on the impingement surface per second and C accounts for inelastic collisions and particle shape effect and was introduced first in this work. The equations described in this section were incorporated in the user-defined subroutine of FLUENT 6 to incorporate the heat transfer due to conduction between the particles and the impingement surface.

3.4 Near wall treatment

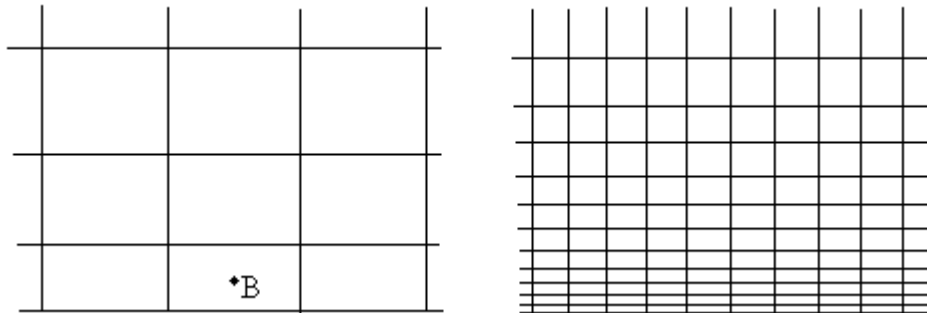
When the flow to be computed involves walls, the wall affects the turbulent flows in the regions close to the walls. First, the presence of the walls changes the turbulence and the mean velocity field is affected by the no-slip condition. Because the near-wall modeling significantly impacts the reliability of the numerical solutions, accurate representation of flow in near-wall region determines successful prediction of wall-bounded turbulent flows.

To handle the near-wall flows two procedures have been suggested. These are:

1. For near wall modeling, use the low-Re k - ϵ model instead of the high Re k - ϵ model.
2. Use a separate model to treat the near-wall boundary

The first method was proposed by Jones and Launder and was successfully used by many researchers, for example, Seyedein et al. (1994). When low-Reynolds number versions of turbulence model are used, the iterations can be carried up to the wall. Some different models of turbulence also had been applied in literature. Patel et al. (1985) compared eight models in their review. In the second method, semi-empirical formula called ‘wall functions’ are used to bridge the viscosity-affected region between the wall and the fully turbulent region. It accounts for the shortcomings of the high-Reynolds number k - ϵ model in the near wall region, where molecular viscosity affects the generation, destruction and transport of the turbulence energy. Since viscous effects are confined to the first grid point close to the wall, near wall functions have the advantage of reducing the grid density required in the near wall region. Figure 3.1 shows the near wall treatments. The wall function approach is popular because it is economical, robust and reasonably accurate. It is a practical option for the near-wall

treatments for industrial flow simulation. The second method using special function is available in FLUENT, which offers two choices of wall function approaches: a. Standard wall function; b. Non-equilibrium wall function.



Wall function approach

- The viscosity-affected region is bridged by the wall functions, instead of it being resolved.
- High-Re turbulence model can be used

Near-wall model approach

- The near-wall region is resolved all the way down to the wall.
- Only low-Re turbulence model can be used.

Figure 3.1 Near wall treatments

The standard wall functions in FLUENT are based on the proposal of Launder and Spalding (1972), which are provided as a default option in FLUENT. The standard wall function introduces the logarithmic law of the wall to describe the velocity profile in absence of pressure gradient and mass transfer. Near the solid wall surfaces, no-slip conditions are imposed for flow analysis. They considered the first grid point close to the wall and assumed that the thin layer of the fluid close to the wall is in local equilibrium.

When the mesh is such that $y^* < 11.225$, at the wall-adjacent cells, the laminar stress-strain relationship is used as $U^* = y^*$ (3.34)

Where
$$U^* \equiv \frac{U_B C_\mu^{1/4} k_B^{1/2}}{\tau_w / \rho} \quad (3.35)$$

$$\text{and } y^* \equiv \frac{\rho C_\mu^{1/4} k_B^{1/2} y_B}{\mu} \quad (3.36)$$

$$\text{That is } \tau_w = \frac{U_B \mu}{y_B} \quad (3.37)$$

The log-law is employed when $y^* > 11.225$,

$$U^* = \frac{1}{k_v} \ln(9.81 y^*) \quad (3.38)$$

$$\tau_w = \frac{\rho U_B C_\mu^{1/4} k_B^{1/2}}{U^*} \quad (3.39)$$

To analyze heat transfer, linear law is used for the thermal conduction sublayer where conduction is important and logarithmic law is used for the turbulent region where the turbulence effects dominate conduction. Generally, the thickness of the thermal conduction layer is different from the thickness of the viscous sublayer and changes with fluid. Once the physical properties of the fluid are specified, its molecular Prandtl number is computed. Then the thermal sublayer thickness, y_T^* , is calculated from the intersection of the linear and logarithmic profiles. During the iteration, depending on the value of y^* , either the linear or the logarithmic profile is applied to compute the wall temperature T_w or heat flux q .

The production of kinetic energy; G_k , and its dissipation rate, ε , at wall-adjacent cell

$$\text{are computed from } G_k \approx \tau_w \frac{\partial U}{\partial y} = \tau_w \frac{\tau_w}{k_v \rho C_\mu^{1/4} k_B^{1/2} y_B} \quad (3.40)$$

$$\text{and } \varepsilon_B = \frac{C_\mu^{3/4} k_B^{3/2}}{k_v y_B} \quad (3.41)$$

In addition to the standard wall function, a two-layer-based, nonequilibrium wall functions of Chieng and Launder (1980) are additional options available in FLUENT for the strong nonequilibrium flows. The nonequilibrium wall functions are described as follows:

- a. Launder and Spalding's log-law for mean velocity is sensitized to pressure gradient effects.
- b. The two-layer-based concept is adopted to compute the budget of turbulent kinetic energy in the wall neighboring cells.

Details of the log-law for mean velocity sensitized to pressure gradients and the turbulent kinetic energy (G_k , ε) are available in the manual of FLUENT. The law of the wall for mean temperature remains the same as in the standard wall function described above.

In conclusion, the standard wall functions give reasonably accurate predictions for most high-Reynolds number, wall-bound flows, and the non-equilibrium wall functions further extend the applicability of the wall function approach by considering the effects of pressure gradient and strong non-equilibrium.

3.5 Numerical techniques for turbulent impinging jet simulations

3.5.1 Boundary conditions

In this part, the boundary conditions needed for both laminar and turbulent jets are considered. Unless stated otherwise, the following boundary conditions were applied for the continuous phase in all cases simulated in this work:

- Impingement surface: the impingement surface was specified as an isothermal or a constant heat flux wall. The velocities satisfy the no-slip condition and temperature value is fixed at T_w or the heat flux value is fixed at q_w .
- Confinement surface: the confinement surface is considered to be an adiabatic wall. The velocities also satisfy the no-slip condition and the heat flux value is fixed to be zero.
- Inlet: the inlet is considered as velocity inlet boundary conditions, at which uniform velocity and temperature profiles are prescribed. Unless otherwise stated, turbulence intensity and length scale at the inlet for all the calculations are chosen to be 2 % and 0.07 D (hydraulic diameter), respectively.
- Outlet: the outlet is considered as fully developed outflow. Thus, $V=0$ and the gradients of other variables are set to zero. Pressure outlet is another choice where the pressure in outlet is specified to be atmospheric and the temperature is equal to the ambient fluid temperature.
- Symmetry line: at the symmetry line, the axial velocity is set to zero and gradients of all other variables are equal to zero.

For multiphase cases, the particles were introduced in the inlet with the same velocity and temperature as the continuous phase. It should be emphasized that all particles were introduced to the flow field at 10 discrete positions. The ten different trajectory positions were determined by numerical experiments, which had shown that 10 trajectory positions were large enough and appropriate for the simulation. A larger number of locations (e.g. 20, 30 and 40) yielded the same results. The dispersion of particles due to gas turbulence is also considered using the statistical method. (FLUENT 6.0)

3.5.2 Numerical parameters

To solve the main variables u , v , p and T , a control volume based on the finite difference method (CVPDM) was used to discretize the governing equations by integration over the control volume. The general form of the algebraic governing equations obtained from discretization can be written as follows:

$$\alpha_P \Phi_P = \alpha_E \Phi_E + \alpha_W \Phi_W + \alpha_N \Phi_N + \alpha_S \Phi_S + b_\Phi \quad (3.42)$$

Where α is the coefficient of the convection and diffusion fluxes; E, W, N and S stand for the grid locations at the east, west, north and south sides of point P, and b is the discretized source term. In order to ensure stable simulation, the momentum equations, energy equation, turbulence kinetic energy equation, turbulence dissipation rate equation and Reynolds stress equations were discretized in FLUENT using the first-order upwind interpolation scheme. The discretized equations were solved using the SIMPLEC algorithm of Patankar (1980). Simulations using higher order interpolation scheme produced the same results as the first-order upwind interpolation.

3.5.2.1 Relaxation factors

To promote smooth convergence of the discretized equations, proper and successive under-relaxation parameters for the variables should be used. For single phase flow, the typical relaxation factors were 0.3, 0.7 and 0.5 for pressure, momentum and Reynolds stresses. For energy, the relaxation factor was 1. For the turbulence kinetic energy, and turbulence dissipation rate, the relaxation factor was 0.8 in each case. For gas-particle suspension flow, to make the cases converge, lower relaxation factors were selected, and the typical relaxation factors used were 0.2 and 0.3 for pressure and discrete phase sources, respectively. For others, the relaxation factor was set at 0.5.

3.5.2.2 Convergence criteria

The convergence criteria commonly require the following aspects. Firstly, the overall mass balance must be satisfied. Secondly, each of the sums of the local residuals must be less than the prescribed level.

In this study, the solution was considered to be converged when the normalized energy residual was less than 10^{-6} and the normalized residuals of all other variables were less than 10^{-4} for the single phase flow, while for gas-particle suspension flow, the solution was considered converged when the normalized energy residual was less than 10^{-5} and the normalized residuals of all the other variables were less than 10^{-4} .

3.5.2.3 Grid independence tests

The choice of grid layouts and density in the simulation domain is a very important aspect in numerical simulations. Generally, in the regions where the velocity or temperature gradients are large, the grid density is needed to be high. In this work, the flow and heat transfer behavior of single semi-confined impinging slot jet with and without cross flow and multiple impinging slot jets are studied. Here we use single semi-confined impinging slot jet without cross flow as an example to illustrate grid definition. This impinging slot jet flow configuration is symmetric, as shown in figure 1.1, therefore simulation of only half-domain is adequate for complete characterization of the flow. Several simulations involving the full domain were also conducted, which produced results in full agreement with the results of the half-domain as shown in Figure 3.2 and hence were not pursued any further. The impingement region is the most difficult domain to simulate accurately due to large gradients at streamline curvature. The grid layout in this region was specified to be much finer than that in the

downstream region. Figure 3.3 is simulation domain and definition of different regions. A non-uniform grid was used in all the simulations and a typical grid distribution is shown in Figure 3.4. Grid-independence tests were conducted for each new case. Figure 3.5 shows the results of one such test. The grid densities, 20×80 , 26×90 , 32×90 and 40×100 in Figure 3.5 refer only to the impingement region (Region A), and not to the whole region. Typically, a grid density of 20×80 in Region A yields grid-independent results for the example shown.

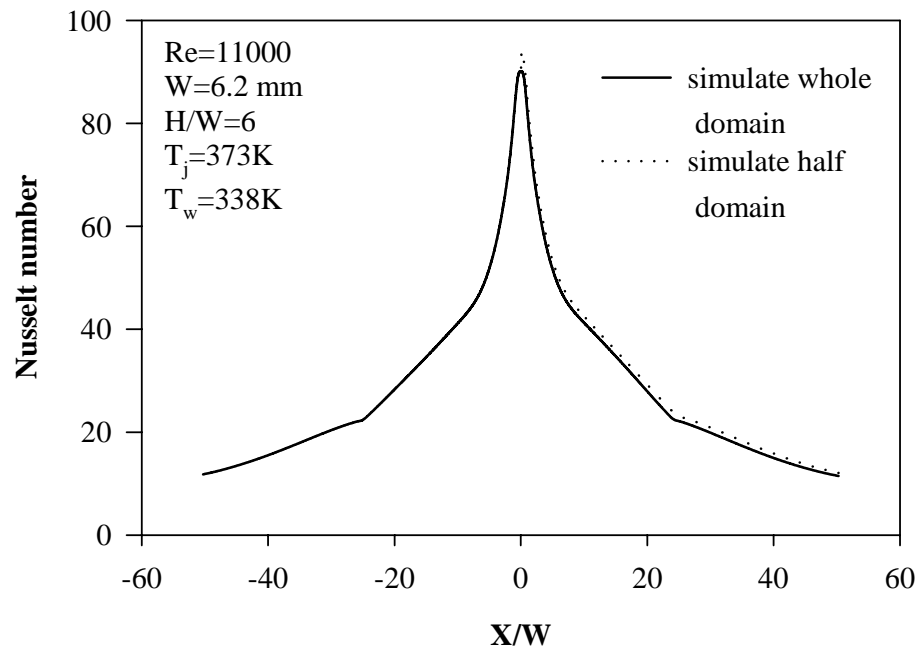


Figure 3.2 Effect of simulation region on results

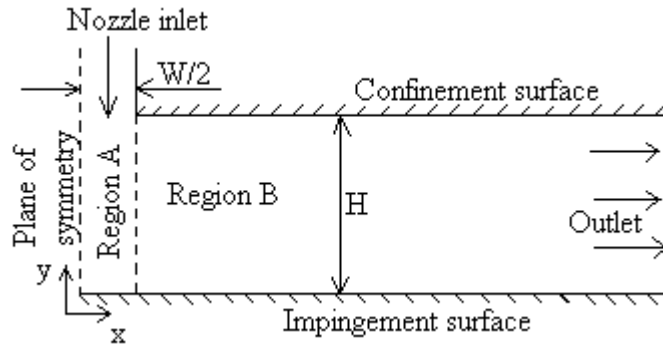
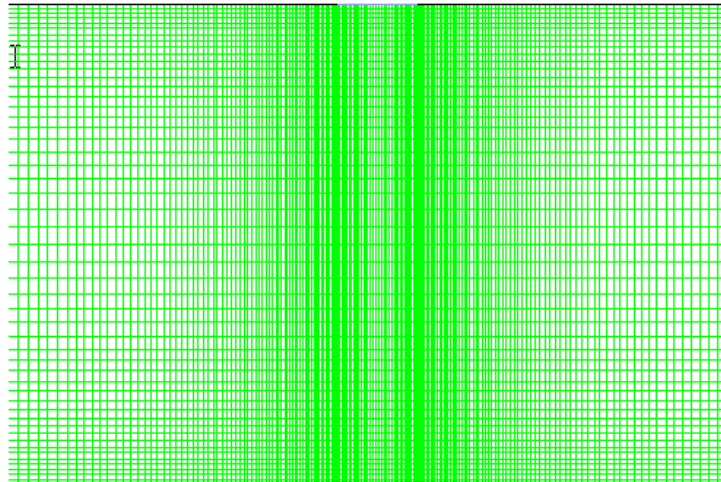


Figure 3.3 Definition of different regions in the computational domain



a: Typical grid structure



b: Second type of grid at the inlet area

Figure 3.4 Examples of typical grid structure

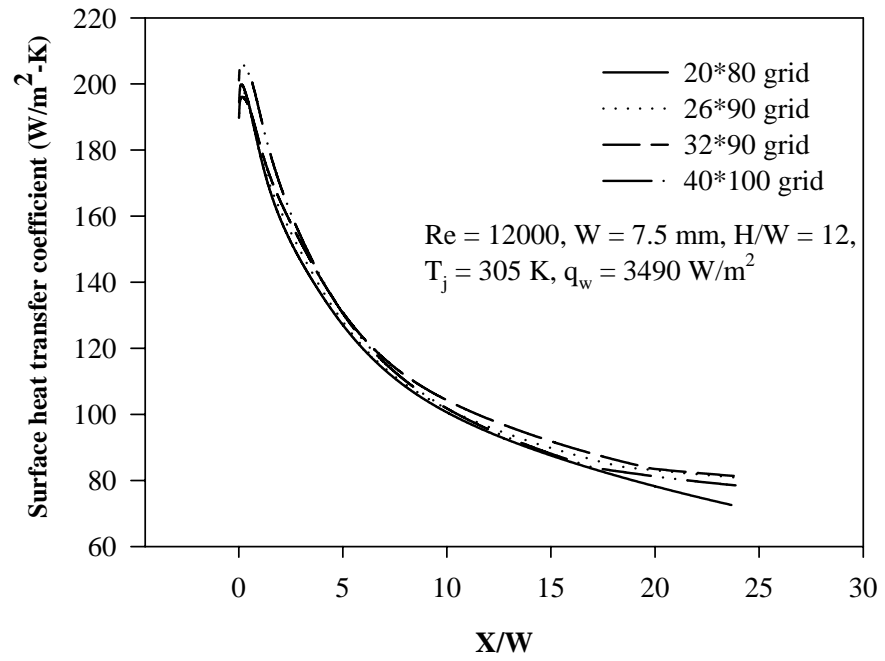


Figure 3.5 Effect of grid size on surface heat transfer coefficient

Chapter 4

Heat transfer under a turbulent impinging slot jet

4.1 Introduction

As mentioned in Chapter 1, impinging jets of various configurations are commonly used in numerous industrial applications such as drying of tissue, paper, textiles, photographic films, and cooling of high power density electronic components, due to their highly favorable heat and mass transfer characteristics. Despite an extensive body of research literature on the subject over the past two decades, impinging jet heat transfer remains an active area of research covering both the experimental and computational fluid dynamics aspects due to its inherently complex fluid and heat flow characteristics. This chapter presents simulation results for a single semi-confined turbulent slot jet impinging normally on a flat plate using FLUENT 5. Effects of various turbulence models, near wall functions, jet turbulence, jet Reynolds number as well as the type of thermal boundary condition at the target surface on heat transfer are discussed in the light of experimental data. The numerical simulation scheme adopted in this work was validated by comparing predicted Nusselt number distributions with experimental data from literature. Four sets of experimental results were selected from the numerous data available in the literature on the basis of how detailed the authors were in describing their experimental setup and procedures, and also the boundary conditions needed for simulation. The geometric parameters and boundary conditions of the selected experimental results are described in the following section in some detail.

For all of the cases studied here, besides the boundary conditions mentioned in Chapter 3, the fully developed outflow boundary condition was used at the outlet and the confinement surface was specified as an adiabatic wall.

4.2 Results and discussion

4.2.1 Comparison of results from various turbulence models

The geometric parameters and the corresponding boundary conditions of the simulated cases for different turbulent models are presented in Table 4.1. The results are presented as the distribution of local Nusselt number in the stream-wise direction. The heat transfer coefficient over the impingement surface was normalized in the form of a local Nusselt number for an isothermal impingement surface as: $Nu_x = \frac{h_x W}{\lambda}$, where

$$h_x = \frac{q}{(T_w - T_j)}$$

and λ is fluid thermal conductivity.

Table 4.1 Geometric parameters and boundary conditions for the two cases tested for turbulence models

	W (mm)	H/W	Re _j	T _j (K)	Boundary Condition at Impingement Surface	Turbulence Intensity on Nozzle Exit
Case 1	6.2	6.0	11000	373	T _w =338 K	2 %
Case 2	14.1	2.6	10200	310	T _w =348 K	2 %

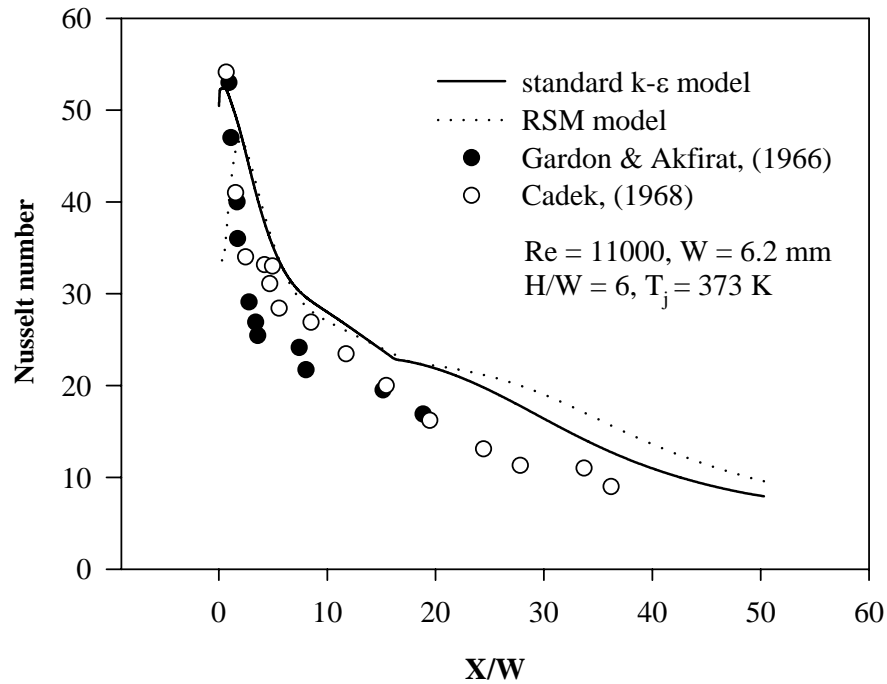


Figure 4.1 Comparison of simulated Nusselt number to the experimental data from literature for case 1

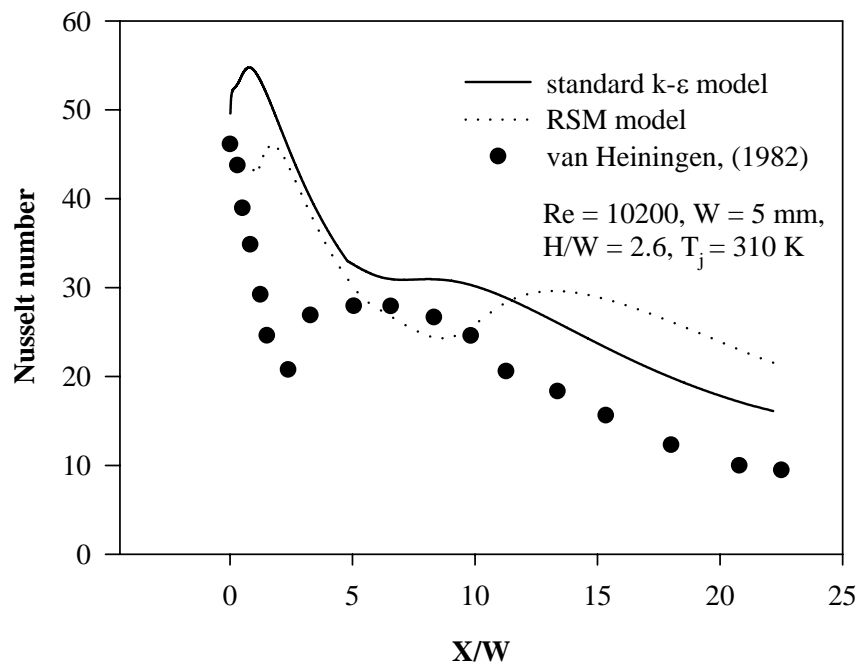


Figure 4.2 Comparison of simulated Nusselt number to the experimental data from van Heiningen for case 2

The computed local Nusselt numbers for two cases using the standard $k-\epsilon$ model and the Reynolds stress model are compared with the experimental data in Figures 4.1 and 4.2. Figure 4.1 compares the simulation results predicted by the two models with the

experimental data of Gardon and Akfirat (1966) from literature for case 1. Whereas Figure 4.2 compares simulation results predicted by the two models with the experimental data from van Heiningen (1982) for case 2. As can be seen from Figures 4.1 and 4.2, both standard k- ϵ and the Reynolds stress models slightly over-predict the Nusselt number in the stagnation region for both the cases, while greater difference (maximum of 20%) occurs for the standard k- ϵ model. The over-prediction of the Nusselt number at the stagnation zone is due to the high level of turbulence kinetic energy generation. The Nusselt number predicted by the Reynolds stress model reaches a maximum at X/W equal to 2 and 1.7 for case 1 and case 2, respectively, while the experimental maximum occurs at the stagnation point for the flow and geometric parameters shown in these figures.

For large nozzle-to-target spacing, $H/W = 6$, prediction by the standard k- ϵ model was better than the RSM model as shown in Figure 4.1, and both the models depict the qualitative trend of the Nusselt numbers very well. For small nozzle-to-target spacing, $H/W = 2.6$, van Heiningen measured two peak values in the local Nusselt number distribution (Figure 4.2). The first peak occurred at the stagnation point, while the second peak was located at X/W of about 6. In semi-confined impinging jet flows, a recirculation bubble develops in the off-stagnation region attached to the confinement surface, which forms a constricted channel with minimum area at the thickest section of the bubble, reducing the channel area and accelerating the fluid in this region. This causes an increase in the local heat transfer coefficient. This effect becomes appreciable only at smaller nozzle-to-target spacings as the experimental data show a clear second peak for $H/W=2.6$. Gardon and Akfirat (1966) and Polat et al. (1985) reported similar results for small H/W values. The RSM model shows a small

secondary hump but at a distance greater than the distance reported in the experimental work of van Heiningen (1982). Although generally the standard k- ϵ model gives a better prediction with respect to the shape of the Nusselt number distribution curve at least over a range of H/W and Re, it does not predict the secondary peak. The RSM model, on the other hand, predicts the numerical value of the secondary peak of Nusselt numbers well, but it does not predict the position of the secondary peak accurately.

4.2.2 Effect of turbulent Prandtl Number

Thakre and Joshi (2000) contended that even for simple flows such as the turbulent pipe flow, turbulent Prandtl number increases steeply and far exceeds unity as the wall is approached. The turbulent Prandtl number is defined as the ratio of the momentum to heat eddy diffusivities: $D_t(T) = \nabla \cdot \left(\left(\frac{\nu}{Pr} + \frac{\nu_t}{Pr_t} \right) \nabla T \right)$ and hence must influence the predictions of heat transfer rates using both the standard k- ϵ and the RSM models. A systematic parametric study was carried out to examine the influence of Pr_t on the Nusselt number distributions. For Case 2, the turbulent Pr value was varied from 0.85 (default) to 1.5 based on Lai & So (1990b) and Kim & Moin (1987).

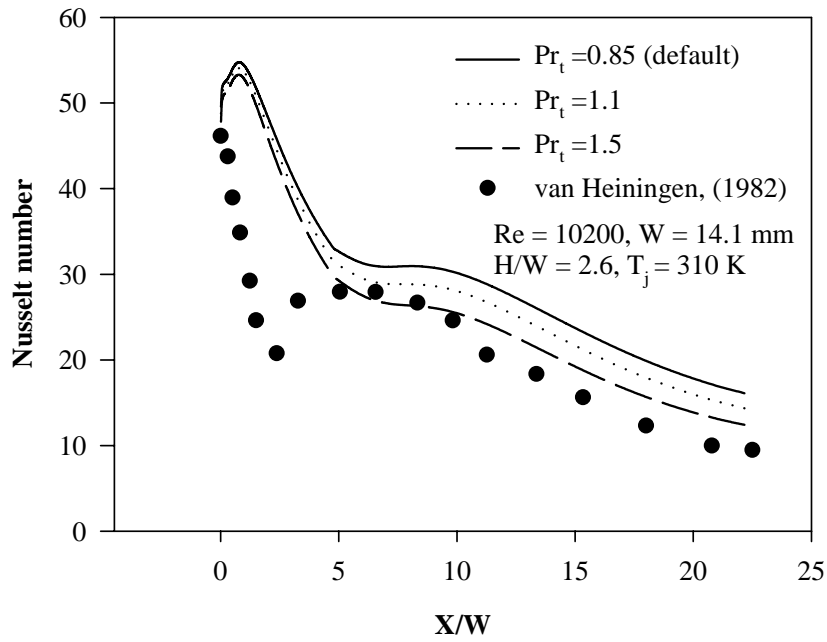


Figure 4.3 Comparison of Nusselt number predicted by standard $k-\epsilon$ model with increasing turbulent Pr no. to the experimental data

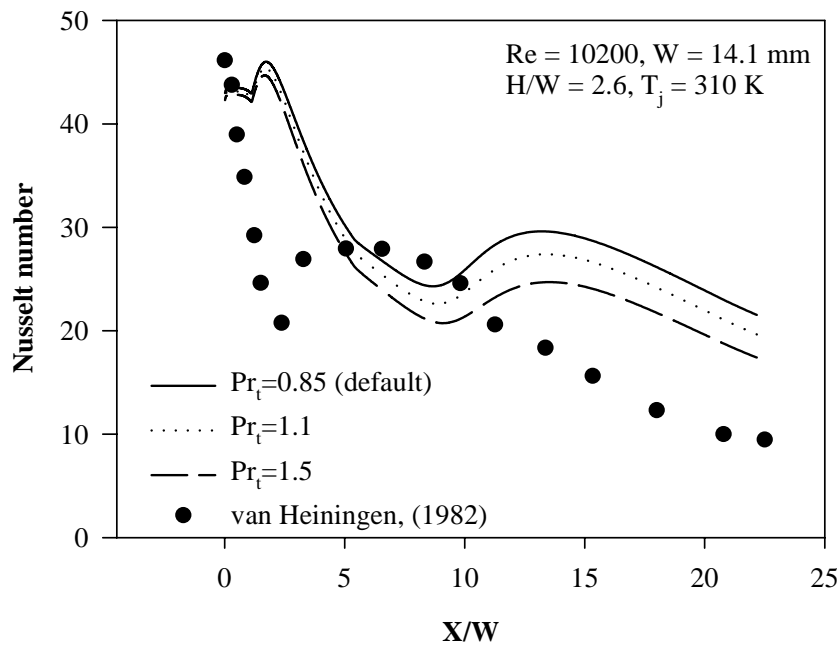


Figure 4.4 Comparison of Nusselt number predicted by the RSM model with increasing turbulent Pr no. to the experimental data

Figures 4.3 and 4.4 show the effect of turbulent Prandtl number on the computed Nusselt number along with the experimental data for case 2 as predicted by the standard $k-\epsilon$ model and the Reynolds Stress Model, respectively. Although, the standard $k-\epsilon$ model over-predicted the Nusselt number, the deviations from the

experimental data were reduced by increasing the turbulent Pr number and the fit with experimental data was much better away from the impingement zone. It seems that the turbulent Pr number affected Nusselt number to a greater extent in the downstream (wall jet) region than in the stagnation region for both the models tested. The Nusselt number decreased with the increase of turbulent Prandtl number for both standard k- ϵ and RSM models, but the magnitude of the turbulent Prandtl number did not change the shape of the Nusselt number profile and the position of the secondary peak of the Nusselt number.

4.2.3 Effect of Reynolds Number

Simulations were carried out for five Reynolds numbers for an impinging jet under constant heat flux conditions. The Reynolds number for the impinging jet flow is defined as, $Re = \frac{U_j L}{\mu}$, while the characteristic length, L , is the width of the slot jet.

The geometric parameters, boundary conditions, and the maximum surface heat transfer coefficients of the cases are presented in Table 4.2. Figure 4.5 shows the effect of the jet Reynolds number on the distribution of the surface heat transfer coefficients. The surface heat transfer coefficients predicted by both the standard k- ϵ model and the Reynolds stress model were compared with the experimental data of Bi (2001). As expected, the impingement surface heat transfer coefficients predicted by both the standard k- ϵ and the RSM model increased with the increase of jet Reynolds number. The agreement with the experimental data for both the models was much better for low Re_j (1500) values. However, interestingly, Bi's data are unlike the results shown in Figures 4.1 and 4.2, as the simulated heat transfer coefficients are lower than the experimental values as shown in Figure 4.5. This is probably due to the fact that a

uniform velocity profile at the end of the jet was used in simulations whereas that was probably not the case in the experiments of Bi, where a nozzle with high level of turbulence was used.

Table 4.2 Geometric parameters, boundary conditions and maximum surface heat transfer coefficient for the test cases for different Reynolds numbers

	W (mm)	H/W	Re _j	T _j (K)	Boundary Condition at Impingement Surface (W/m ²)	Turbulence Intensity at Nozzle Exit	Maximum Heat Transfer Rate (W/m ² -K)
Case 3	7.5	12	12000	305	3490	2 %	200
Case 4	7.5	12	9000	305	2830	2 %	158
Case 5	7.5	12	6000	305	1960	2 %	113
Case 6	7.5	12	3000	305	1260	2 %	80
Case 7	7.5	12	1500	305	870	2 %	61

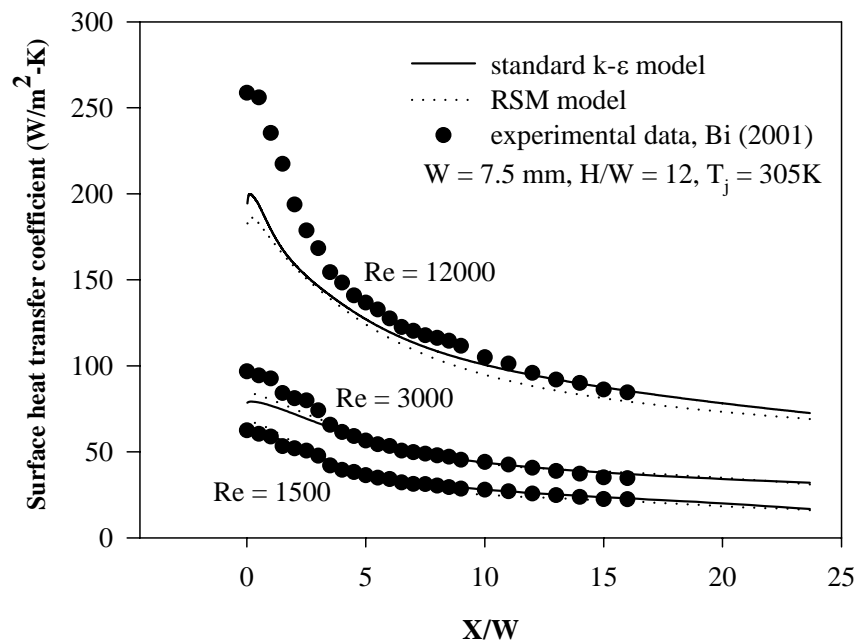


Figure 4.5 Effect of the jet Reynolds number on the surface heat transfer coefficients

Usually, the dependence of an average Nusselt number on Reynolds number is expressed as $Nu_{ave} = A Re^b$. Based on the simulations, relationships between Nu and

Re over a range of $X/W = 0 \sim 24$ such as $Nu_{ave} = 0.1023Re^{0.603}$ and $Nu_{ave} = 0.126Re^{0.576}$ were developed by standard k- ϵ model and RSM model, respectively, with the correlation coefficient, $R^2 = 0.996$ for both the models. The majority of the studies reported “b” values ranging from 0.5 to 0.8. For example, Saad (1981) found that the exponent “b” was constant at a value of 0.65 for all practical purposes and Martin (1977) reported it to be 0.67.

4.2.4 Effect of turbulence level at the nozzle exit on heat transfer

The turbulence intensity and length scale at the nozzle exit are important factors to represent the turbulence. The turbulence intensity, I , is defined as the ratio of root-mean-square of the velocity fluctuations, u , to the mean flow velocity, u_{avg} , while the turbulence length scale, l , represents the size of the large eddies that contain the energy in turbulent flows. Higher turbulence levels are commonly associated with high heat transfer coefficients. However, exploratory computations by Morris et al. (1996) showed that the turbulence intensity at the inlet (nozzle exit) had a negligible effect on the exit profile by using the standard k- ϵ model in FLUENT. In this work, effects of turbulence intensity and turbulence length scales on the flow characteristics, heat transfer and turbulent kinetic energy distributions were evaluated. The geometric parameters and boundary conditions for the cases studied are listed in Table 4.3.

Table 4.3 Geometric parameters and boundary conditions for the test cases

	W (mm)	H/W	Re _j	T _j (K)	Boundary Condition at Impingement Surface	Turbulence Length Scales	Turbulence Intensity on Nozzle Exit %
Case 8	14.1	2.6	10200	310	T _w =348 K	l=D	2, 4, 6, 8 and 10
Case 9	14.1	2.6	10200	310	T _w =348 K	l=0.07 D	2, 4, 6, 8 and 10

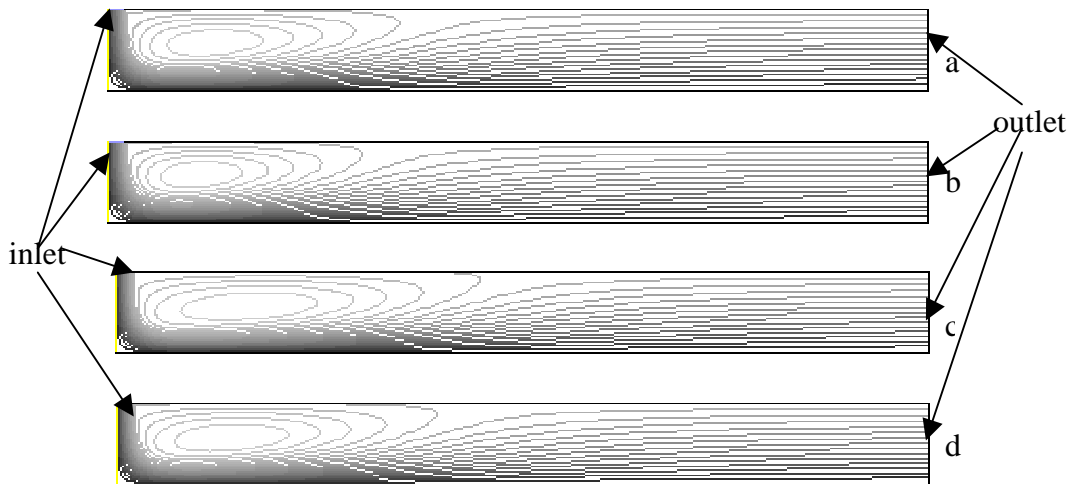


Figure 4.6 Streamline contour predicted by the standard k - ϵ model for different turbulence intensities and length scales

a: turbulence intensity = 2% (0~0.1448 kg/s), turbulence length scale = D ;

b: turbulence intensity = 10% (0~0.1446 kg/s), turbulence length scale = D ;

c: turbulence intensity = 2% (0 ~ 0.129 kg/s), turbulence length scale = $0.07D$;

d: turbulence intensity = 10% (0 ~ 0.1446 kg/s), turbulence length scale = $0.07D$

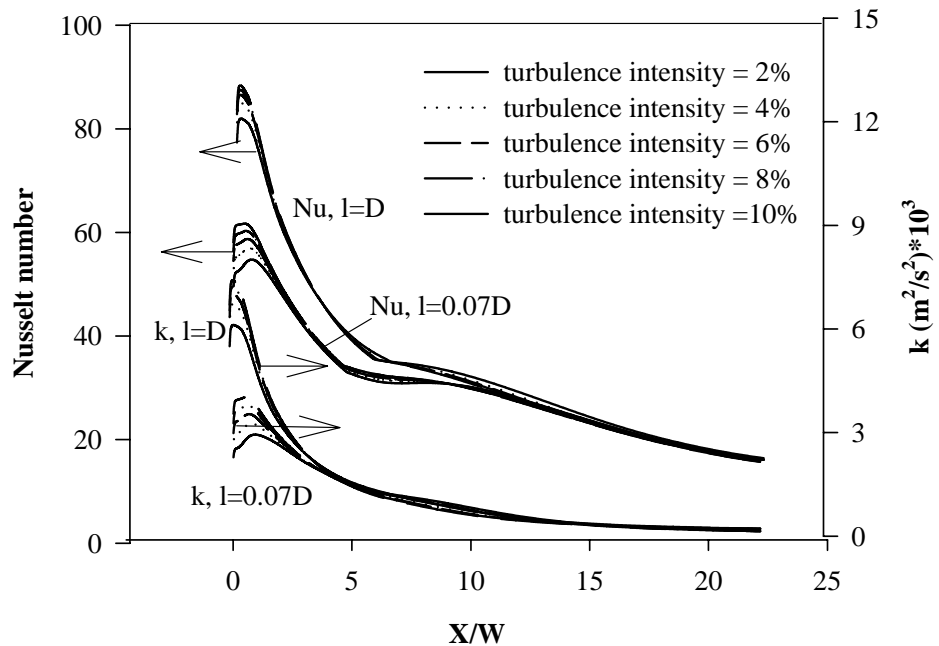


Figure 4.7 Effect of turbulence intensities and turbulence length scales on Nusselt number and turbulent kinetic energy predicted by the standard k - ϵ model

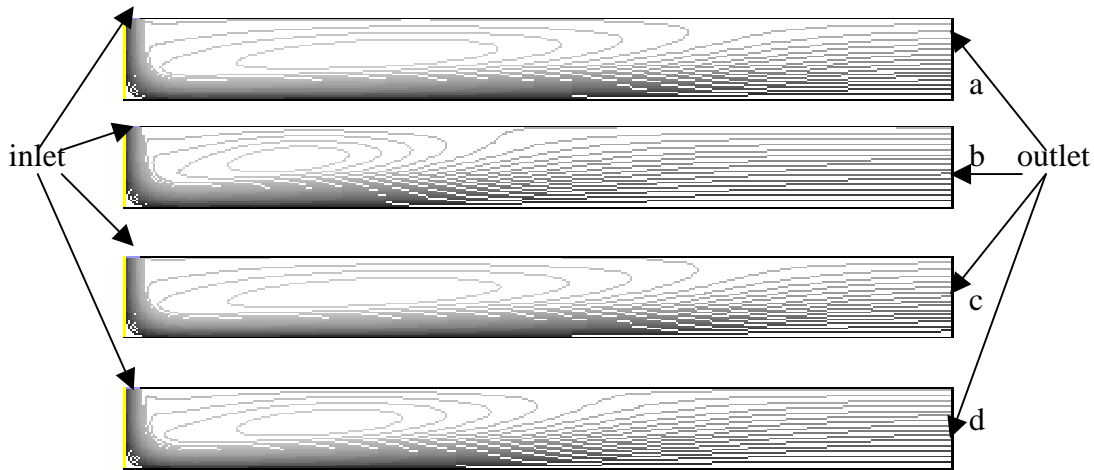


Figure 4.8 Streamline contour predicted by RSM model for different turbulence intensities and length scales

- a: turbulence intensity = 2% (0~0.1364 kg/s), turbulence length scale = D ;
 b: turbulence intensity = 10% (0~0.1397 kg/s), turbulence length scale = D ;
 c: turbulence intensity = 2% (0 ~ 0.121 kg/s), turbulence length scale = $0.07D$;
 d: turbulence intensity = 10% (0 ~ 0.125 kg/s), turbulence length scale = $0.07D$

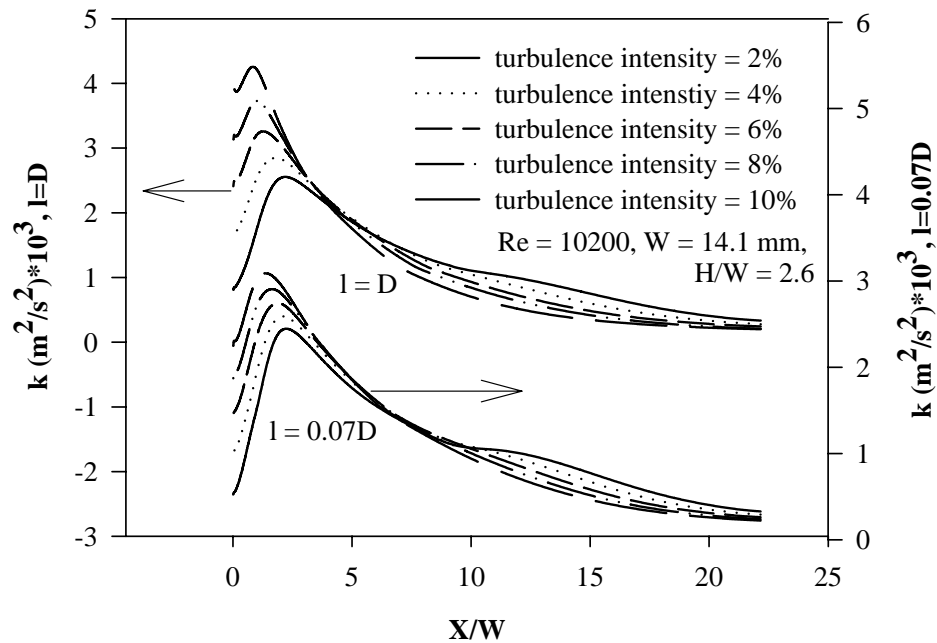


Figure 4.9 Effect of turbulence intensities and turbulent length scales on turbulent kinetic energy predicted by RSM model

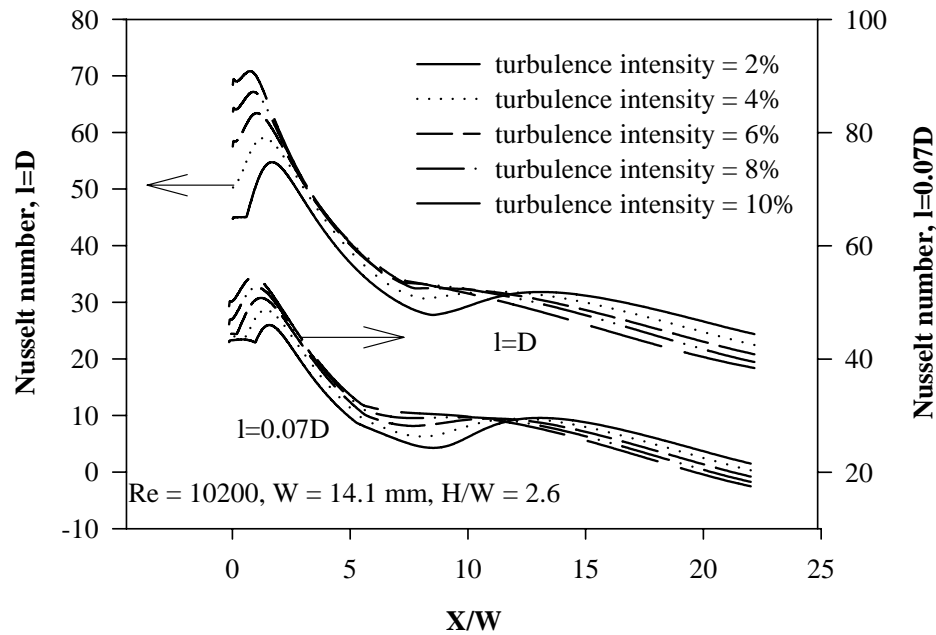


Figure 4.10 Effect of turbulence intensities and turbulent length scales on Nusselt number predicted by RSM model

The streamline contours for different turbulence intensities and length scales predicted by the standard $k-\epsilon$ model in the whole domain (Figure 4.6) show small effect of the turbulence intensity and large effect of the turbulence length scales at the nozzle exit. When the turbulence intensity increased, the size of the main vortex decreased slightly, while it decreased significantly when the turbulence length scales increased from $0.07D$ to D (D is the hydraulic diameter). Modest changes can be seen in the Nusselt number and turbulent kinetic energy distributions in the stagnation region when the turbulence intensity increased from 2% ~ 10% predicted by the standard $k-\epsilon$ model in Figure 4.7. For example, when the turbulence intensity increased from 2% to 10%, the turbulent kinetic energy and Nusselt number at the stagnation zone increased by 32.9% and 10.7%, respectively (for $Re_j=10,200$, $H/W=2.6$). Away from the stagnation zone, turbulent kinetic energy and Nusselt number distributions showed no influence of turbulence intensity. These results are similar to those of Morris et al. (1996) where turbulence intensity did not influence the exit flow profiles. Greater impact in turbulent kinetic energy (126% increase) and the Nusselt number (53% increase) at the

stagnation zone was seen when the turbulence length scale was increased from $0.07D$ to D . Thus, turbulence intensity and length scales at the nozzle exit affected the Nusselt number distributions more in the impingement region than in the downstream region for the standard k - ϵ model.

Greater difference in streamline contours can be seen when RSM was used to characterize the effect of turbulence intensity and length scales at the nozzle exit (Figure 4.8). The recirculation zone shifted upstream and the size of the recirculation decreased when the turbulence intensity and length scale increased. Similarly, much greater effects of both the turbulence intensity and length scale were observed on the maximum turbulent kinetic energy and Nusselt number as shown in Figures 4.9 and 4.10, respectively. In addition to the impingement region, the Nusselt number and turbulence kinetic energy in the downstream zone were also affected by the turbulence intensity and the magnitude of turbulence length scale at the nozzle exit, which is quite different from the standard k - ϵ model.

4.2.5 Effect of the near wall function on the predicted Nusselt number

As mentioned in chapter 3, the nonequilibrium wall function partly accounts for the effect of pressure gradients and the departure from equilibrium. The nonequilibrium wall function is commonly claimed to be suitable for complex and separated flows. Morris et al. (1999) in their work on jet impingement heat transfer used the standard wall function over the Re_j range of 2000-13,000, and $H/D = 2\sim 4$ and the nonequilibrium wall function for the cases with $Re_j \geq 13,000$. However, no comparison of the effects of chosen wall functions on the heat transfer rate distributions was presented. In this work, we present a case for $H/W = 2.6$ and $Re_j = 71,300$. It is noted

that the standard wall function predicts slightly higher Nusselt numbers than the nonequilibrium wall function at the stagnation and downstream zones for both the turbulence models used (Figure 4.11). Since the simulated Nusselt number values are generally higher than the experimental data, use of nonequilibrium wall function can be considered to be marginally better than the standard wall function. However, generally the standard wall function is more stable and converges faster than the nonequilibrium wall function. Thus, for low Re_j , the standard wall function was chosen and nonequilibrium wall function was used for Re_j greater than 20,000. On passing, it was observed that at high Reynolds number, $k-\varepsilon$ model produces much greater stagnation Nusselt number than the Reynolds Stress Model.

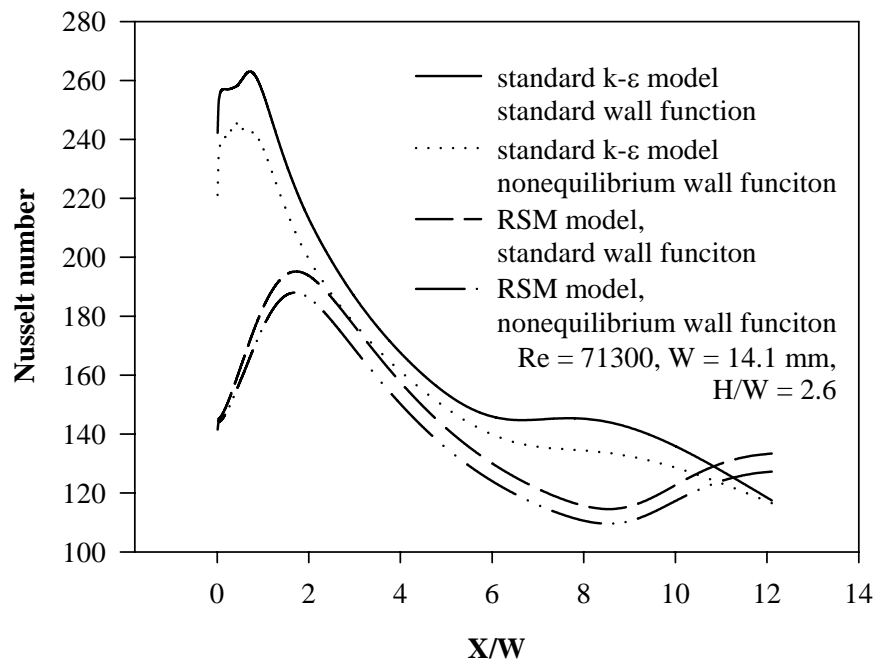


Figure 4.11 Effect of wall functions on Nusselt number distributions

4.2.6 Effect of the magnitude of the heat flux

Four cases were selected to evaluate the effect of heat fluxes applied at the impingement surface on heat transfer. The geometric parameters and boundary

conditions for these four cases are listed in Table 4.4. The properties of the materials were treated as constant for cases 10-12 as a small range of temperature difference was used in these computations, while the properties of the materials were defined as temperature-dependent for case 13 where large range of temperature difference (>100K) was used in calculations.

Table 4.4 Geometric parameters and boundary conditions for the test cases

	W (mm)	H/W	Re _j	T _j (K)	Boundary Condition at Impingement Surface (W/m ²)	Boundary Condition at Confinement Surface (W/m ²)	Turbulence Intensity on Nozzle Exit
Case 10	5	6	12000	302	1000	0	2 %
Case 11	5	6	12000	302	3000	0	2 %
Case 12	5	6	12000	302	5450	0	2 %
Case 13	5	6	12000	302	50000	0	2 %
Case 14	5	6	12000	302	310 (K)	0	2 %

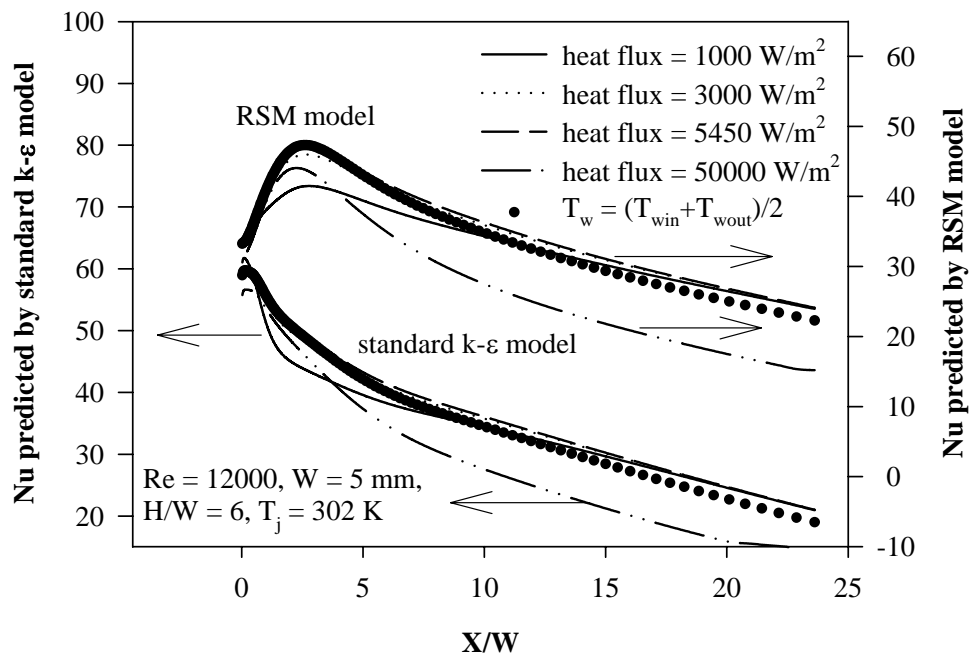


Figure 4.12 Comparison of Nusselt number at different thermal boundary conditions

The effect of heat flux on the impinging surface as predicted by the standard k- ϵ and RSM models on the Nusselt number is shown in Figure 4.12. Both models showed that the variable heat fluxes did not influence the numerical values of Nusselt number at low heat flux values (Figure 4.12). When the heat flux at the impingement surface was increased from 1000 W/m² to 5450 W/m², the greater difference of Nusselt number occurred at X/W about 2.5. With the increase of the heat flux of the impingement surface from 1000 W/m² to 5450 W/m², the Nusselt number (at X/W at about 2.5) increased only by 11% by the standard k- ϵ model and 14% by the RSM model, respectively. Beyond X/W=13, the Nusselt number changed slightly for different heat flux values. However, when the heat flux at the impingement surface was increased to a very high value, 50,000 W/m², the Nusselt numbers were decreased significantly (as shown in Figure 4.12). Interestingly, the difference in Nusselt number with increased heat flux was higher with the increasing X/W.

The effect of heat flux on Nusselt number and wall temperature distributions has important significance in practice since it permits one to use data and empirical design correlations carried out using isothermal, constant heat flux or variable temperature impingement surface. For example, the two dotted lines in Figure 4.12 are the Nusselt number distributions with the constant temperature boundary condition (the constant temperature is the average temperature of the inlet and outlet temperatures on the impingement surface for case 12). By comparing the Nusselt numbers under the constant temperature boundary conditions with those under the constant heat flux boundary conditions, it can be seen that for low heat flux values, the Nusselt number distributions with the constant temperature boundary condition were quite similar to those of constant heat flux boundary conditions (constant temperature was the average

temperature of the impingement surface with the constant heat flux boundary conditions).

4.3 Conclusions

Two turbulence models, namely the standard k- ϵ model and the RSM, were used to calculate the heat transfer under a semi-confined turbulent impinging slot jet for various flow and geometric parameters. It was found that the qualitative trends predicted by both turbulence models compared very well with the experimental trend in most cases. The simulated results compare favorably with the experimental results for large nozzle-to-target spacing, but the predictions for small nozzle-to-target spacing call for further improvement in the simulation. Considering that all experimental results are subject to an uncertainty level, which is rarely quantitatively reported by the authors, and inadequate description about the flow conditions at the nozzle exit, the agreement between simulation and experimental data is quite encouraging. Some specific conclusions can be drawn from the study conducted in this chapter as follows:

- i) The standard k- ϵ model was not successful in predicting the secondary flow patterns, which occur for small H/W ratios, whereas RSM could predict a secondary peak for such cases, albeit at a different distance than the experimental value.
- ii) The turbulent Pr number brought about noticeable effects on the computed Nusselt number in the downstream direction, and a better match between the simulated and experimental data was observed when the turbulent Pr was increased from its default value of 0.85 to 1.5.

- iii) Differences between the simulated and experimental heat transfer coefficients in the stagnation zone increased with increasing Reynolds number from 1500 to 12,000.
- iv) The standard wall function predicted slightly higher Nusselt number distributions than the nonequilibrium wall function for both the standard $k-\epsilon$ and the Reynolds Stress models.
- v) The turbulence length scale at the nozzle exit brings forth significant changes in the Nusselt number distribution by both the models, whereas the effect of turbulence intensity at the nozzle exit is more remarkable in case of only RSM model.
- vi) For low heat flux values (1000~6000 W/m²), the physical properties of air are temperature-independent and the heat flux has negligible effect on the Nusselt number distribution. However, for large heat flux (50,000 W/m²), the physical properties of air become temperature-dependent and the heat flux has significant effect on the Nusselt number distribution.

In this chapter, we demonstrate the use of CFD as a successful prediction tool for flow problems involving impinging jet by comparing experimental data with the simulations, although further improvement in prediction is necessary for small nozzle-to-target spacing, especially in the impingement region.

Chapter 5

Effect of temperature difference between the jet and impingement surface on heat transfer

5.1 Introduction

In heating, cooling or drying applications involving large temperature differences between the jet and the target surface, it is necessary to incorporate the temperature-dependence of fluid properties on the flow and temperature fields. Despite their frequent occurrence in industrial practice, there is little research reported in the literature on this subject. It is also necessary to distinguish between heating and cooling applications since the thermo-physical properties of the fluid in the vicinity of the target surface vary in different directions for the two cases. In this chapter, CFD simulation results for heat transfer in a semi-confined slot turbulent jet under thermal boundary conditions where temperature-dependence of the fluid properties affect the flow and thermal fields are presented. A comparative analysis of the performances of standard k- ϵ and RSM models at constant target surface temperature in turbulent flow regimes is presented.

This chapter examines the effect of small and large temperature differences, ΔT , ranging from 12 K to 272 K, between the jet and the impingement surface on the local Nusselt number distributions under isothermal boundary conditions. The local Nusselt number for an isothermal impingement surface can be defined as $Nu_x = \frac{h_x W}{\lambda}$, where λ is the fluid thermal conductivity, $h_x = q / \Delta T$ and ΔT is the temperature difference between the jet and impingement surface. The fluid thermal conductivity can be

calculated according to different reference temperatures. The most popular method is to calculate the λ by film temperature, $T_f = \frac{(T_w + T_j)}{2}$.

In this work, λ is calculated at jet, film and impingement wall temperatures and the corresponding Nusselt numbers are denoted by Nu_j , Nu_f and Nu_w , respectively. A comparison is made between the Nusselt number distributions under these three definitions of Nu. The choice of flow configuration and geometric parameters for this aspect of study is same as presented before in Chapter 4.

5.2 Results and discussion

Initially, the effects of temperature difference between the jet and impingement surface on Nusselt number were carried out by studying four temperature difference values ($\Delta T = 12$ K, 52 K, 172 K and 272 K) for both heating and cooling conditions with the nozzle-to-target spacing, $H/W = 6$, by both the standard k- ϵ and RSM turbulence models.

5.2.1 Small temperature difference case

Figures 5.1 - 5.3 show the effects of small temperature differences between the jet and impingement surface on the variously defined Nusselt number distributions (Nu_j , Nu_f and Nu_w) predicted by both the standard k- ϵ as well as the RSM models for both cooling and heating conditions.

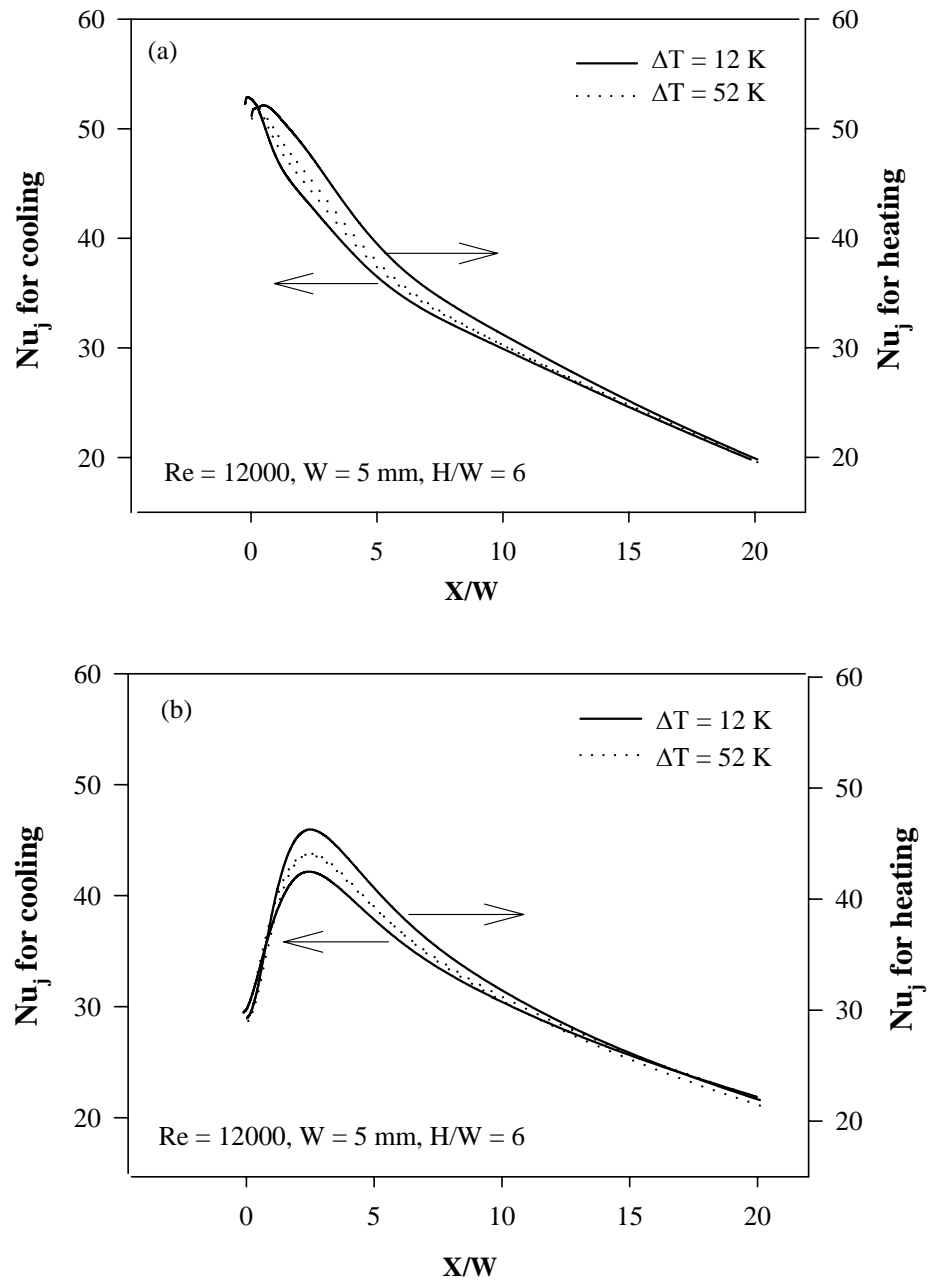


Figure 5.1 Effect of small ΔT between the jet and the impingement surface on Nu_j for cooling and heating. a: standard $k-\epsilon$ model; b: RSM model

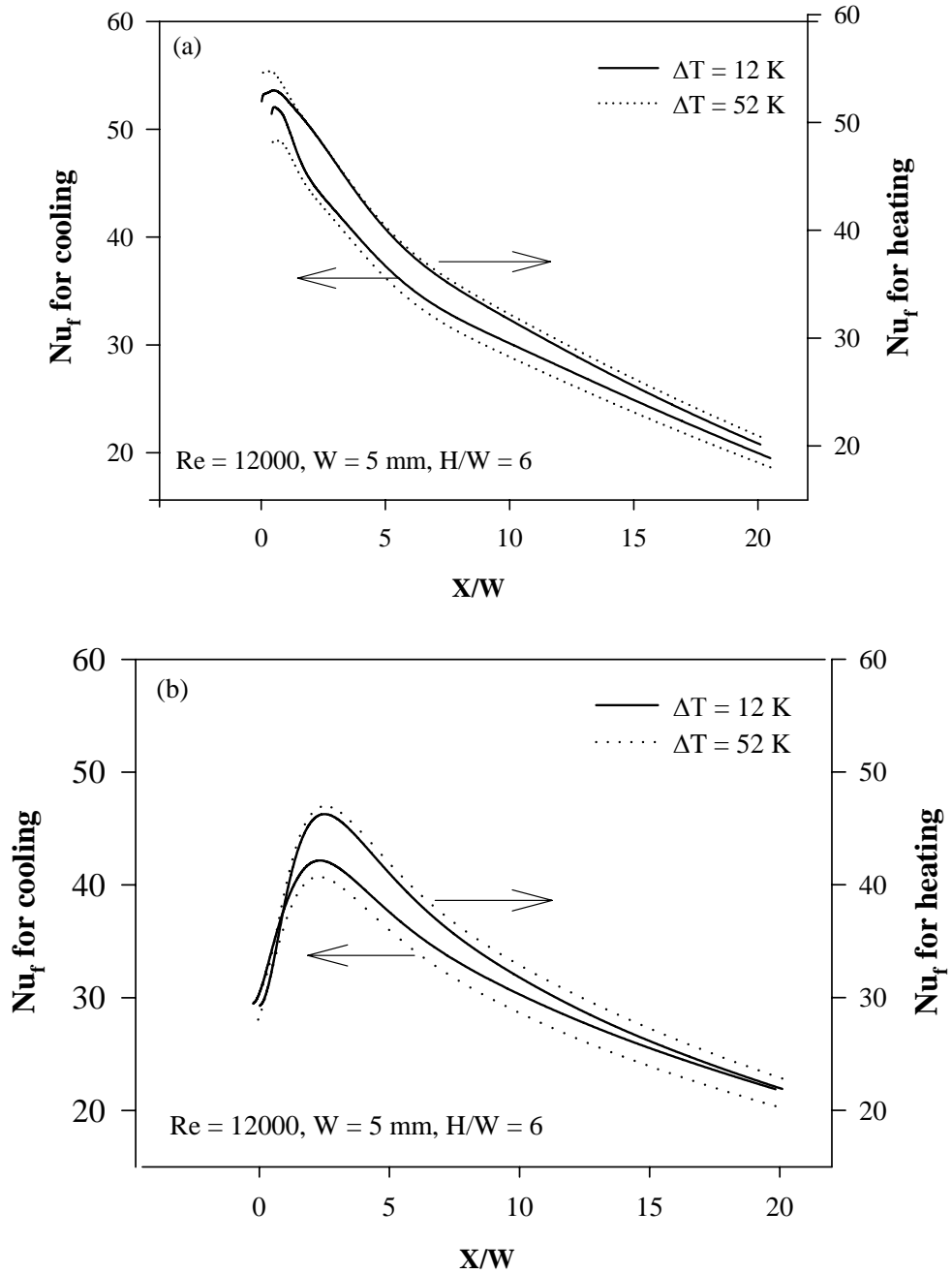


Figure 5.2 Effect of small ΔT between the jet and the impingement surface on Nu_f for cooling and heating. a: standard $k-\epsilon$ model; b: RSM model

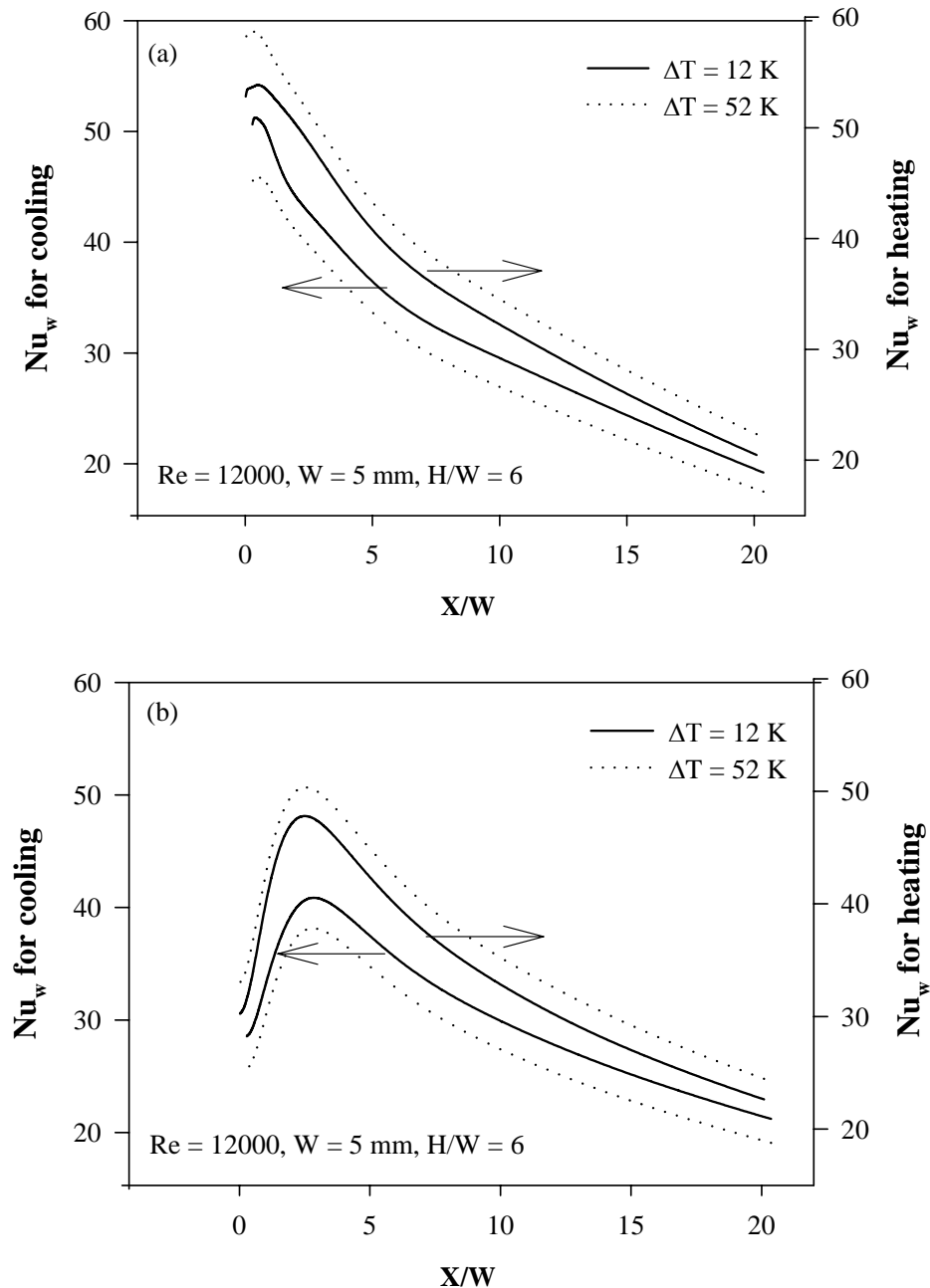


Figure 5.3 Effect of small ΔT between the jet and the impingement surface on Nu_w for cooling and heating. a: standard $k-\epsilon$ model; b: RSM model

In these three figures, Nu_j , Nu_f and Nu_w predicted by RSM all reach a maximum at $X/W = 2.5$, while the standard $k-\epsilon$ model predicts the maximum Nusselt number at the stagnation point. Both the standard $k-\epsilon$ and RSM models showed that the Nusselt number changed in opposite directions with increase of the temperature difference for cooling and heating conditions since the thermo-physical properties of the fluid in the

vicinity of the target surface vary in different directions for heating and cooling conditions.

These figures also show that the three definitions of Nusselt number, Nu_j , Nu_f and Nu_w , yield comparable results, i.e., Nu_j , Nu_f and Nu_w have nearly the same values at small ΔT s. When the temperature difference between the jet and impingement surface increased from 12 K to 52 K, the difference in the wall Nusselt number (λ is calculated at impingement wall temperature) was larger than that in the film Nusselt number (λ is calculated at film temperature) and the jet Nusselt number (λ is calculated at jet temperature). The largest difference in wall Nusselt number was about 10%, while the jet and film Nusselt number changed little when temperature difference increased from 12 K to 52 K. These results suggest that, under small temperature differences between the jet and impingement surface, the physical properties of the fluid do not change considerably and the fluid properties can be treated as temperature-independent for small temperature difference.

5.2.2 Large temperature difference case

Figures 5.4 – 5.6 present the results for large temperature differences between the jet and impingement surface. Similarly as for small temperature differences, the shape of the Nusselt number distributions (Nu_j , Nu_f and Nu_w) predicted by RSM model are different from those predicted by the standard k- ϵ model; the peak values of the three Nusselt numbers predicted by the standard k- ϵ model and RSM model are at stagnation point and at $X/W = 2.5$, respectively.

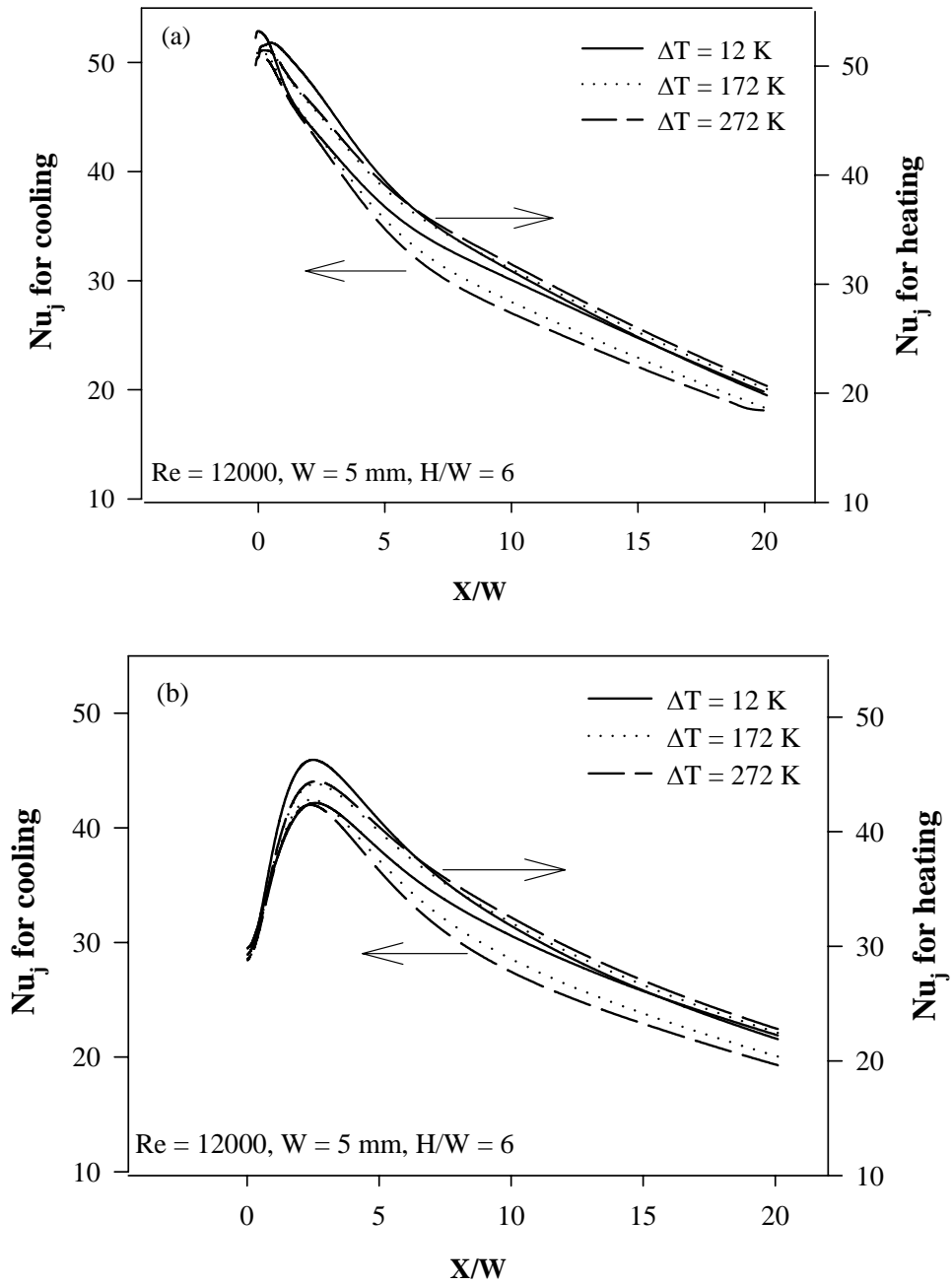


Figure 5.4 Effect of large ΔT between the jet and impingement surface on Nu_j for cooling and heating. a: standard $k-\epsilon$ model; b: RSM model

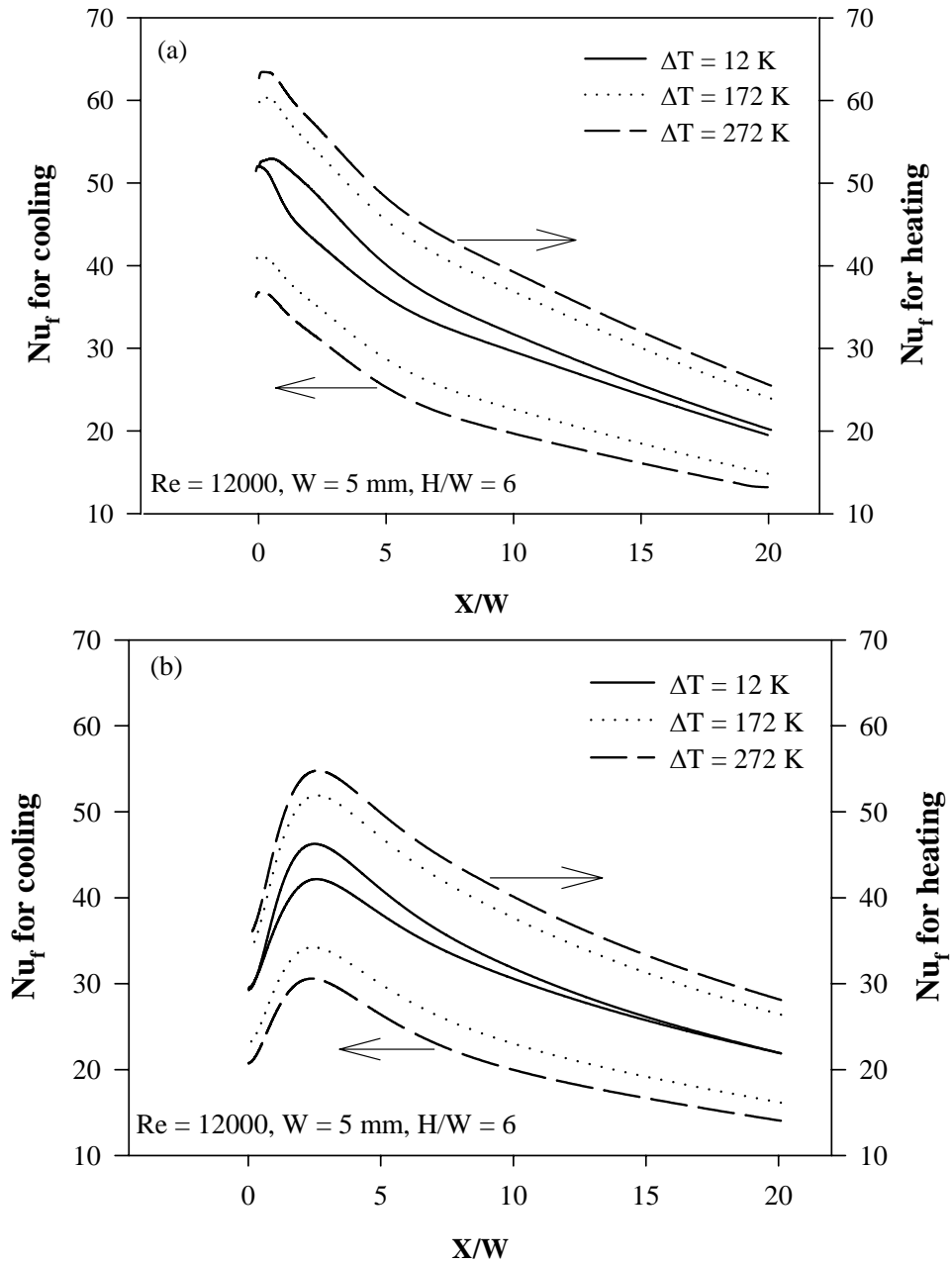


Figure 5.5 Effect of large ΔT between the jet and impingement surface on Nu_f for cooling and heating. a: standard $k-\epsilon$ model; b: RSM model

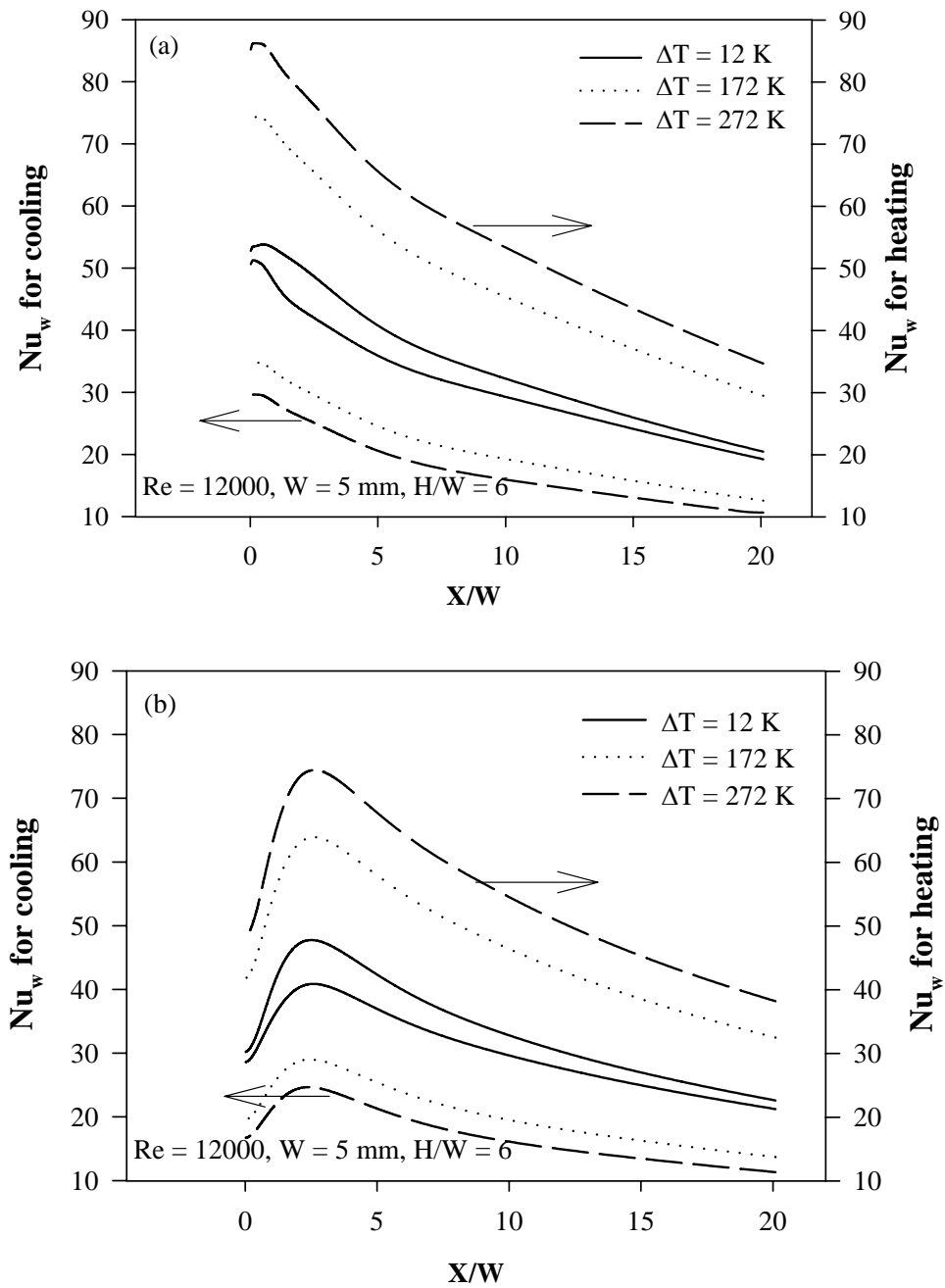


Figure 5.6 Effect of large ΔT between the jet and impingement surface on Nu_w for cooling and heating. a: standard $k-\epsilon$ model; b: RSM model

In Figure 5.4, the spread in jet Nusselt number distribution was the least when the temperature difference between the jet and impingement wall increased from 12 K to 272 K for both cooling and heating conditions predicted by the standard $k-\epsilon$ as well as RSM turbulence models. Despite the large variation in T , the jet Nusselt numbers were almost unchanged at the stagnation point for both cooling and heating conditions. At

the exit, the jet Nusselt number varied the largest, but by only 7.5% according to the standard k- ϵ model and only 10% according to the RSM model for the cooling condition. For heating, the jet Nusselt number varied by only 2% and 4.5% as computed using the standard k- ϵ and RSM models, respectively.

When the temperature difference increased from 12 K to 272 K, the difference in the film Nusselt number and wall Nusselt number increased greatly according to both models. The Nusselt number changed with increase of ΔT in opposite directions for the cooling and heating conditions, which is also because the thermo physical properties of the fluid in the vicinity of the target surface vary in opposite directions for the two cases.

For the same variation in T as above, for cooling, the peak film Nusselt number varied by 29% and 27% as predicted by the standard k- ϵ and RSM models, respectively. For the heating condition, the peak film Nusselt number varied by about 20% as predicted by the two turbulence models tested. Also for the same range of ΔT for cooling, at the exit, the film Nusselt number varied by 30% and 36%; for heating, by 27.5% and 30% as predicted by the standard k- ϵ model and RSM model, respectively (Figure 5.5).

From Figure 5.6, we notice that, with the increase of ΔT , the difference in the wall Nusselt number was the largest among the three definitions. When ΔT increased from 12 K to 272 K, the peak Nusselt number decreased by 41% and 39% for cooling condition by the standard k- ϵ model and RSM model, respectively and increased 59% and 56% for heating condition by the standard k- ϵ model and RSM model, respectively. At the exit, the wall Nusselt number decreased by 42% and 48% for

cooling by the standard k- ϵ model and RSM model, respectively and increased by 75% and 115% for heating by the standard k- ϵ model and RSM model, respectively.

Based on the above results, we extended the numerical experiments for variable H/W values (H/W = 2.6, 6 and 12), and different jet Reynolds number values (Re = 1500, 3000, 6000 and 12,000). Only the standard k- ϵ model was used because although the standard k- ϵ model and RSM model produce different numerical values for Nusselt number distributions, both models produce the same conclusion about the effect of temperature difference on Nusselt number. Figures 5.7-5.10 show the effects of temperature differences between the jet and impingement surface on Nu_j predicted by the standard k- ϵ model for three nozzle-to-target spacing, H/W = 2.6, 6 and 12, for four jet Reynolds numbers, Re = 1500, 3000, 6000 and 12,000, respectively. Figures 5.11-5.14 and Figures 5.15-5.18 are similar to the Figures 5.7-5.10, however, presenting the results for Nu_f and Nu_w , respectively.

From the above figures, we observe that for both small and large nozzle-to-target spacings, and for the range of jet Reynolds number from 1500 to 12,000, the Nu_j shows the least spread among the three Nusselt number definitions under the range of temperature differences between the jet and impingement surface from 12 K to 272 K and Nu_w shows the largest spread under the same range of ΔT . We also found that the difference in Nu_f and Nu_w increases with the increase of jet Reynolds numbers. For example, impingement region, for H/W = 12, the difference of Nu_f increased from 10% for Re = 1500 to 25% for Re = 12,000, similarly, also for H/W = 12, Nu_w increased from 40% for Re = 1500 to 70% for Re = 12,000.

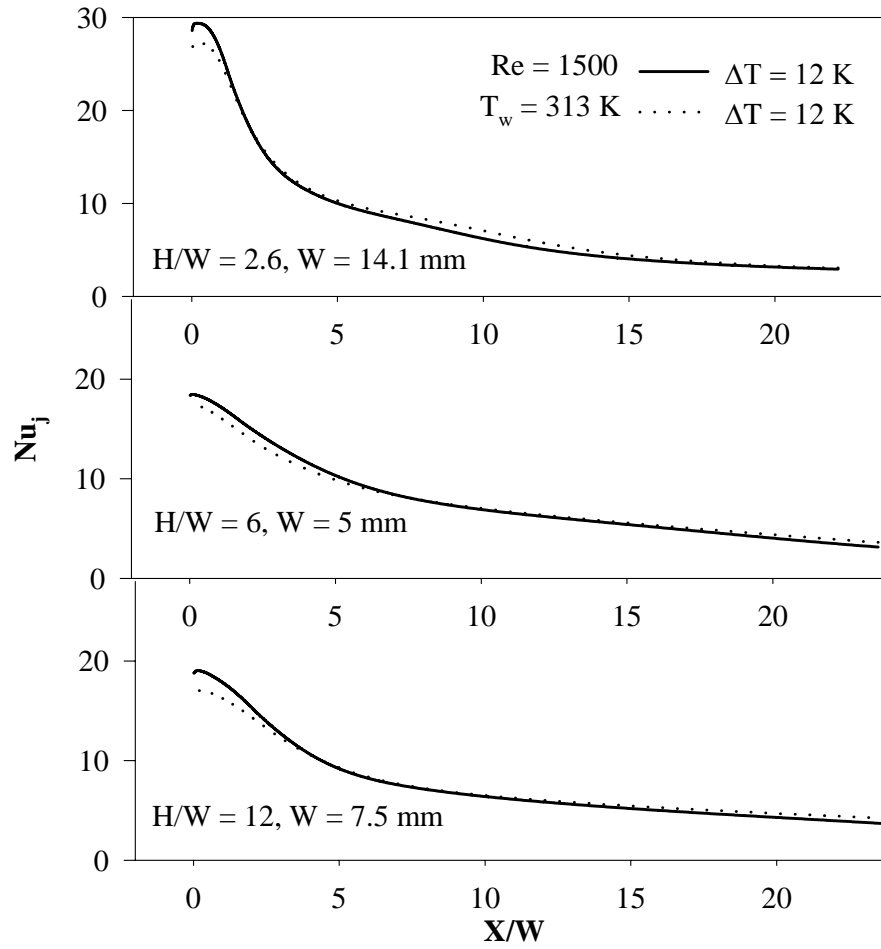


Figure 5.7 Effect of temperature difference between the jet and impingement surface on jet Nusselt number for heating condition by the standard $k-\epsilon$ model

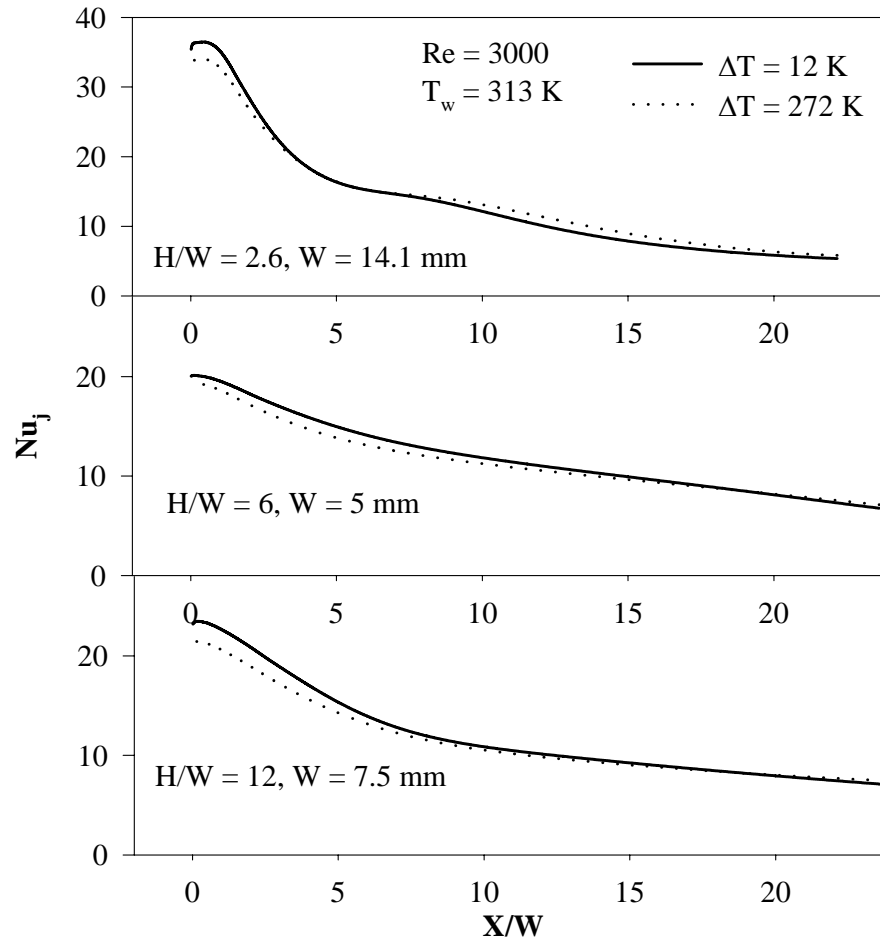


Figure 5.8 Effect of temperature difference between the jet and impingement surface on jet Nusselt number for heating condition by the standard $k-\epsilon$ model

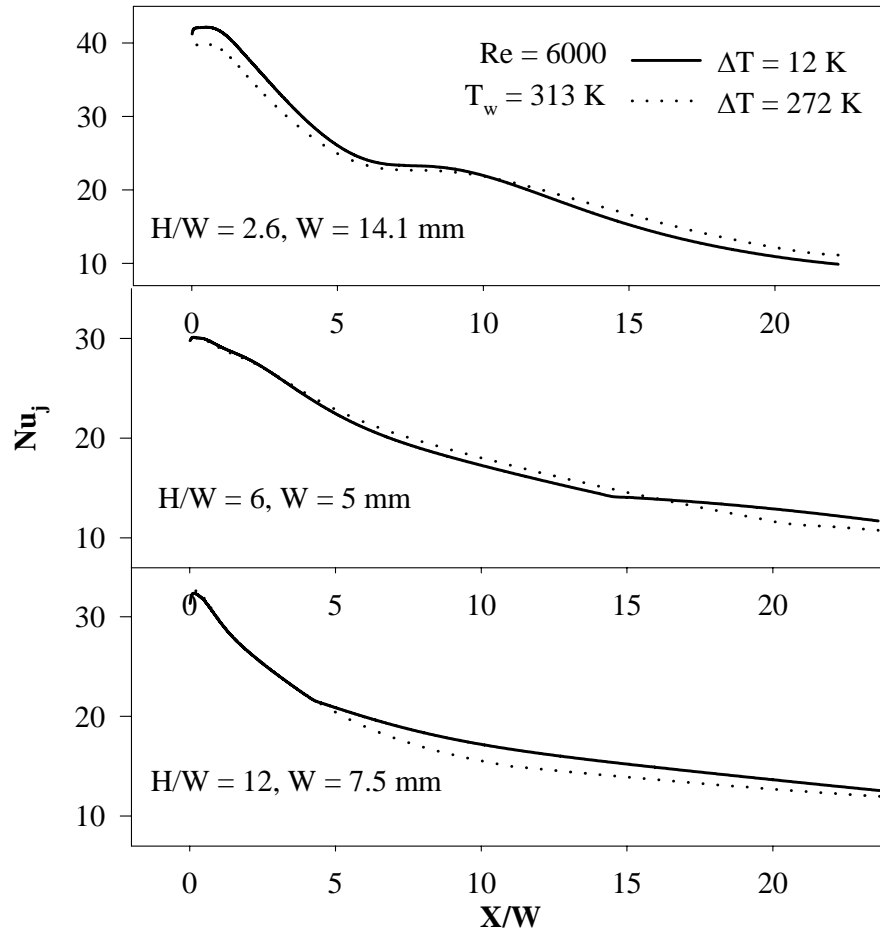


Figure 5.9 Effect of temperature difference between the jet and impingement surface on jet Nusselt number for heating condition by the standard $k-\epsilon$ model

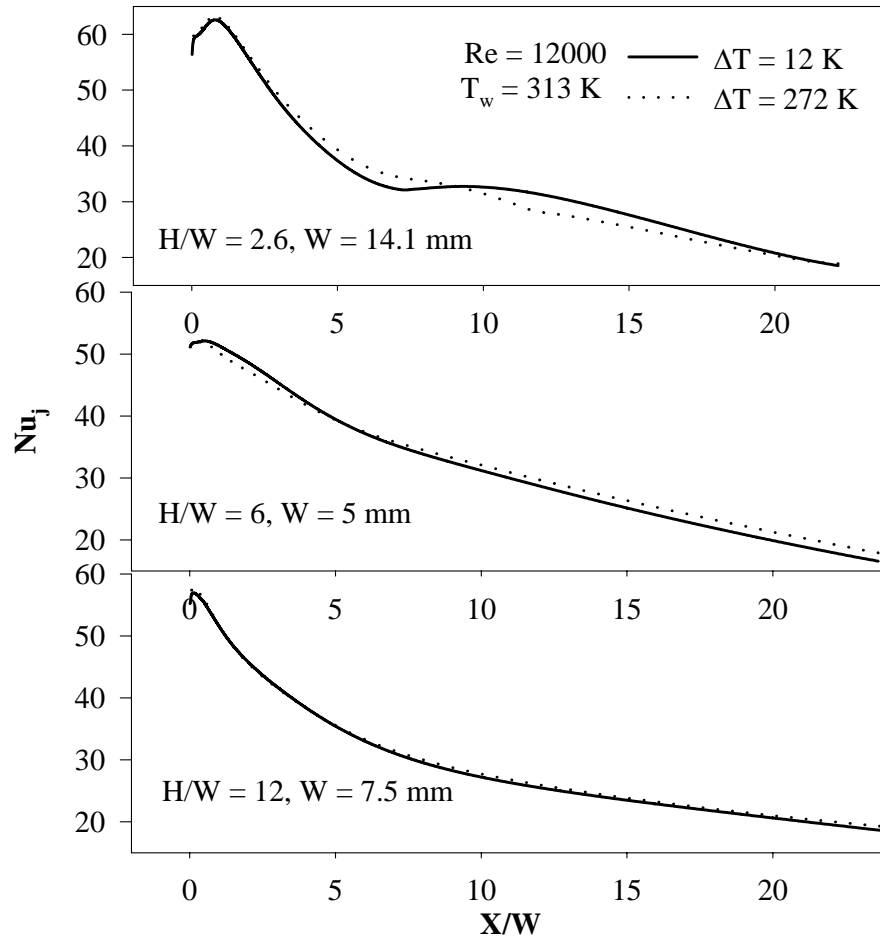


Figure 5.10 Effect of temperature difference between the jet and impingement surface on jet Nusselt number for heating condition by the standard k- ϵ model

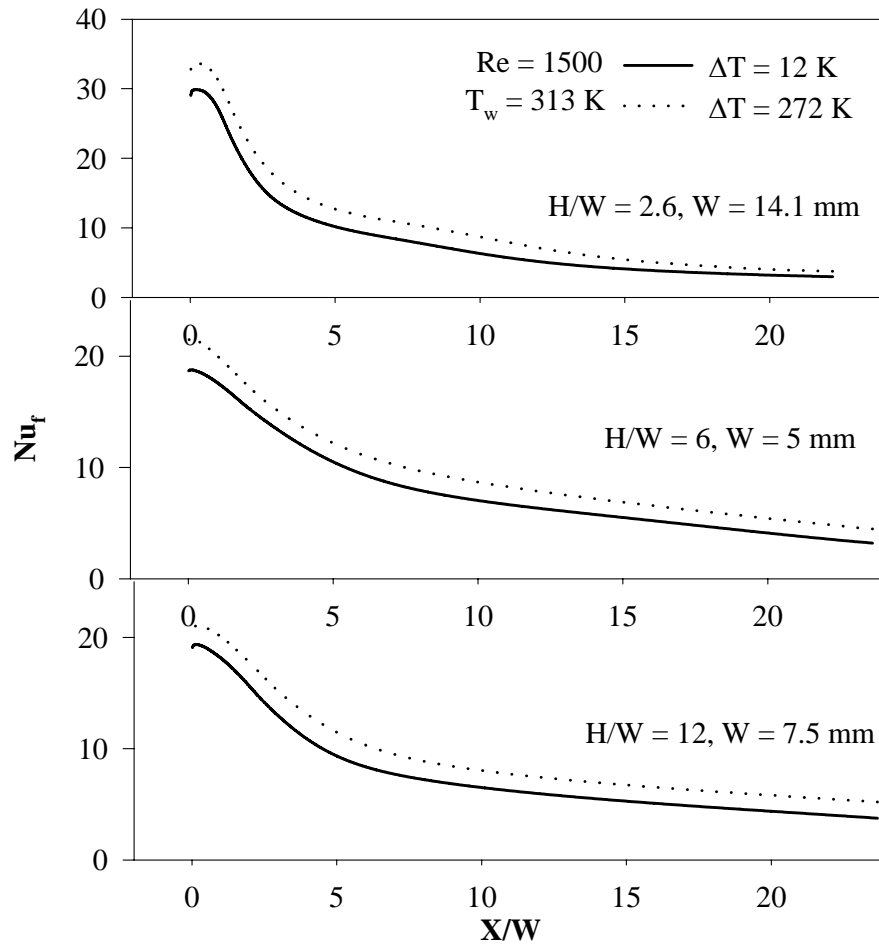


Figure 5.11 Effect of temperature difference between the jet and impingement surface on film Nusselt number for heating condition by the standard k- ϵ model

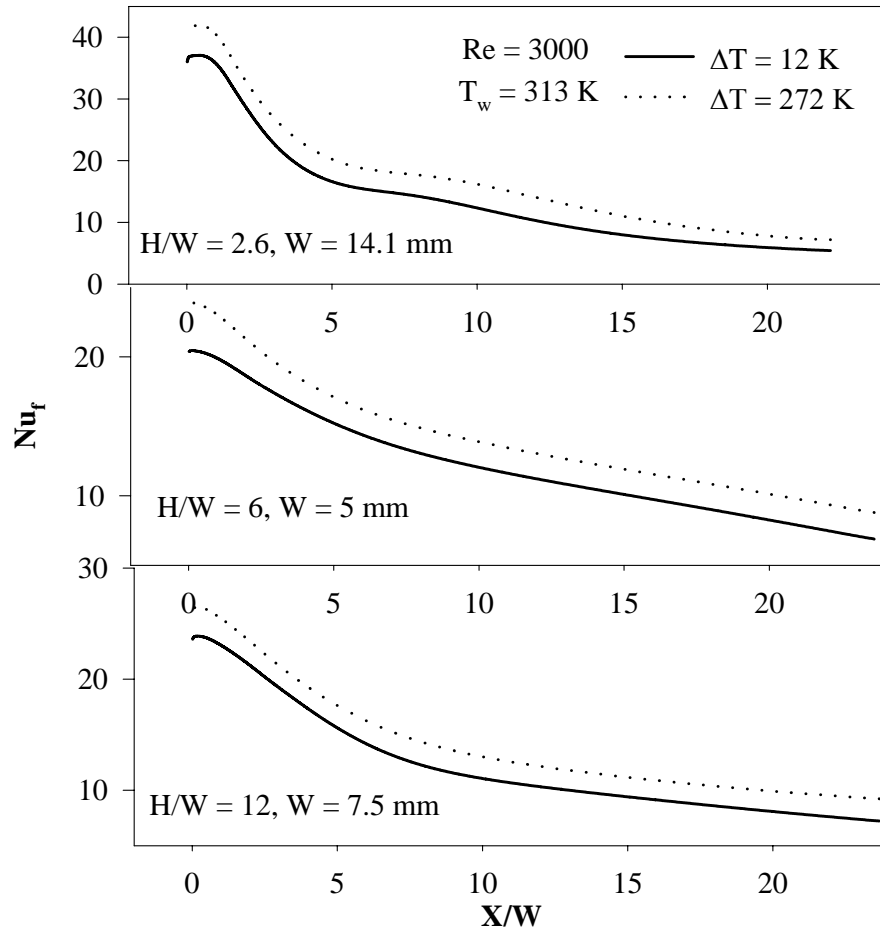


Figure 5.12 Effect of temperature difference between the jet and impingement surface on film Nusselt number for heating condition by the standard k- ϵ model

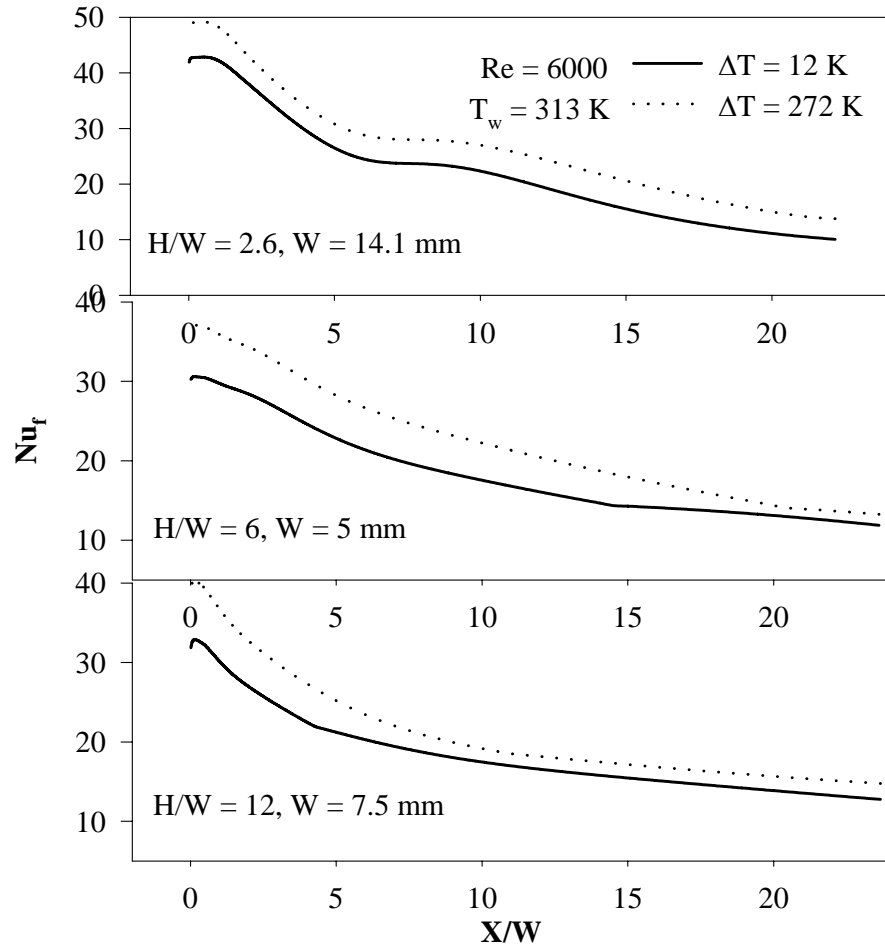


Figure 5.13 Effect of temperature difference between the jet and impingement surface on film Nusselt number for heating condition by the standard k - ϵ model

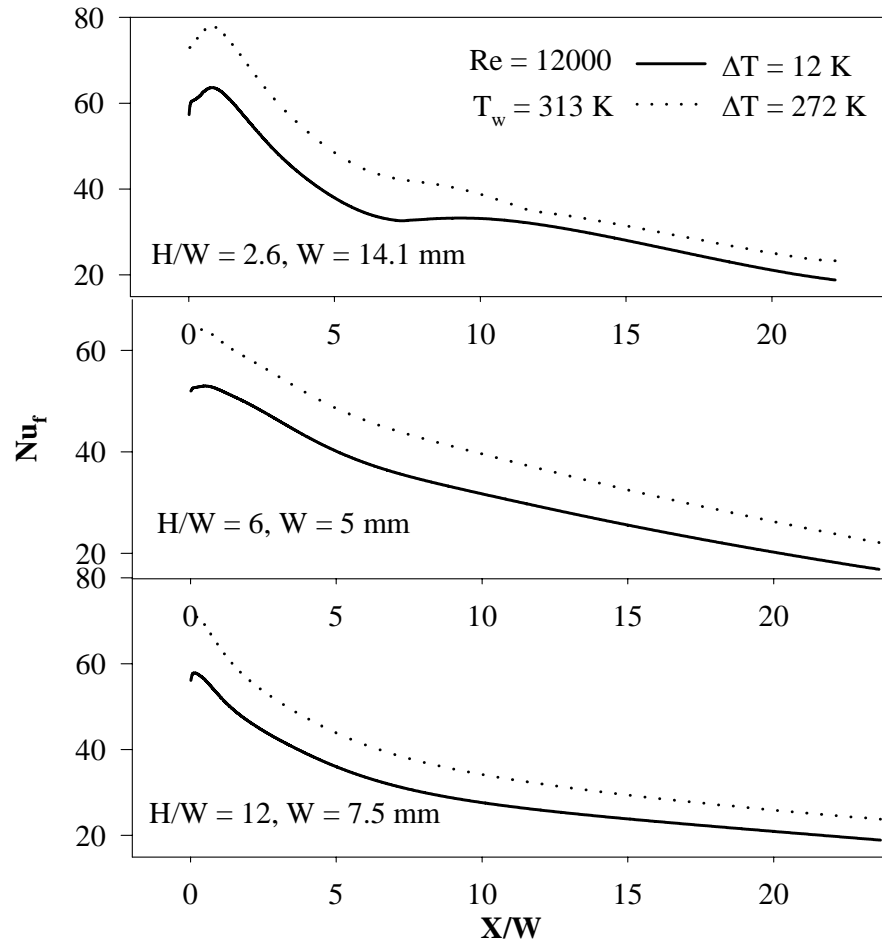


Figure 5.14 Effect of temperature difference between the jet and impingement surface on film Nusselt number for heating condition by the standard k- ϵ model

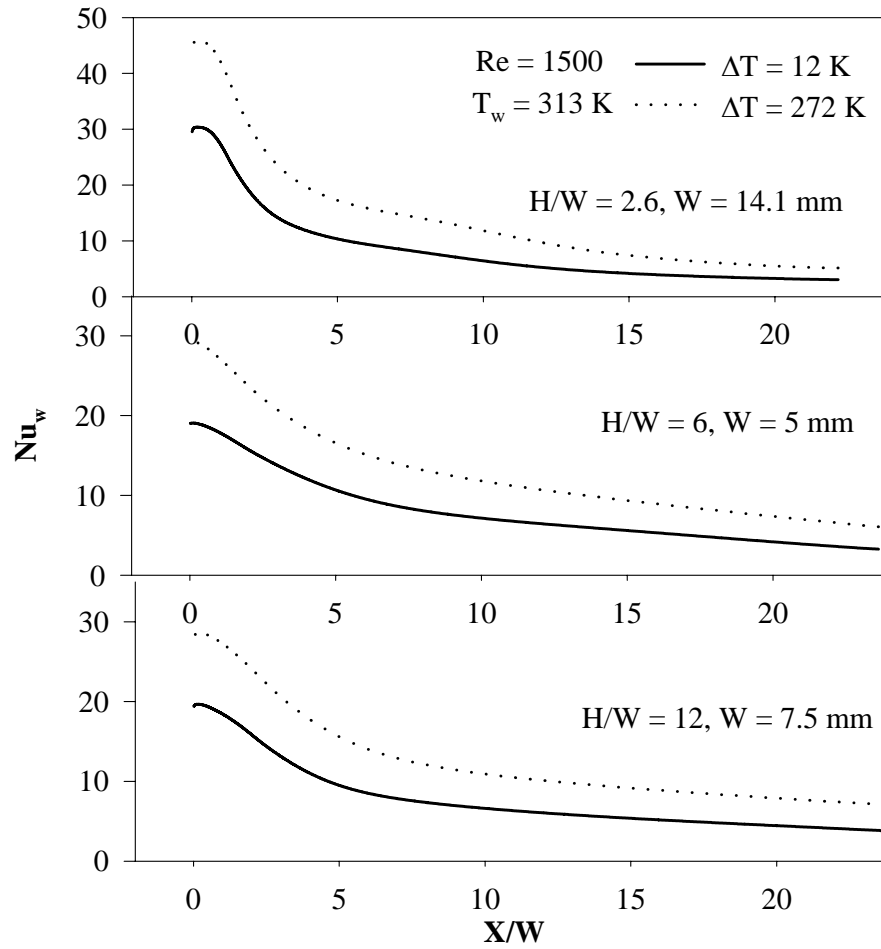


Figure 5.15 Effect of temperature difference between the jet and impingement surface on wall Nusselt number for heating condition by the standard k - ϵ model

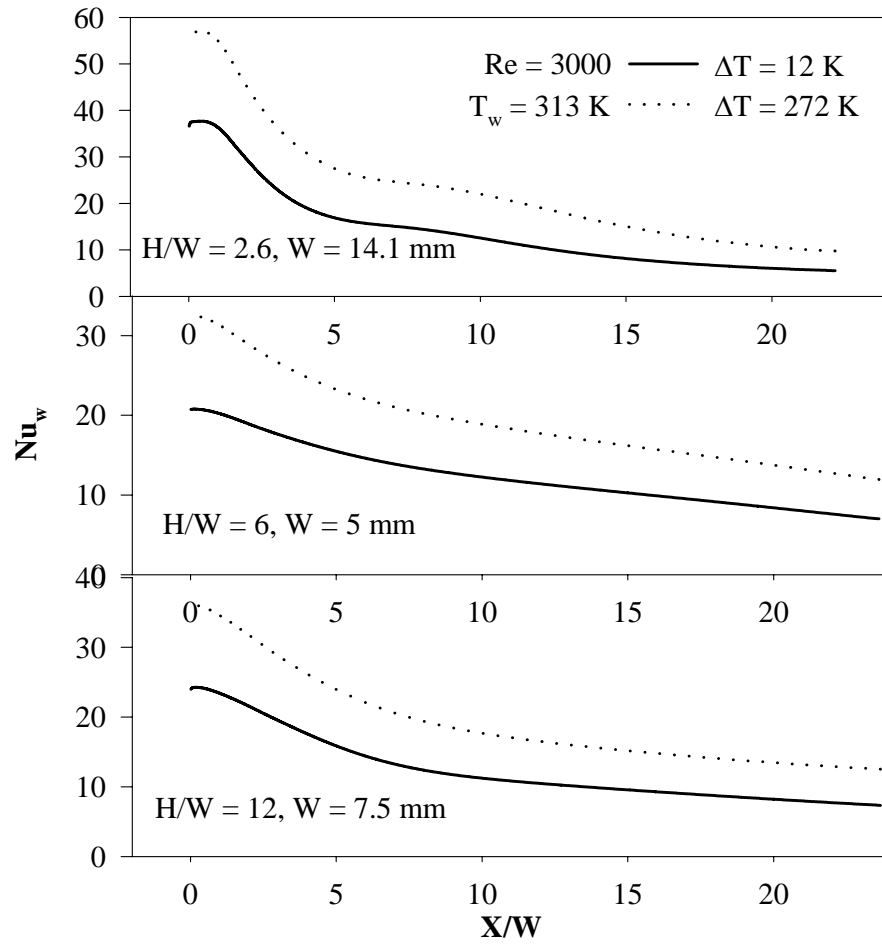


Figure 5.16 Effect of temperature difference between the jet and impingement surface on wall Nusselt number for heating condition by the standard k- ϵ model

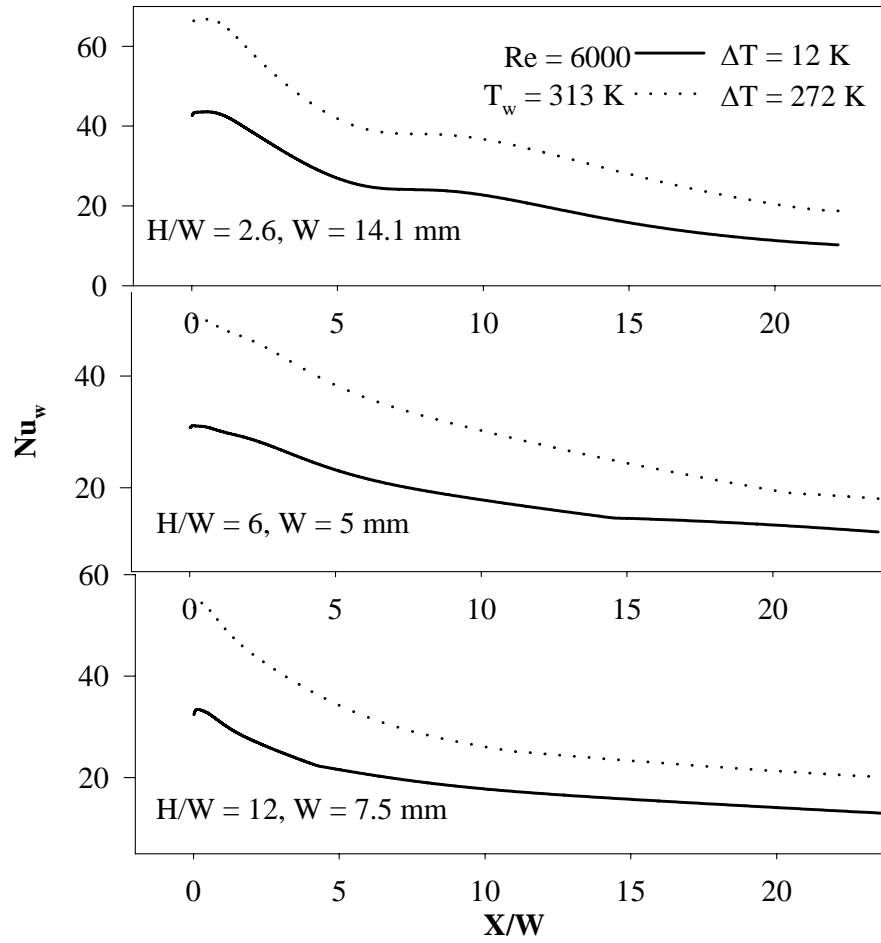


Figure 5.17 Effect of temperature difference between the jet and impingement surface on wall Nusselt number for heating condition by the standard k- ϵ model

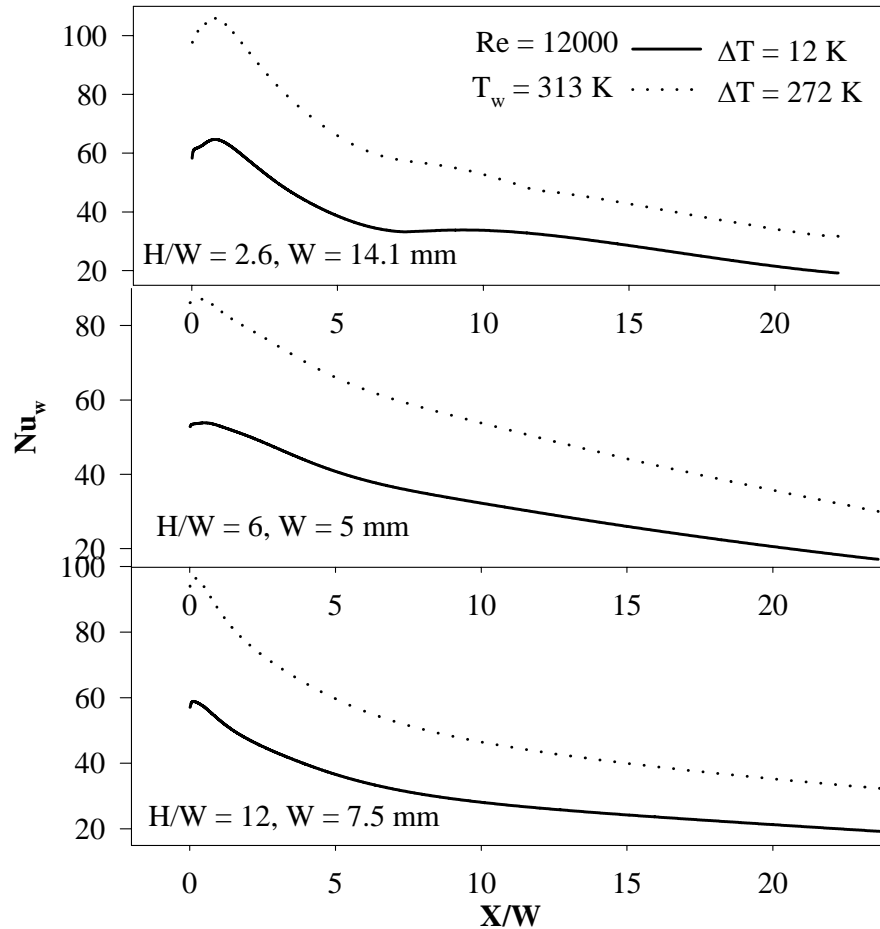


Figure 5.18 Effect of temperature difference between the jet and impingement surface on wall Nusselt number for heating condition by the standard k- ϵ model

All of the above discussion relating to the effect of large temperature differences between the jet and impingement surface on Nusselt number distributions indicates that, under large temperature differences between the jet and impingement surface, the physical properties of the fluid should be defined as temperature-dependent as the large temperature difference between the jet and impingement surface has great effect on film and wall Nusselt number distributions. The Nu_j is the most suitable definition for the Nusselt number distributions in impinging jet heat transfer since it exhibited the least variation under large ΔT compared to those of Nu_f and Nu_w .

5.2.3 Effect of jet Reynolds number on the Nu_{jave} and Nu_{j0}

From the above discussion, we note that the jet Nusselt number is the best among the three definitions (Nu_j , Nu_f and Nu_w) to represent the impinging jet heat transfer, especially for large temperature differences between the jet and the impingement surface due to its least spread with the increase of ΔT . Usually, the dependence of the average Nusselt number and Reynolds number can be expressed as $Nu_{ave} = A Re^B$. Based on the above study, we investigated the effect of jet Reynolds number on the average jet Nusselt number, Nu_{jave} and the stagnation jet Nusselt number, Nu_{j0} .

Figures 5.19 and 5.20 show the effect of jet Reynolds number on Nu_{jave} and Nu_{j0} , respectively, for the nozzle-to-target spacing equals 2.6, 6 and 12 by the standard k- ϵ model. The relationships between the jet Nusselt number and Re over a range of $X/W = 0 - 20$ were $Nu_{jave} = 1.502 Re^{0.654}$, $Nu_{j0} = 0.943 Re^{0.697}$ and $Nu_{jave} = 1.382 Re^{0.649}$ with the correlation coefficients, $R^2 = 0.999, 0.993$ and 0.998 for $H/W = 2.6, 6$ and 12 , respectively (Figure 20). The majority of the studies reported “b” values ranging from 0.5 to 0.8. For example, Saad (1981) found that the exponent “b” was constant at a value 0.65 for all practical purposes and Martin (1977) reported it to be 0.67.

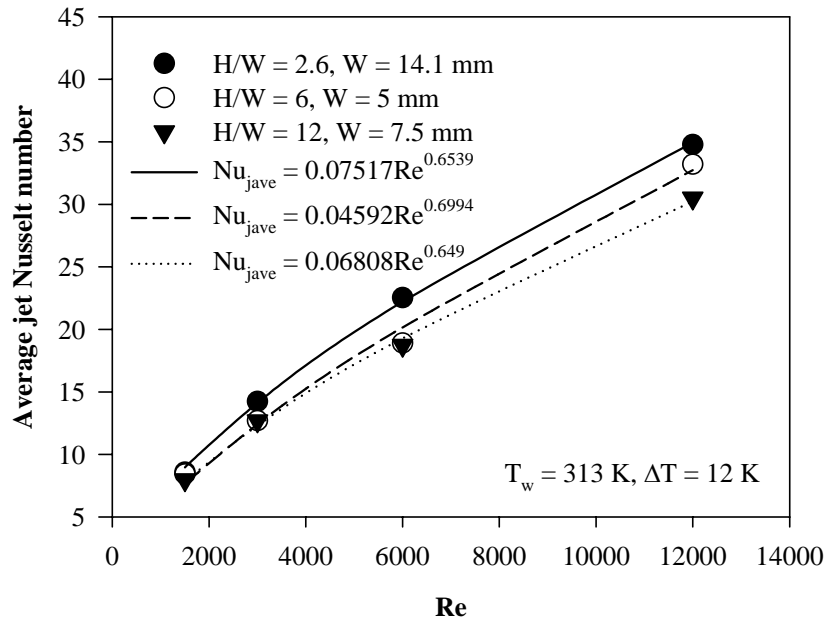


Figure 5.19 Effect of jet Reynolds number on average jet Nusselt number for heating predicted by the standard k- ϵ model

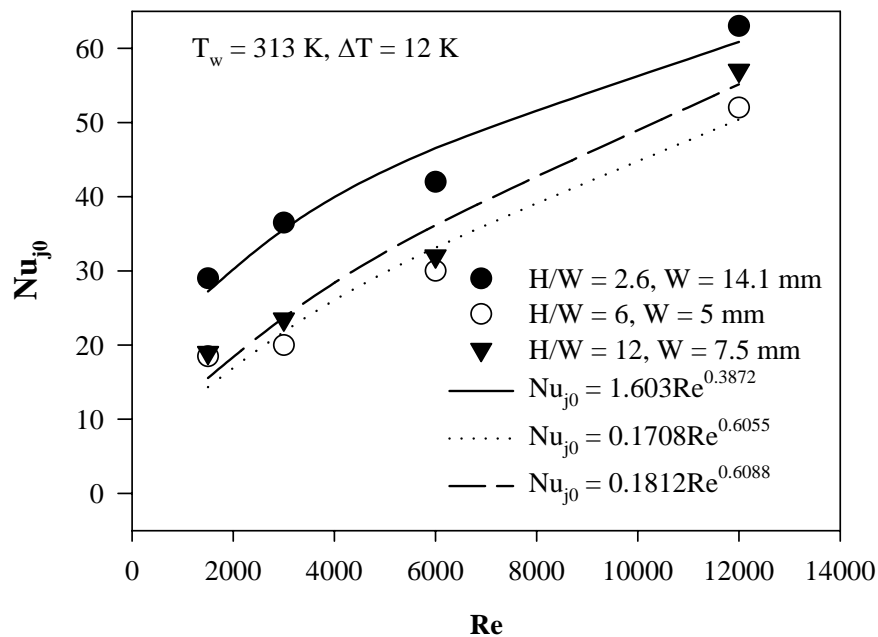


Figure 5.20 Effect of jet Reynolds number on stagnation jet Nusselt number for heating predicted by the standard k- ϵ model

Finally, an empirical correlation of form $Nu_{j0} = ARe^B$ was developed based on the CFD predictions. The exponent values of the correlations were 0.3872 for $H/W = 2.6$, 0.6055 for $H/W = 6$ and 0.6088 for $H/W = 12$ predicted by the standard k- ϵ model, as shown in Figure 5.21. In Chapter 4 we had seen that for small nozzle-to-target spacing

$H/W = 2.6$, the standard $k-\varepsilon$ model over predicted the stagnation Nusselt number, while for large nozzle-to-target spacing, $H/W = 12$, the standard $k-\varepsilon$ model under predicted the heat transfer coefficient at the stagnation point and when $H/W = 6$, the deviation of the numerical stagnation Nusselt number from the experimental stagnation Nusselt number was quite small. Hence, the correlation $Nu_{j0} = 0.1708Re^{0.6055}$, for $H/W = 6$, could be more accurate than the other two correlations. That means that the exponent value of 0.6 should be quite reasonable. But these exponents have been evaluated only with 4 points, so they are subject to uncertainty. The slope of 0.5 in stagnation point had been widely cited in the literature (Lytle & Webb (1994) and Lee et al. (1995)).

5.3 Conclusions

Results of the CFD modelling of turbulent impinging jets show that large temperature differences between the jet and the impingement surface lead to significant differences in the heat transfer coefficients. Small temperature differences (e.g. up to 50 K) show only minor differences between the local Nusselt numbers calculated using thermal conductivity values at the jet, film or wall temperatures. However, large temperature differences (over 100 K) can result in significant differences between the three possible definitions of the Nusselt numbers. This is true for both heating and cooling conditions with impinging jets. It is shown that use of the jet temperature as the reference temperature for the calculation of the Nusselt numbers shows the least spread. This result allows the designer to use previously published correlations, which are obtained at small temperature differences between the jet and the impingement surface. This conclusion is valid regardless of the jet Reynolds number and nozzle-to-surface spacing. Also, the same conclusion is drawn from the use of the standard $k-\varepsilon$ as

well as the Reynolds stress models of turbulence. Finally, empirical correlations are provided for the average and stagnation jet Nusselt numbers under a semi-confined turbulent slot jet based on the numerical results. The exponent values in the above two correlations based on CFD models are comparable with the values reported in literature which are based on experimental data.

Chapter 6

Effects of Pr on impinging jet heat transfer under a slot jet

6.1 Introduction

Despite the extensive literature dealing with impinging jet heat transfer, little attention has been directed at the effect of fluid Prandtl number. Almost without exception, earlier studies, both experimental and numerical, deal with air or water as the jet fluids. In this chapter, we carry out numerical experiments to examine the effect of different thermal properties of the fluid (gas or liquid phase) on heat transfer and to correlate the effect of the fluid Prandtl number on heat transfer under a semi-confined impinging slot jet. Both laminar and turbulent flows were studied. New results are presented for different gases viz. air, argon, nitrogen, hydrogen, helium, ammonia and ethylene and several liquids viz. water, benzene, ethanol, turpentine and iso-butyl alcohol. Local, stagnation and average values of the impingement Nusselt number as well as the heat transfer coefficient were reported by FLUENT 5. The configuration of the impinging slot jet was that shown in Chapter 1. Empirical correlations are derived for the stagnation and average Nusselt numbers as a function of the fluid Prandtl number on the basis of extensive numerical experiments. The average Nusselt number is given by

$$Nu_{ave} = \frac{1}{L} \int_0^L Nu(x) dx, \text{ where } L \text{ is the length of the impingement surface.}$$

6.2 Results and Discussion

The fluids Prandtl number studied in this chapter varied from 0.67-71. Table 6.1 lists the properties of all the fluids investigated here. The results are presented as surface heat transfer coefficient as well as the corresponding Nusselt number distribution in the stream-wise direction. For liquids, the temperature of the impinged surface was well below the fluid boiling point.

Table 6.1 Thermal properties of fluids studied here at $T = 300$ K

No.	Materials	λ (W/m K)	C_p (J/kg K)	Pr
1	Argon (Ar), gas	0.0176	521	0.68
2	Nitrogen (N ₂), gas	0.0267	1043	0.69
3	Ammonia (NH ₃), gas	0.0246	2200	0.90
4	Hydrogen (H ₂), gas	0.1980	14780	0.67
5	Helium (He), gas	0.1490	5200	0.70
6	Air, gas	0.0267	1005	0.69
7	Ethylene (C ₂ H ₂), gas	0.0209	2229	1.10
8	Water (H ₂ O), liquid	0.6098	4181	6.00
9	Benzene (C ₆ H ₆), liquid	0.1439	1735	7.00
10	Ethanol (C ₂ H ₅ OH), liquid	0.1676	2474	15.00
11	Turpentine (C ₁₀ H ₁₆), liquid	0.1260	1800	21.20
12	Iso-butyl alcohol (C ₄ H ₁₀ O), liquid	0.1260	2313	71.10

6.2.1 Laminar flow

6.2.1.1 Effect of fluid Prandtl number on heat transfer rates

The local and average Nusselt numbers and surface heat transfer coefficients were investigated numerically as a function of fluid Prandtl number over the range of 0.7-71 for $H/W = 6$ and $Re = 100$. The effect of the Prandtl number on local Nusselt number distributions can be seen from Figure 6.1. As expected, the Nusselt number increases

with increase of Pr from 0.7 to 71, with the notable exception of air. Although the Prandtl number of air ($Pr = 0.69$) is lower than that of ethylene (gas, $Pr = 1.1$), the Nusselt number for air is found to be consistently greater than that for ethylene. One possible reason for this is that the fluid Prandtl number is not sufficient to account fully for the heat transfer rate distributions. A second peak value was found for laminar flow when fluid Prandtl number was greater than 1.1. Moreover, with the increase of the fluid Prandtl number, the second peak value of Nusselt number becomes predominant.

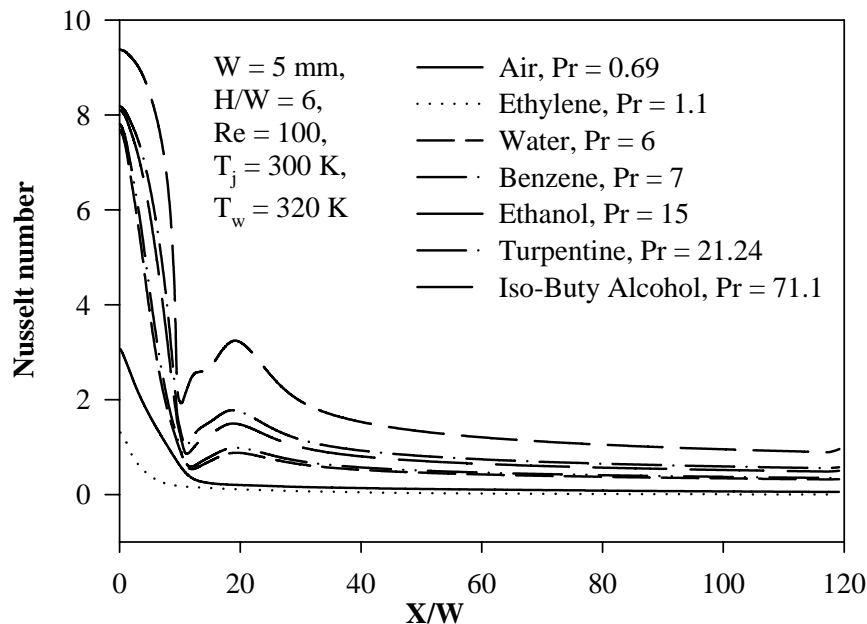


Figure 6.1 Effect of Pr number on the local Nusselt number distributions for laminar flow

The distributions of the computed heat transfer coefficients are shown in Figure 6.2. For all fluids the maximum values of the heat transfer coefficients are located in the impingement region, the minimum values occur at the exit and the second peak value of heat transfer rate occurs only when fluid Prandtl number is greater than 1.1. However, the surface heat transfer coefficients do not increase with increase of the fluid Prandtl number. In Figure 6.2, we find that the surface convective heat transfer coefficient for the liquid water jet is much higher than those of other fluids studied

here. The stagnation point heat transfer coefficient for the water jet is 50 times greater than that for air. Thermal conductivity of water is much higher than those of other fluids, as shown in Table 6.1. Higher thermal conductivity improves heat transfer in the boundary layer and therefore results in a higher heat transfer rate.

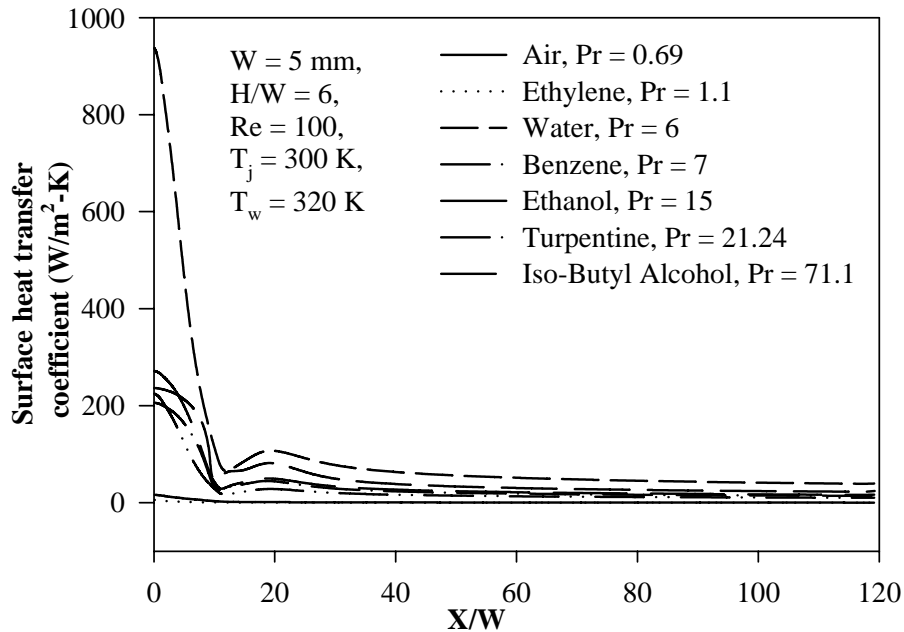


Figure 6.2 Effect of Pr number on surface heat transfer coefficient distributions for laminar flow

Figures 6.3 and 6.4 show the distributions of the local Nusselt number and surface heat transfer coefficient of 5 different gases with similar fluid Prandtl number (0.9 for NH₃ and about 0.7 for others), respectively. As expected, the local Nusselt number distributions of the gases with similar Prandtl number are quite similar, as shown in Figure 6.3. However, much greater differences in the predicted surface heat transfer coefficients were noticed among the gases. From the Figure 6.4, it can be seen that the surface heat transfer coefficient distributions for air, argon and ammonia are similar, while the surface heat transfer coefficients for hydrogen and helium are much greater than those for other gases. The stagnation point heat transfer coefficient for the hydrogen jet is about 7 times greater than those for air, argon, nitrogen and ammonia.

As seen in the earlier section, thermal conductivity values of hydrogen and helium are much higher than those of the other gases tested here, Table 6.1.

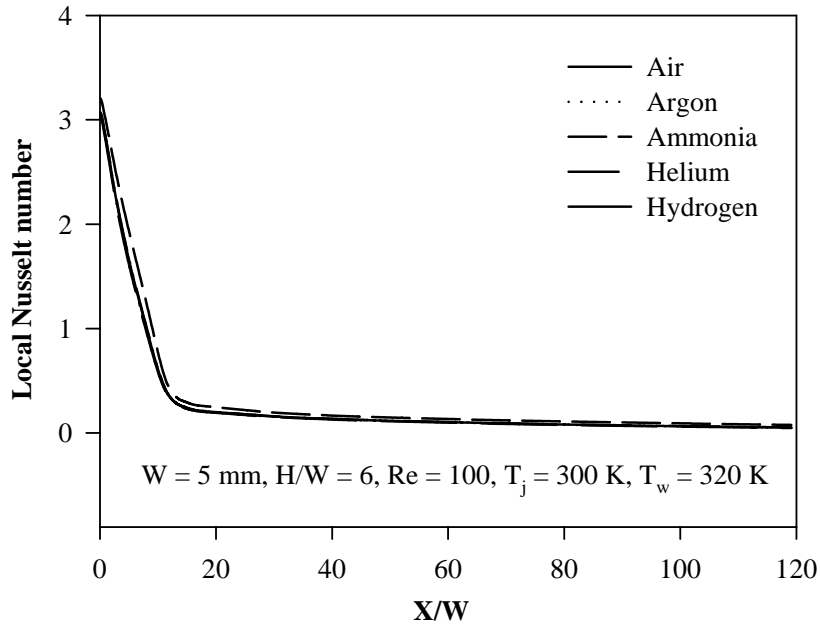


Figure 6.3 Local Nu distributions for gases with similar fluid Pr number for laminar flow

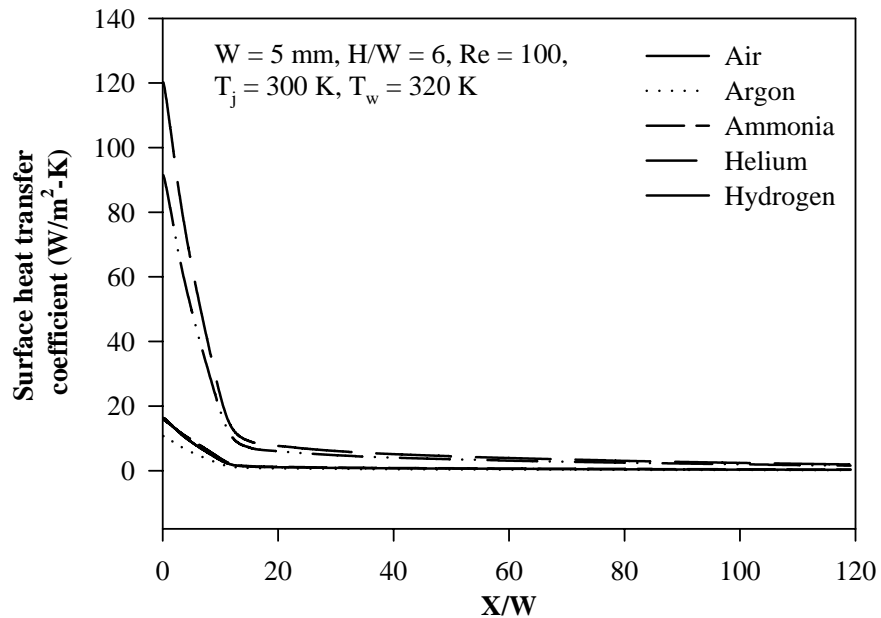


Figure 6.4 Heat transfer coefficient distributions for gases with similar fluid Pr number for laminar flow

6.2.1.2 Correlations between Prandtl number and Nusselt number

Based on the numerical results obtained over a wide range of fluid physical thermo properties, empirical correlations were obtained for the stagnation and average Nusselt numbers in a semi-confined laminar slot impinging jet. Heat transfer correlations by regression analysis of numerical results of 11 test fluids (except the N₂) (Pr = 0.67 – 71.1) were developed.

The left and right axes of Figure 6.5 show the best-fit correlations for the stagnation Nusselt number and the average Nusselt number, respectively. The relations between stagnation and average Nusselt numbers and the fluid Prandtl number can be expressed as $Nu_0 = A Pr^b$ and $Nu_{ave} = A' Pr^{b'}$, respectively. The correlations between Nu_{ave} and Pr were conducted over a range of $X/W = 0 - 60$. Our simulation results showed that the values of R^2 for the correlations of Nu_0 and Nu_{ave} were 0.81 and 0.97, respectively. The exponent values of Nu_0 and Nu_{ave} were 0.2512 and 0.4095, respectively. Bejan's scaling analysis (Bejan (1995)) shows that, for laminar boundary layers flow $Nu \propto Pr^{1/2}$ for fluids ($Pr \ll 1$) and $Nu \propto Pr^{1/3}$ for fluids ($Pr \gg 1$). Figure 6.5 also indicated that the fluid Prandtl number alone does not fully correlate the Nu data, perhaps the Prandtl number exponent should not be taken as a constant. Additional studies are needed to resolve this issue.

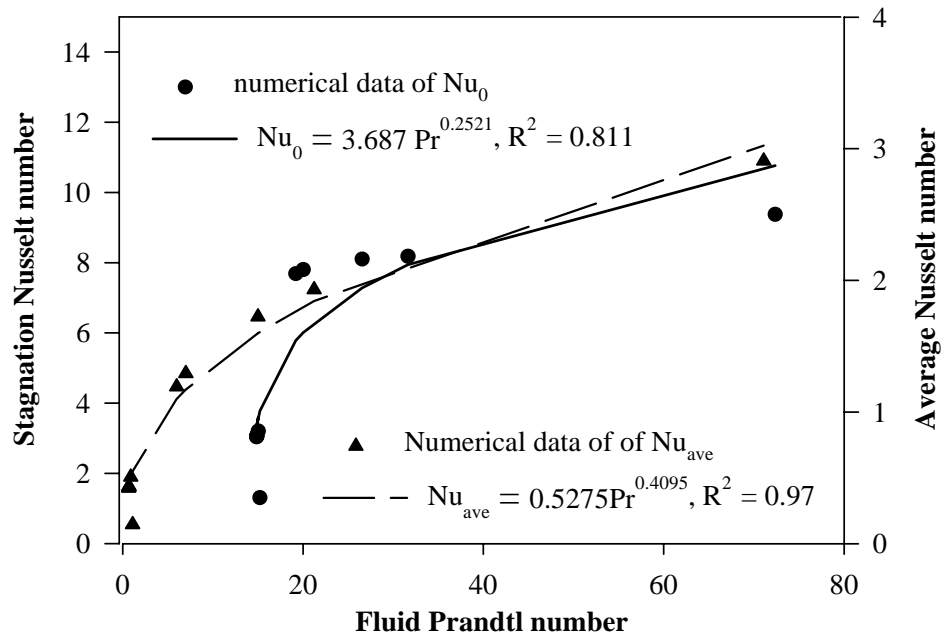


Figure 6.5 Effect of Pr number on stagnation and average Nusselt numbers for laminar flow

6.2.2 Turbulent flow

6.2.2.1 Effect of fluid Prandtl number on heat transfer rates

The effect of Prandtl number on local Nusselt number distributions for turbulent flow predicted using the standard $k-\varepsilon$ model is shown in Figure 6.6. Similar to the corresponding results for laminar flow, the Nusselt number increases with the increase of Pr from 0.7 to 71, with the noticeable exception of air. Although the Prandtl number of air is lower than that of ethylene, the Nusselt number for air is found to be consistently greater than that for ethylene. Moreover, with the increase of fluid Prandtl number, the location of the maximum Nusselt number shifted from the stagnation point (e.g. air) in the downstream direction; the Nusselt number then decreases monotonically from the peak towards the exit. For example, for the iso-butyl alcohol jet, the maximum Nusselt number is located at $X/W = 2.3$. That is a notable difference from the laminar flow case, where two peak values of Nusselt number occurred. The differences in Nusselt number distributions among the different fluids are the largest in

the impingement region and are the smallest in the exit region of the wall jet of the channel.

The distributions of the computed surface heat transfer coefficients are shown in Figure 6.7. As noted earlier, for all fluids the maximum values of the surface heat transfer coefficients are located in the impingement region and the minimum values occur in the exit of section. However, the surface heat transfer coefficients do not increase with increase of the fluid Prandtl number. In Figure 6.7, we find that the surface heat transfer coefficient for the water jet is much higher than those of other fluids studied here. The stagnation point heat transfer coefficient for the water jet is 17 times greater than that for air. In our previous study of laminar impinging jets, the stagnation point heat transfer coefficient for the water jet was 50 times greater than that for air. Li and Garimella (2001) also showed that the stagnation heat transfer coefficient for water jet was 3.7 times higher than that for the FC-77 jet ($Pr = 25$). The reason for this observation is the same as that for laminar flow. It is that the thermal conductivity of water is much higher than those of the other fluids. Higher thermal conductivity improves heat transfer in the boundary layer and therefore results in a higher heat transfer rate.

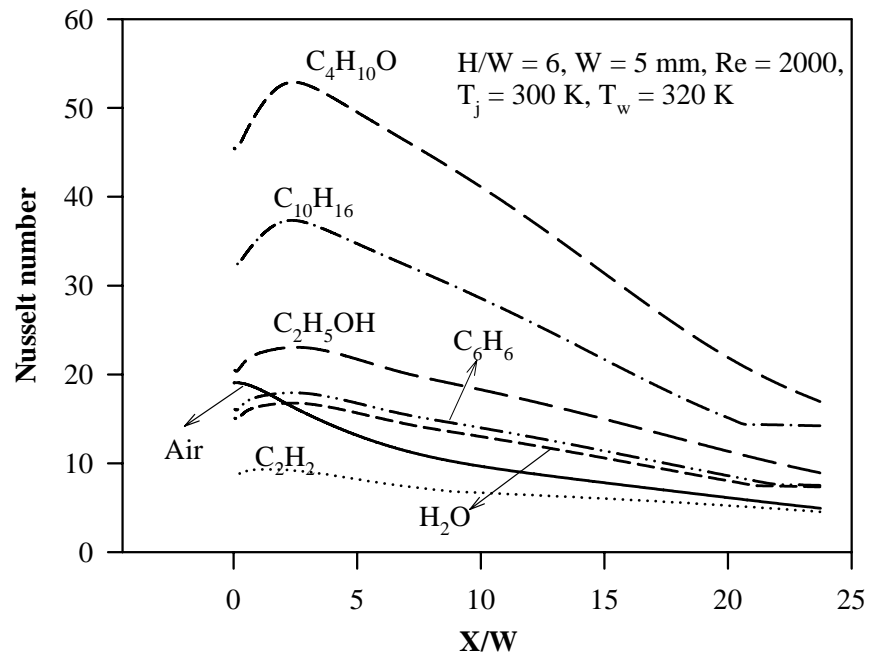


Figure 6.6 Effect of Pr number on Nusselt number distributions for turbulent flow

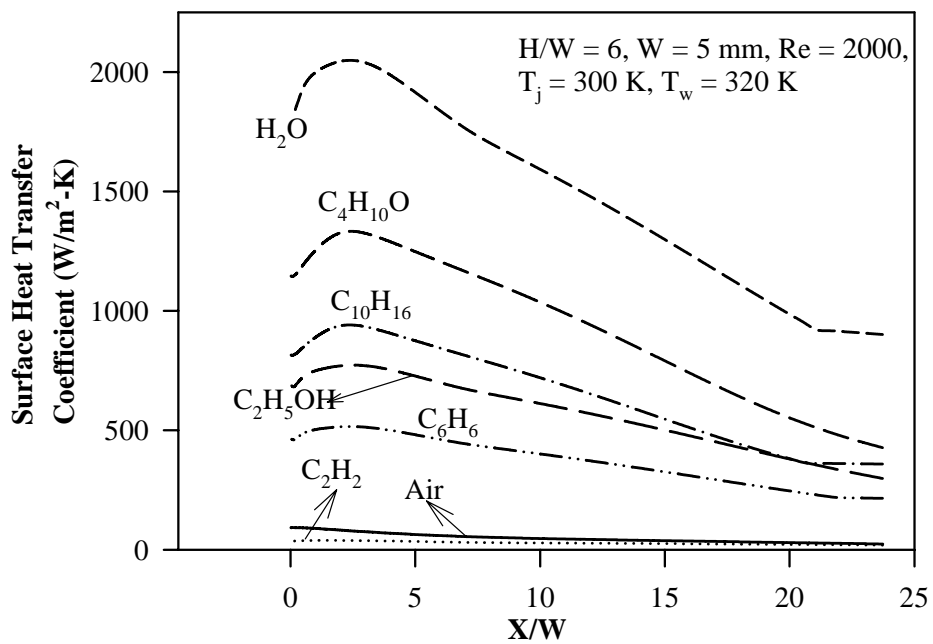


Figure 6.7 Effect of Pr number on surface heat transfer coefficient distributions for turbulent flow

Distributions of the local Nusselt number and surface heat transfer coefficient for jet of 6 different gases with similar fluid Prandtl number (0.9 for NH_3 and about 0.7 for others) for turbulent flow are shown in the Figures 6.8 and 6.9, respectively. Similar to

the results in our previous study of laminar jets, gases with similar Prandtl number in turbulent flow produce similar values of the local Nusselt number. At the stagnation point, the largest difference among the predicted Nusselt number was only about 15%. However, much greater differences in the predicted surface heat transfer coefficients were noticed among the gases. From the Figure 6.9, it can be seen that the surface heat transfer coefficient distributions for air, argon, nitrogen and ammonia are similar, while the surface heat transfer coefficients for hydrogen and helium are much greater than those for other gases. The stagnation point heat transfer coefficient for the hydrogen jet is 5.5 times greater than that for air, argon, nitrogen and ammonia. In our previous study of laminar flow, this factor was 7. As seen in the earlier section, thermal conductivity values of hydrogen and helium are much higher than those of the other gases tested here, shown in Table 6.1.

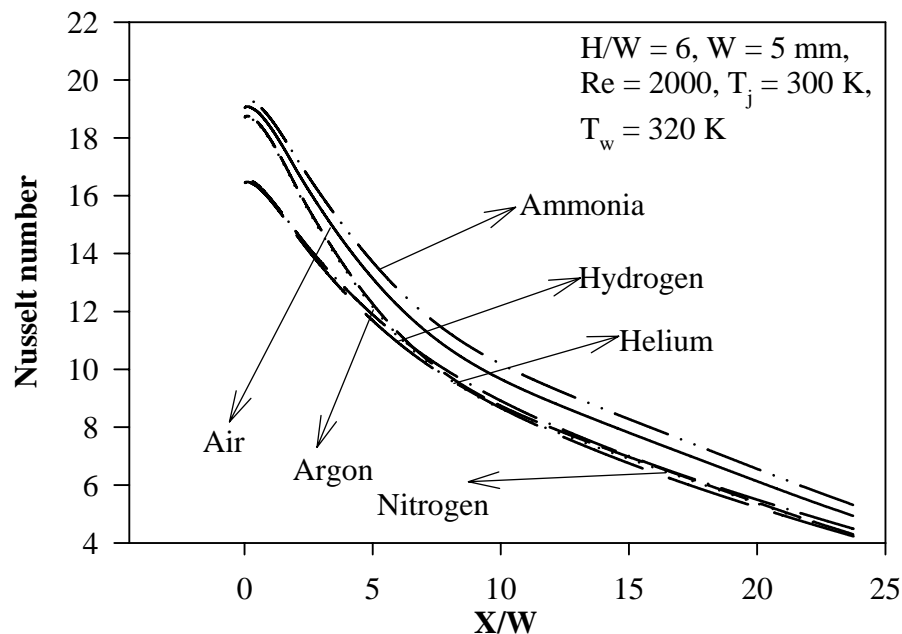


Figure 6.8 Local Nusselt number distributions of different gases with similar fluid Prandtl number predicted by the standard $k-\epsilon$ model

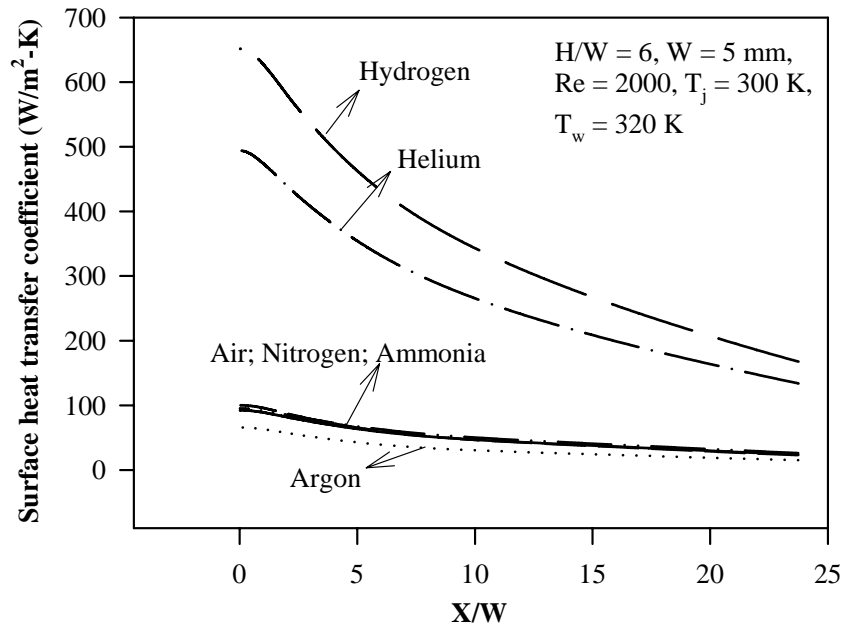


Figure 6.9 Surface heat transfer coefficient distributions of different gases with similar fluid Prandtl number for turbulent flow

6.2.2.2 Correlations between Prandtl number and Nusselt number

Based on the numerical results obtained over a wide range of fluid thermo physical properties, empirical correlations are obtained for the stagnation and average Nusselt numbers in a semi-confined turbulent slot impinging jet. The heat transfer correlations by regression analysis of numerical results using 3 different databases were compared. The correlations were first developed for all 12 fluids tested here ($Pr = 0.67 - 71.1$). For the next sets of data for regression, we separated the database into two sets: one consisting of 6 gases ($Pr < 1$) and the other for 6 fluids ($Pr > 1$). Note that only for $Pr = 1$, the thermal and velocity boundary layers coincide.

The left and right axes of Figure 6.10 show the best-fit correlations for the stagnation Nusselt number and the average Nusselt number, respectively. The relations between stagnation and average Nusselt numbers and the fluid Prandtl number can be expressed as $Nu_0 = A Pr^b$ and $Nu_{ave} = A' Pr^{b'}$, respectively. The correlations between Nu_0 and Pr

as well as Nu_{ave} and Pr over a range of $X/W = 0 - 20$ are summarized in Table 6.2 for the data sets of all test fluids and 6 fluids ($Pr > 1$). The correlations of Nu_0 and Nu_{ave} for 6 gases ($Pr < 1$) are not listed in Table 6.2. The database of the 6 gases ($Pr < 1$) is not suitable for regression since the 6 gases have quite similar Prandtl numbers (about 0.7), which results in very high relative error in regression.

Table 6.2 Stagnation and average Nusselt number correlations

Materials	Correlations (Nu_0)	R^2	Correlations (Nu_{ave})	R^2
12 fluids	$Nu_0 = 15.39 Pr^{0.215}$	0.63	$Nu_{ave} = 8.56 Pr^{0.351}$	0.93
6 fluids ($Pr > 1$)	$Nu_0 = 6.173 Pr^{0.4408}$	0.97	$Nu_{ave} = 7.393 Pr^{0.4275}$	0.95

Our simulation results showed that the values of R^2 for the correlations of Nu_0 and Nu_{ave} for 6 gases ($Pr < 1$) were as low as 0.2 and 0.32, respectively. By comparing the numerical results in Table 6.2 with the published experimental data of Li and Garimella (2001), we find that the exponents of Prandtl number for the 6 fluids ($Pr > 1$) are comparable with the published data. Li and Garimella (2001) reported the Prandtl number exponents to be 0.444 and 0.441 for stagnation Nusselt and average Nusselt numbers, respectively. From Table 6.2, we find that the R^2 of the correlations for both Nu_0 and Nu_{ave} for 12 fluids are lower than those for the 6 fluids ($Pr > 1$) jets. According to Bejan's scale analysis (Bejan (1995)), the Nusselt number depends on Pr number with different exponent values for low Prandtl number fluids ($Pr \ll 1$) and high Prandtl number fluids ($Pr \gg 1$). As mentioned in previous part, Bejan's scale analysis shows that, for laminar boundary layers flow $Nu \propto Pr^{1/2}$ for fluids ($Pr \ll 1$)

and $Nu \propto Pr^{1/3}$ for fluids ($Pr \gg 1$). Thus, it is reasonable to obtain separate correlations for high and low Prandtl number fluids.

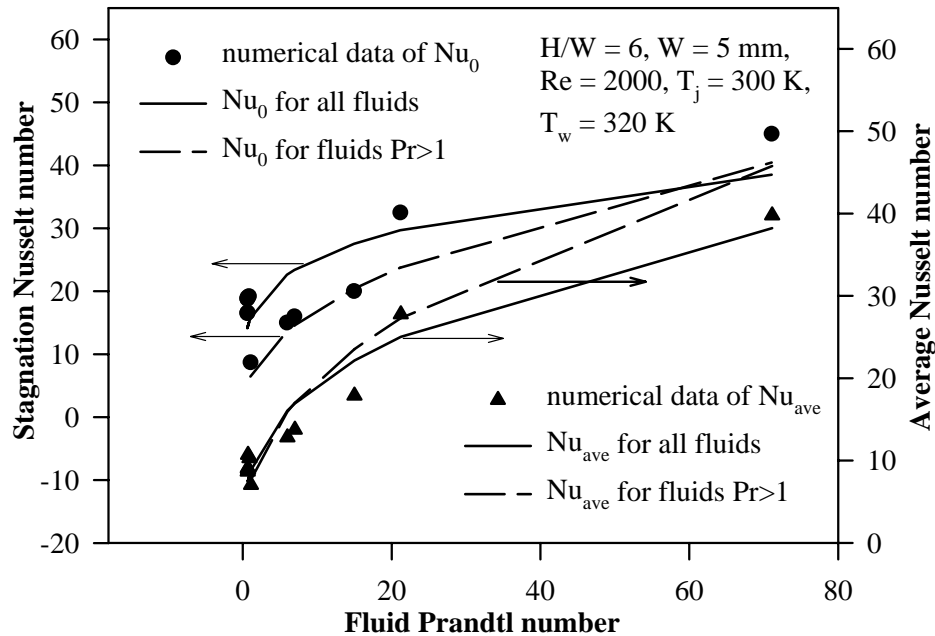


Figure 6.10 Effect of Prandtl number on stagnation and average Nusselt number for turbulent flow

6.3 Conclusions

The local and average Nusselt numbers and surface heat transfer coefficients on a semi-confined laminar and turbulent slot impinging jets were investigated numerically as a function of fluid Prandtl number over the range of 0.7-71. The variations of Nusselt number for all the test fluids are similar to those for air. The Nusselt number increases with increase of fluid Pr number from 0.7 to 71. For laminar flow, when fluid Prandtl number is higher than 1.1, there are two peak values in the local Nusselt number distributions for $H/W = 6$; the second peak value of Nusselt number becomes predominant with increase of the Prandtl number. On the contrary, for turbulent flow, there is only one peak value of Nusselt number for the fluids studied here and with the

increase of fluid Prandtl number, the location of the maximum Nusselt number shifted from the stagnation point (e.g. air) in the downstream direction. Gases with similar Prandtl number exhibit similar values of Nusselt number, but different values of the surface heat transfer coefficient for both laminar and turbulent flows due to their widely different thermal conductivity. Predictive correlations are proposed for the effect of Prandtl number on the stagnation and average Nusselt numbers.

Chapter 7

Effect of cross flow on turbulent flow and heat transfer characteristics under normal and oblique semi-confined impinging slot jets

7.1 Introduction

Impinging jets are commonly used in industrial dryers and electronics chip cooling. Since in industrial practice it is necessary to use multiple jets, the interaction between jets can have important effect on their heat transfer performance. Hence, the study of cross-flow caused by the spent flow of upstream jets is obviously significant. Despite their practical implications, the normal and oblique impinging jets in cross flow have received very little attention both experimentally and numerically. Few researchers have studied the effect of cross-flow as well as jet inclination angles on slot jet impingement flow and heat transfer behavior. The effect of cross-flow on Nusselt number distributions has important significance in practice and much experimental and modeling work is needed for efficient design of the multiple impinging jet heat transfer devices by accounting for the adverse effects of the cross-flow.

In this chapter, flow and heat transfer characteristics for a single semi-confined turbulent slot jet of air impinging normally or obliquely into an imposed air cross-flow of the same or different temperature are simulated by FLUENT 5. The standard k - ϵ and the Reynolds stress models were used as before. Effects of the various flow parameters (e.g. jet-to-cross-flow mass ratio) and geometric parameters (e.g. nozzle-to-target spacing and jet angle) were evaluated at a fixed Reynolds number for equal and unequal temperatures of the jet and cross-flow. These models are selected mainly due

to their earlier applications and good performance for prediction of flow and heat transfer in impingement heat transfer in the presence of cross-flow (Kalita et al. (2002)), and also due to our past experience with these models (chapter 4).

7.2 Results and Discussion

In this work, because the computational domain is asymmetric, the simulation is conducted over the whole domain. Grid-independence tests were conducted for each case. The flow domain simulated is shown in Figure 7.1. The following boundary conditions were applied: i) the impingement surface was specified as an isothermal wall, ii) the confinement surface was considered to be an adiabatic wall, iii) the jet inlet and cross-flow inlet were considered as velocity inlets with uniform velocities, and iv) the outlets were considered as fully developed outflow. The values of 2 and 4.5 percent were chosen arbitrarily for the turbulence intensity for jet inlet and cross-flow inlet, respectively. The turbulence length scale at the inlets for all the calculations was defined to be equal to 0.07 times the respective hydraulic diameter. The turbulence intensity at the boundary is expected to have negligible effect on the impingement heat transfer in the region of interest. As correct velocity field description is essential for the accurate prediction of the temperature field, in this chapter, the flow patterns are discussed first; subsequently heat transfer results will be discussed.

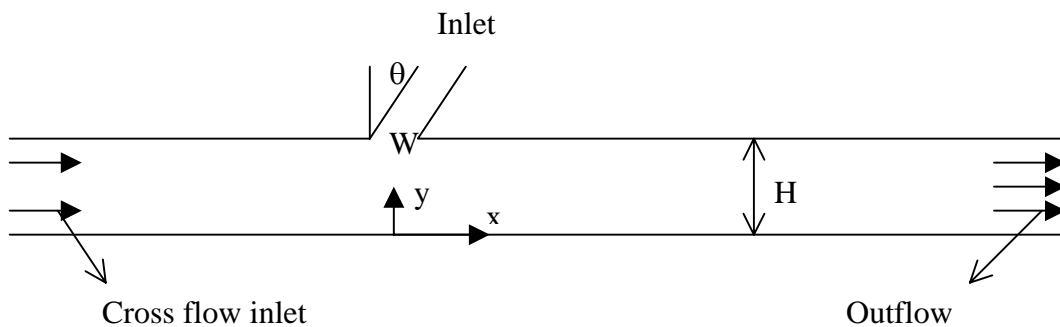


Figure 7.1 Flow geometry of the impinging slot jet with cross-flow

7.2.1 Effect of cross flow and jet angles on flow pattern

In this work, four cross-flow mass ratios ($M = 0, 0.05, 0.25$ and 1), four jet angles ($\theta = -30^\circ, -15^\circ, 15^\circ$ and 30°) and two nozzle-to-target spacings ($H/W = 2.6$ and $H/W = 8$) were simulated by both the standard $k-\varepsilon$ and RSM turbulence models. In this part, for brevity, we only show the streamline contour results for $M = 0.05$ and 1 ; $\theta = -30^\circ$ and 30° . Also, because of the small differences in the streamline contour predictions by the standard $k-\varepsilon$ model and the RSM model, we only show the streamline contours predicted by the standard $k-\varepsilon$ model in this section.

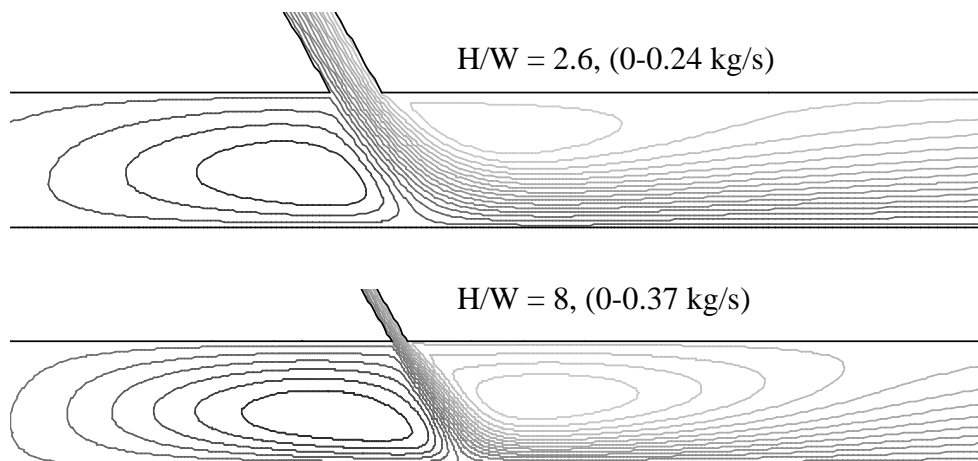


Figure 7.2 Streamline contours for $\theta = -30^\circ$ for two structures under small cross flow value, $M = 0.05$ (two figures are not under same scale)

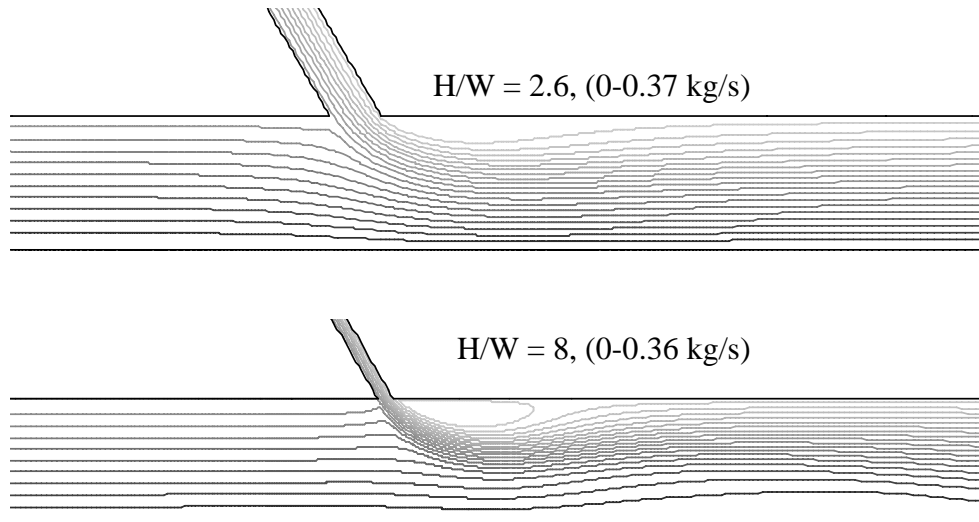


Figure 7.3 Streamline contours for $\theta = -30^\circ$ for two structures under large cross flow value, $M = 1$ (two figures are not under same scale)

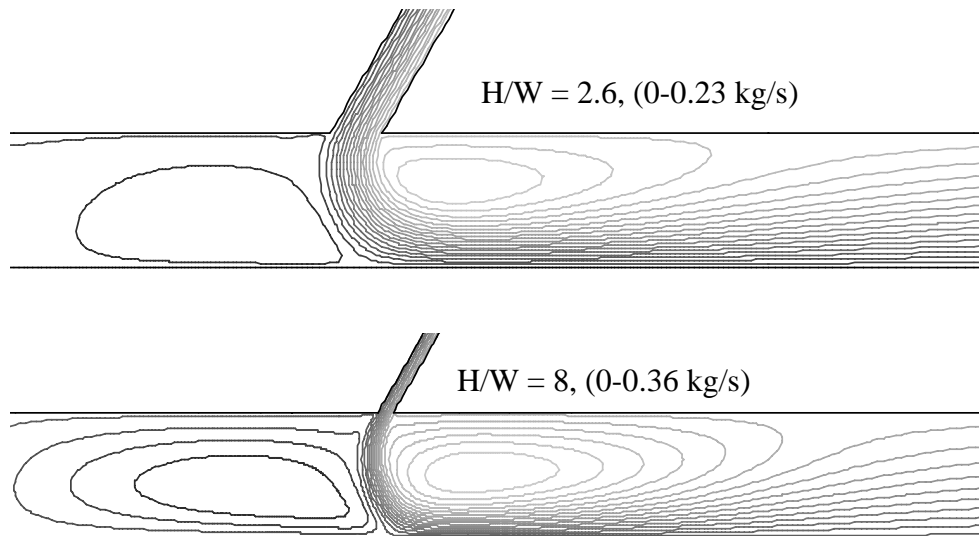


Figure 7.4 Streamline contours for $\theta = 30^\circ$ for two structures under small cross flow value, $M = 0.05$ (two figures are not under same scale)

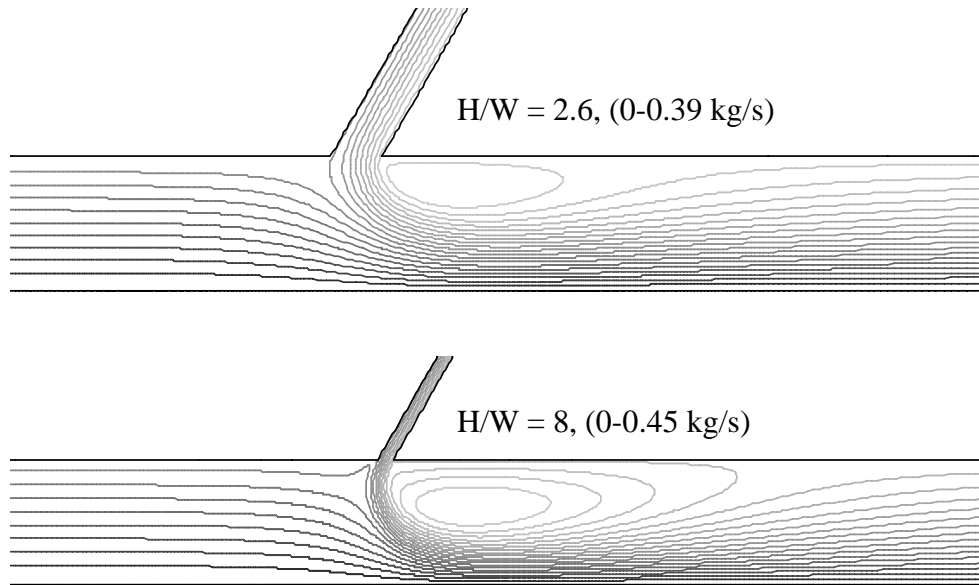


Figure 7.5 Streamline contours for $\theta = 30^\circ$ for two structures under large cross flow value, $M = 1$ (two figures are not under same scale)

Figures 7.2 through 7.5 show the streamline contours for different cross-flow mass values and different jet angles for two H/W values as predicted by the standard $k-\epsilon$ model. From these figures, we can draw the following conclusions for both small nozzle-to-target spacing, $H/W = 2.6$, and large nozzle-to-target spacing, $H/W = 8$, and for both positive and negative jet angles when M increases from a small value, $M = 0.05$, to a relatively large value, $M = 1$.

- When M equals 0.05, it is difficult to identify the stagnation point. When M equals 1, there is no stagnation point; the jet does not reach the impingement surface.
- There are two main vortices for the smaller cross flow value, $M = 0.05$. One is located upstream of the jet, the other is located downstream.
- The upstream main vortex disappears and the downstream main vortex becomes smaller and shifts to the confinement surface when the cross-flow value increases to 1.

- d) When the cross flow value M equals 1, the downstream main vortex, which is near the confinement surface, increases with the angle of inclination of the jet.

These results indicate that when a small amount of cross-flow ($M=0.05$) is introduced, a recirculation region develops near the impingement surface on the upstream side of the jet. At a higher cross-flow value ($M=1$), the recirculation region disappears. When the cross-flow mass is increased, the reattachment length of the main recirculation bubble on the side of outflow boundary decreases in size and shifts towards the confinement surface.

For a fully developed turbulent slot jet, the maximum heat transfer rate occurs typically at the stagnation point. However, for a turbulent impinging flow, subjected to a cross-flow, the separation point for the maximum heat transfer is different from that for the impingement jet without cross-flow. Therefore, in this section, we first present the effect of cross-flow on the heat transfer rate distributions and compare the simulation results with earlier reported data by Mujumdar et al. (1985). Subsequently, the studies of the effect of cross flow, jet angles, nozzle-to-target spacing and temperature difference between the jet and cross flow on heat transfer are presented. The heat transfer coefficient over the impingement surface was normalized in the form of a local Nusselt number for an isothermal impingement surface.

7.2.2 Effect of cross-flow on normal impinging jet heat transfer rate

Figure 7.6 shows the effect of cross-flow on the local Nusselt number distributions predicted by the standard $k-\epsilon$ model. The results show that the maximum value of the Nusselt number decreased and shifted downstream as M increased; also, its value in

the downstream region increased. Mujumdar et al. (1985) reported similar results. The decrease and shift of the maximum Nusselt number may be explained by examining the streamline contours when cross-flow is introduced. According to the streamline contours shown earlier, the stagnation point disappears and the size of the main recirculation bubble on the side of the outflow boundary (downstream) decreases. Cross-flow decreases the pressure gradient in the impingement wall region reducing the size of the recirculation bubbles, and consequently reducing the Nusselt number.

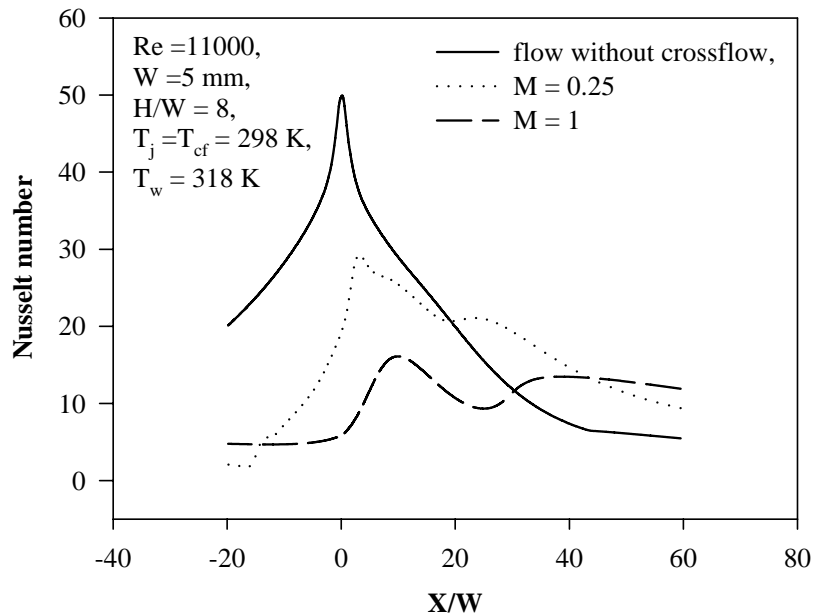


Figure 7.6 Effect of cross-flow on Nusselt number distributions predicted by the standard $k-\epsilon$ model

Based on the above comparison, we studied the effects of cross-flow and jet inclination angle on heat transfer characteristics. As with the flow study, four values of the cross-flow parameters were chosen ($M = 0, 0.05, 0.25$ and 1) with four cases of varying jet angle ($\theta = -30^\circ, -15^\circ, 15^\circ$ and 30°) for both small and large nozzle-to-target spacings, $H/W = 2.6$ and 8 .

7.2.3 Effect of jet angle on local heat transfer rate distribution

As noted earlier, jet impinging at an angle on a higher temperature plate creates an asymmetrical flow pattern. In Figures 7.7-7.10, the local Nusselt number predicted by both the standard k- ϵ and RSM models are plotted vs X/W for different angles of θ at constant values of H/W and Re for M = 0, 0.05, 0.25 and 1, respectively.

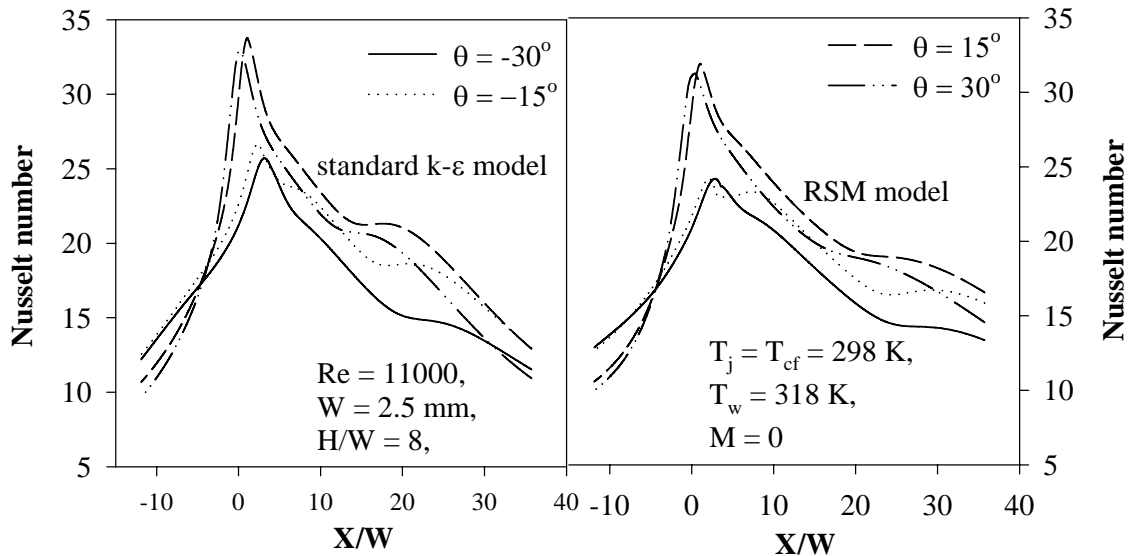


Figure 7.7 Effect of θ on Nusselt number predicted by the standard k- ϵ and RSM models for M = 0

(The values of H/W, Re, M, θ , T_j , T_{cf} , T_w , and W are same for both sides)

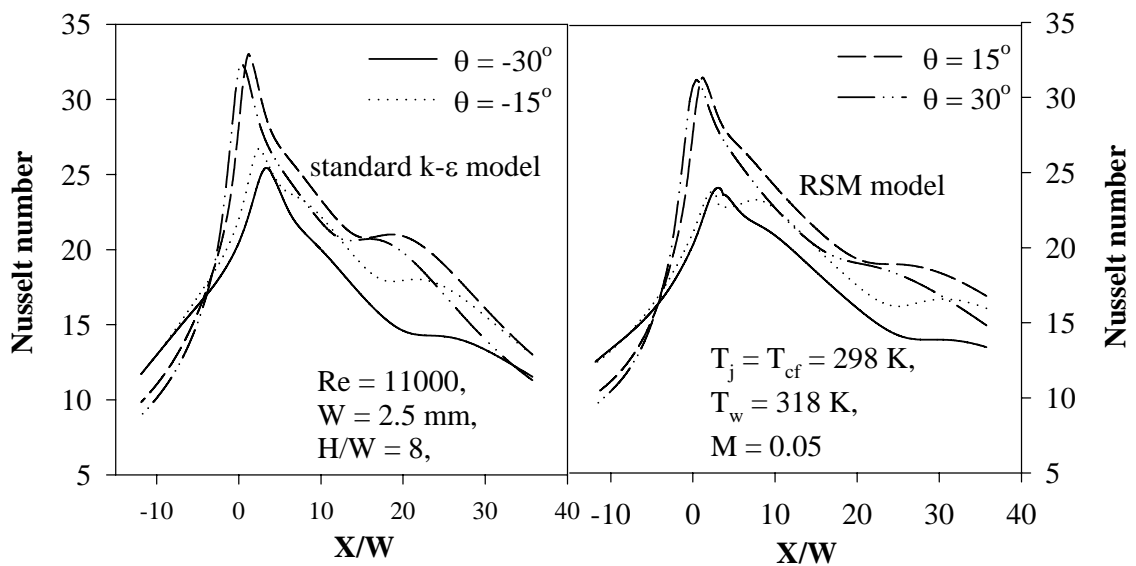


Figure 7.8 Effect of θ on Nusselt number predicted by the standard k- ϵ and RSM models for M = 0.05

(The values of H/W, Re, M, θ , T_j , T_{cf} , T_w and W are same for both sides)

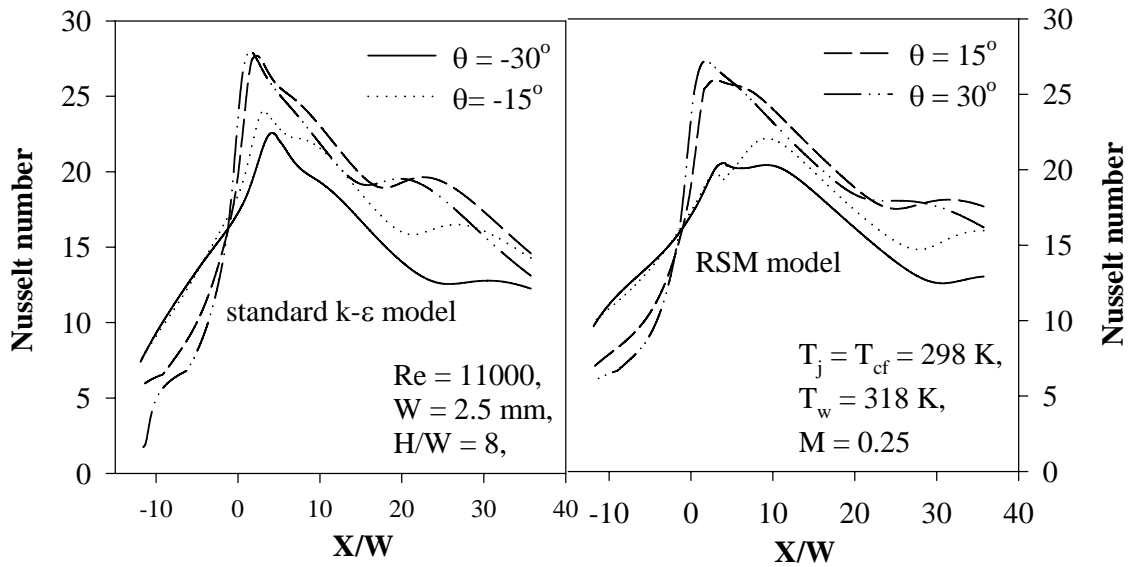


Figure 7.9 Effect of θ on Nusselt number predicted by the standard $k-\epsilon$ and RSM models for $M = 0.25$
(The values of H/W , Re , M , θ , T_j , T_{cf} , T_w and W are same for both sides)

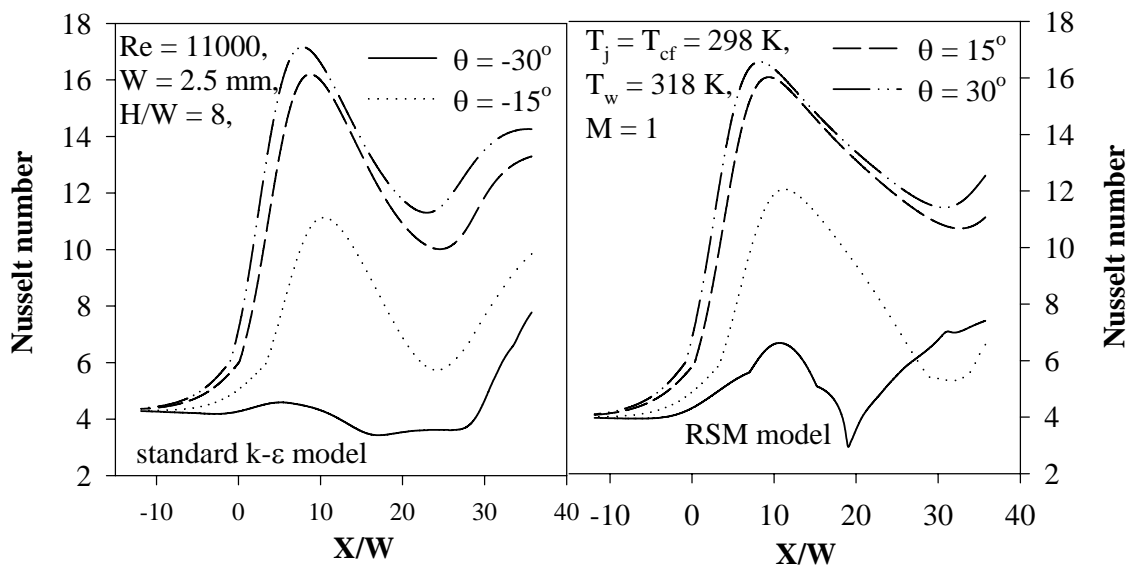


Figure 7.10 Effect of θ on Nusselt number predicted by the standard $k-\epsilon$ and RSM models for $M = 1$
(The values of H/W , Re , M , θ , T_j , T_{cf} , T_w and W are same for both sides)

From the above figures, we note that the peak values of the Nusselt number are still in the downstream region from the stagnation plane for the range of θ from -30° to 30° when the values of M change from 0 to 1. However, the location of the peak value of Nusselt number shifts upstream (i.e., moving towards the stagnation point) when the

angle θ increases from -30° to 30° for the range of cross-flow values from 0 to 1. In addition, the value of the peak Nusselt number increases when the angle θ changes from negative to positive. In terms of the values and shapes of the Nusselt number distributions, the standard k- ϵ and RSM models produce similar results.

7.2.4 Effect of cross-flow and jet angles on the average Nusselt number

Many authors investigated the average Nusselt number in the impingement region for the normal impinging jet without cross flow. For example, Abdlmonem et al. (2000) reported average Nusselt numbers for obliquely impinging turbulent jets. However, there is little information available on the average Nusselt number for obliquely impinging jets in cross-flow. In this section, we present the average Nusselt number vs cross flow values, M , for different jet angles as predicted by both the standard k- ϵ and RSM turbulence models.

Figures 7.11 and 7.12 show the effect of M on the average Nusselt number for different jet angles for $H/W = 2.6$ and $H/W = 8$, respectively. From these figures, we find that, for both $H/W = 2.6$ and $H/W = 8$, the average Nusselt number increases with the increase of the jet angles for the range of cross-flow values from zero to one. Figure 7.12 shows that for $H/W = 8$, the average Nusselt number decreases with increase of the cross-flow value from 0 to 1. However, interestingly for $H/W = 2.6$, the average Nusselt number remains nearly unchanged when cross-flow values increased from 0.25 to 1 as shown in Figure 7.11. A possible reason for this observation is that for small the nozzle-to-target spacing, $H/W = 2.6$, the flow behaves more like channel flow, (Figures 7.2 and 7.3), and there is little effect of the cross-flow on the Nusselt number.

When the cross-flow value is small, $M < 0.25$, the decrease in mass of the wall jet for $H/W = 2.6$ is faster than that for $H/W = 8$ causing a steeper slope of Nu_{ave} for $M < 0.25$.

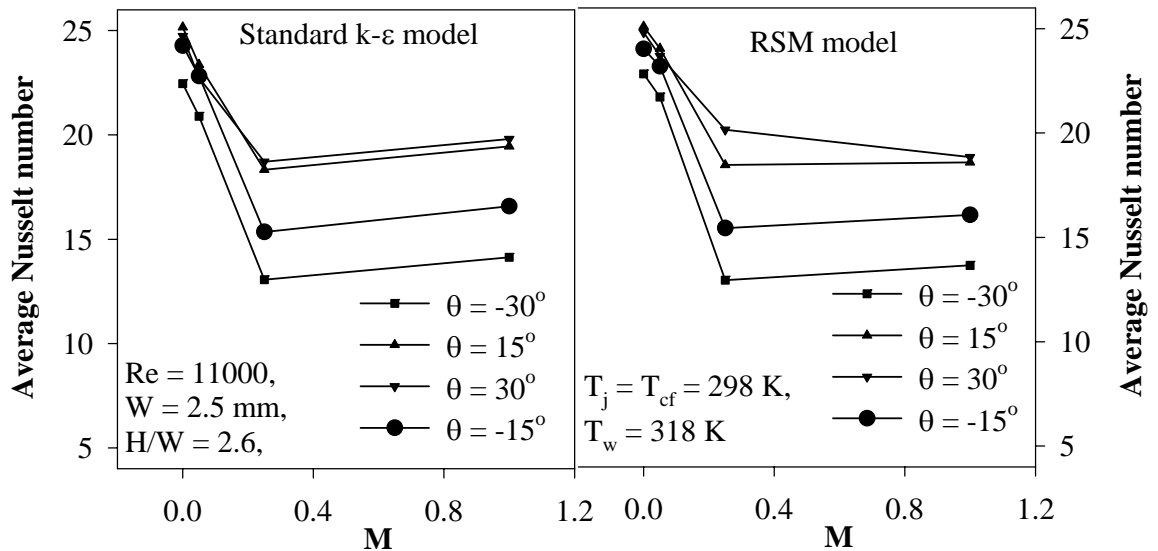


Figure 7.11 Effect of M on average Nusselt number predicted by the standard $k-\epsilon$ and RSM models for $H/W = 2.6$

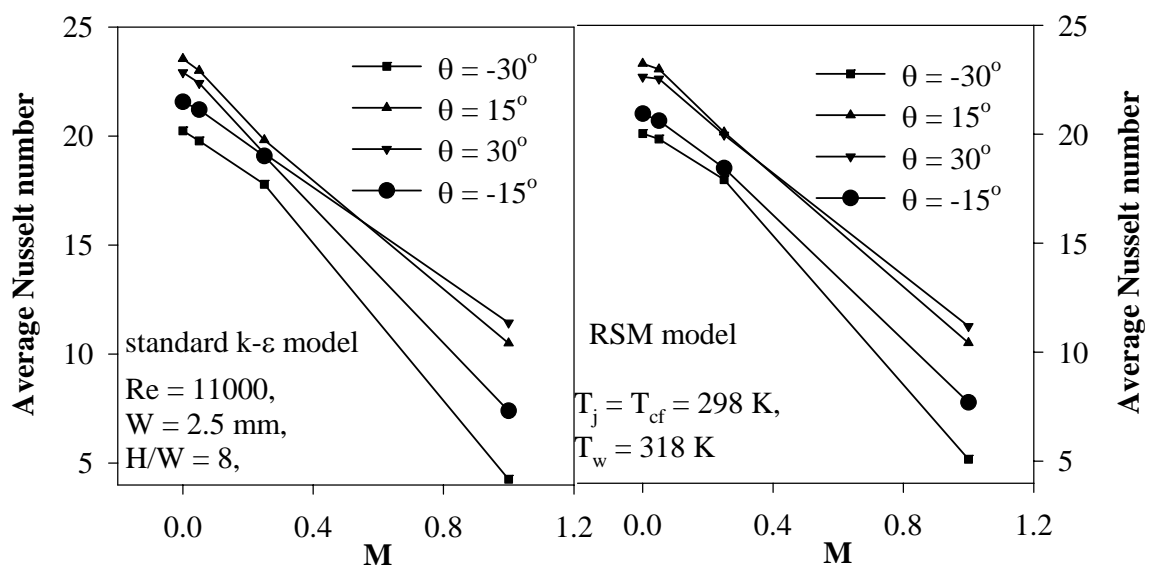


Figure 7.12 Effect of M on average Nusselt number predicted by the standard $k-\epsilon$ and RSM models for $H/W = 8$

7.2.5 Effect of temperature difference between the jet and cross-flow

Figure 7.13 shows the effect of temperature difference between the jet and the cross-flow on Nusselt number predicted by the standard $k-\epsilon$ and the Reynolds stress

turbulence models. As above, the standard $k-\varepsilon$ model and the Reynolds stress model produce similar results for the Nusselt number distributions for the same temperature difference. As expected, the temperature difference between the jet and the cross-flow has a noticeable effect on the Nusselt number distributions. The Nusselt number for the whole flow region increased with the increase of cross-flow temperature; however, the increase is not very significant. For example, when the cross-flow temperature increased from 320 K to 430 K, the maximum Nusselt number increased by only 30% as predicted by both the standard $k-\varepsilon$ and Reynolds stress models.

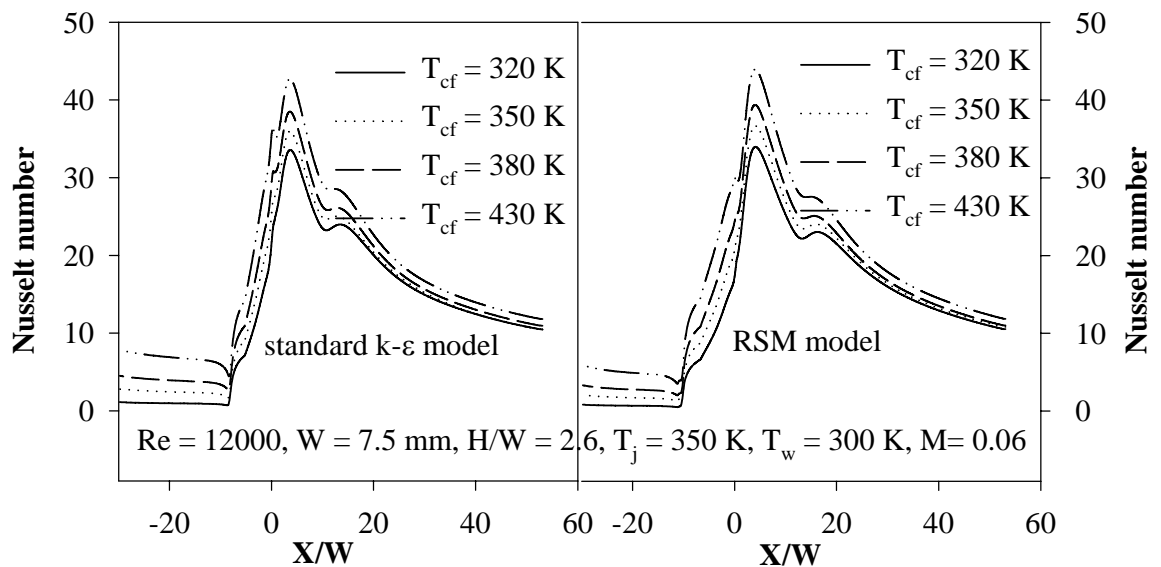


Figure 7.13 Effect of temperature difference between the jet and cross-flow on the Nusselt number predicted by the standard $k-\varepsilon$ model

7.3 Conclusions

In this chapter, the effect of jet-to-cross-flow mass ratio and jet angle on both local and average Nusselt numbers under a semi-confined impinging turbulent slot jet at different nozzle-to-target spacings was studied. Analysis of the numerical results shows that the maximum values of the Nusselt number decreased and shifted downstream as M increased from zero to one, while the Nusselt number values in the

downstream region increased. The peak Nusselt number increased and shifted upstream when the jet angle changed from negative 30° to positive 30° . The average Nusselt number decreased with the increase of the cross-flow value, however, with different slopes for different H/W values. Moreover, the temperature difference between the jet and the cross-flow has an effect on the Nusselt number distributions. The maximum Nusselt number increased by 30% when the cross-flow temperature increased from 320 K to 430 K.

Chapter 8

Heat transfer under turbulent multiple slot impinging jets of gas-particle suspension

8.1 Introduction

This chapter presents the heat transfer characteristics for a dilute gas-particle flow through multiple slot impinging jets computed numerically. A new Eulerian-Lagrangian model was employed in the CFD computation. The two-phase turbulent flow is simulated using the standard k - ϵ model and Lagrangian particle tracking, which includes coupling terms to simulate the fluid-particle interactions. Version 6 of FLUENT was used to solve the relevant governing equations. User Defined Functions (UDF) capability was used to modify the model to include the conduction heat transfer between the particles and the wall. The numerical results are compared with the available experimental data. It is shown that good agreement between the experiment and simulation is obtained only if the conduction heat transfer due to particle-wall collisions is considered in the model. Effects of wall parameters (properties of wall materials, wall reflection coefficient, and impingement wall temperature), particle factors (particle diameter, particle material properties, and loading ratios) and inlet conditions (jet Reynolds number, and direction of the gravitation vector) on the heat transfer rate are discussed.

The multiple slot impinging jets investigated in this work are symmetric and the flow configuration simulated is shown in Figure 8.1. The following boundary conditions were applied for the different cases considered: i) the impingement surface was specified as a constant temperature wall, ii) the confinement surface is considered to be

an adiabatic wall, iii) the gas and particles were introduced at the inlet with the same and constant values of velocity and temperature, iv) the pressure in outlet was specified to be atmospheric, and v) symmetry boundary conditions were applied along the lines of symmetry. The turbulence intensity at the inlet and outlet for all the calculations was specified to be 2 %. In all of the following numerical simulations, the nozzle width W , nozzle-to-target non-dimensional distance H/W and the temperature of inlet particle and gas are fixed at 4 mm, 2 and 300 K, respectively.

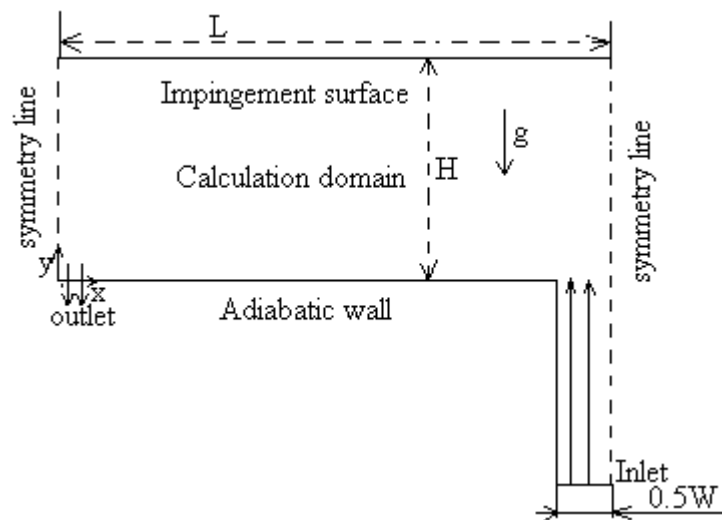


Figure 8.1 Flow configuration of the multiple impinging slot jets

8.2 Results and Discussion

8.2.1 Comparison between experiment and simulation

In this section, local heat transfer coefficient predicted by FLUENT 6.0 is compared with the experimental data reported by Yokomine et al. (2002). In Figure 8.2, the local heat transfer coefficient is plotted vs dimensionless length (X/W) for non-dimensional jet separation spacing $L/W = 5$ and $L/W = 7$. In Figure 8.2, heat transfer is calculated without considering the conduction heat transfer due to particle wall collision.

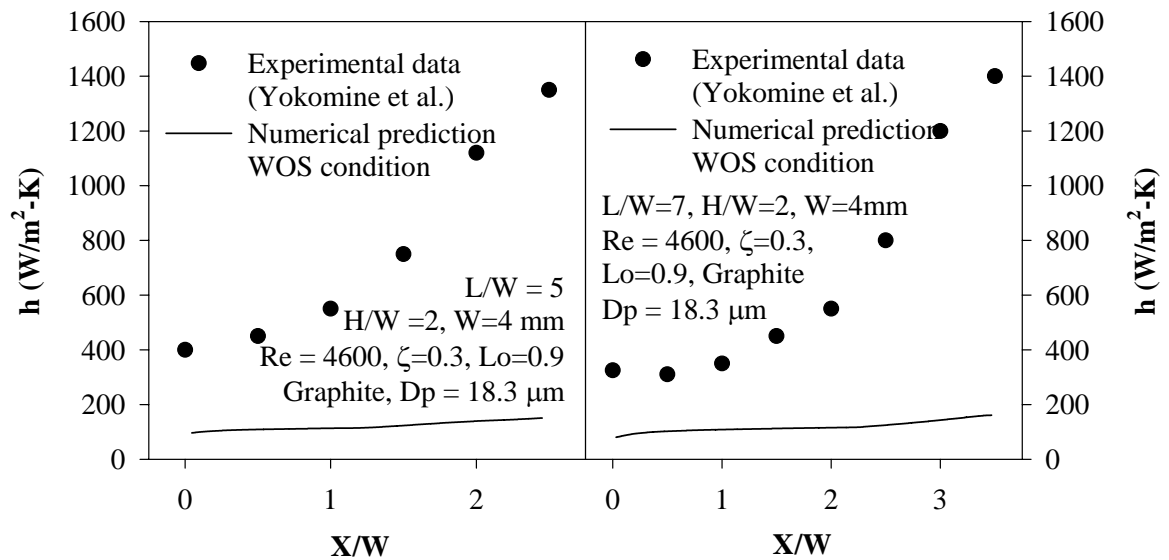


Figure 8.2 Comparison between the experimental results and the numerical results for WOS condition

From Figure 8.2, it is noted that, for both $L/W = 5$ and $L/W = 7$, the numerical model greatly under-predicts the local heat transfer coefficients under multiple slot impinging jets of gas-particle suspensions. For both the L/W values, the maximum difference between experimental results and numerical results was located at stagnation point and the minimum difference occurred at the exit. The experimental heat transfer coefficient at the stagnation point was nearly 9 times higher than the simulated heat transfer coefficient, while the experimental minimum value of heat transfer coefficient at exit was about 4 times higher than the simulated one. The average experimental heat transfer rates were 6.4 and 5.6 times higher than the numerically predicted values for $L/W = 5$ and $L/W = 7$, respectively.

One plausible reason for this deviation is that the conduction heat transfer between the particle and wall is neglected in the original gas-particle heat transfer model in FLUENT 6. It seems that the conduction heat transfer between particles and the wall is

important in impinging jet flows. We have incorporated conduction heat transfer due to the particle-wall collisions in the simulations described in the following sections.

8.2.2 Effect of conduction heat transfer

In this section, the influence of the addition of the conduction heat transfer due to particle-wall collisions is discussed for two multiple impinging jet cases for which the boundary conditions and structural parameters are the same as those of Yokomine's experiment (2002) and shown in Table 8.1. The total heat transfer Q is plotted for two cases with different L/W values. Q is expressed as:

$$Q = m_g c_{pg} (T_{outg} - T_{ing}) + m_p c_{pp} (T_{outp} - T_{inp}) \quad (8.1)$$

Table 8.1 Structure and operating parameters

L/W	W (mm)	H/W	Re _j	T _j (K)	T _w (K)	Lo	Dp (μm)	ξ
5	4	2	4600	300	400	0.9	18.3	0.9
7	4	2	4600	300	400	0.9	18.3	0.9

From Figure 8.3, it is found that the conduction heat transfer due to the particle-wall collisions has a significant effect on the total heat transfer rate. The heat transfer rate increased 5.4 and 6.8 times when the conduction heat transfer due to particle-wall collisions was included for the structural parameters $L/W = 5$ and $L/W = 7$, respectively. Earlier in Figure 8.2, it was shown that the numerical gas-particle models significantly under-predicted the impinging jet heat transfer rate. The average experimental heat transfer rate was 6.4 and 5.6 times higher than the predicted values for $L/W = 5$ and $L/W = 7$, respectively. Therefore, if the additional conduction heat transfer due to particle-wall collisions is considered, the simulated results for both $L/W = 5$ and $L/W = 7$ compared favorably with the experimental data.

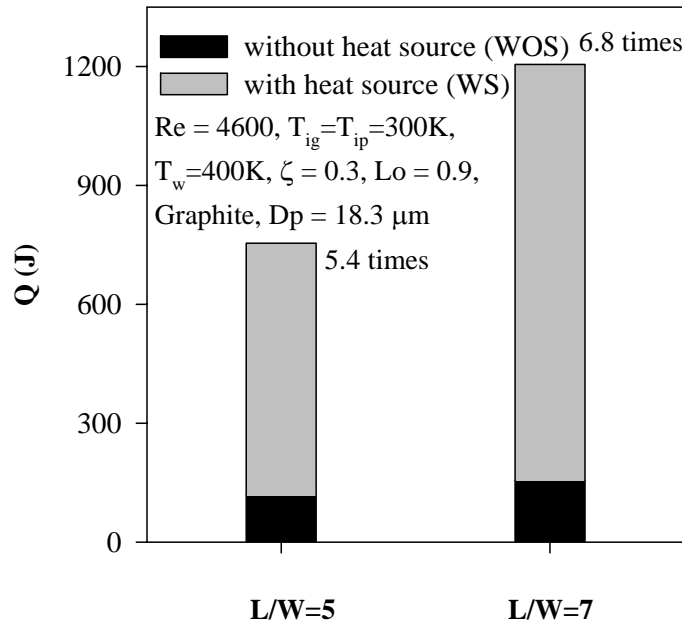


Figure 8.3 Effect of conduction heat transfer between particles and wall on heat transfer for both WOS and WS conditions

The magnitude of the conduction heat transfer between particles and wall depends on many factors including particle and wall properties. The effects of different numerical and experimental parameters such as wall factors (properties of wall materials, wall reflection coefficient, and impingement wall temperature), particle factors (particle loading ratios, particle diameter, and particle material properties), and inlet conditions (jet Reynolds number, and direction of the gravitation vector) are discussed in the following sections. Five materials, graphite, glass, copper, aluminum and steel are studied in this chapter. Table 8.2 lists their properties.

Table 8.2 Material properties of graphite, glass, copper, aluminum and steel

Materials	Density (kg/m ³)	Heat Capacity (J/kg)	Conductivity (W/m-K)	Elastic Modulus (N/m ²)
Graphite	2250	690	24	4.80×10 ⁹
Glass	2460	737	35	8.69×10 ⁹
Aluminum	2705	900	227	6.90×10 ¹⁰
Copper	8940	385	391	1.15×10 ¹¹
Steel	7870	486	52	2.05×10 ¹¹

8.2.3 Effects of wall factors

8.2.3.1 Effect of wall material

Three wall materials, aluminum, copper and steel, were studied in this work. Their properties are listed in Table 8.2. Figure 8.4 shows the effect of impingement surface materials on heat transfer rate. When the conduction heat transfer contribution was neglected, the wall materials with the same roughness had no influence on the flow and heat transfer behavior. However, as before, when conduction heat transfer was considered, the total heat transfer rate significantly increased, although the heat transfer difference between the three wall materials, aluminum, copper and steel, was small. In other words, Figure 8.4 shows that the thermo-physical properties of the wall material have negligible effect on the heat transfer rate. This is probably due to the fact that the thermal boundary condition (isothermal wall) is forced externally on the wall.

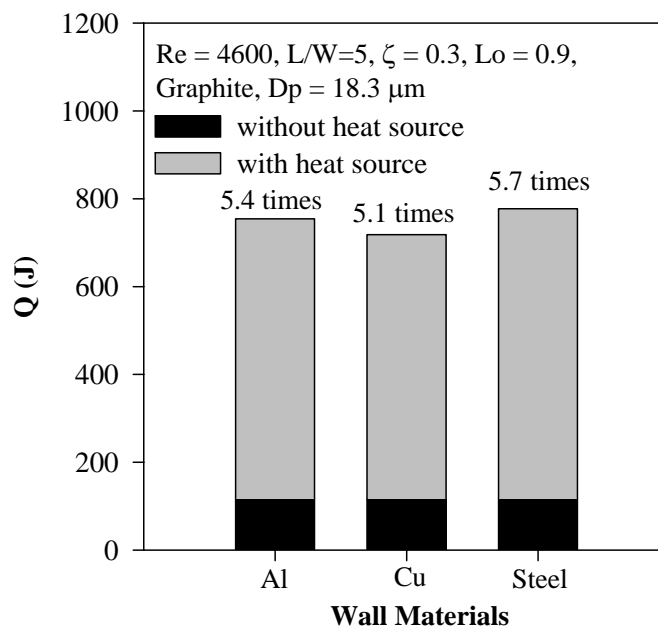


Figure 8.4 Effect of wall materials on heat transfer for both WOS and WS conditions

8.2.3.2 Effect of reflection coefficient on heat transfer

In Figure 8.5, it is shown that the wall reflection coefficient has only a secondary effect on heat transfer for both WOS and WS conditions. Under the present boundary conditions, when the conduction heat transfer between particle and wall was included, the maximum heat transfer rate occurred when the reflection coefficient was equal to 0.6. The effect of reflection coefficient on total heat transfer is nonlinear. The reflection coefficient not only affected the flow behavior of gas and suspended particles, but also affected the magnitude of the heat transferred by the conduction between the particle and wall. However in the present study, the heat transfer due to particle wall collision is calculated under the assumption of elastic collision, which makes the study of effect of reflection coefficient is not very practical. Nonetheless, to characterize the effect of gas-particle suspension on heat transfer in impinging jets systems, further fundamental work is needed to correlate the reflection coefficient with the heat transfer rate.

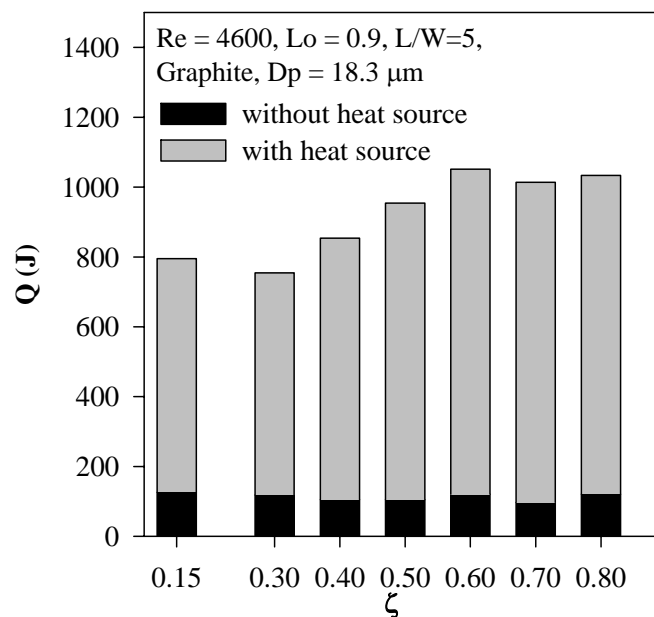


Figure 8.5 Effect of reflection coefficient on heat transfer for both WOS and WS conditions

8.2.3.3 Effect of impingement wall temperature

It is well known that the temperature difference between the impingement wall and inlet gas and particles not only affects the convection heat transfer but also affects the conduction heat transfer between the particles and the wall. Figure 8.6 shows the predicted heat transfer behavior for three values of the impingement wall temperature for both WOS and WS conditions. Figure 8.6 shows that the heat transfer rate increases with the increase of the impingement wall temperature for both WS and WOS conditions. However, under WS conduction, the heat transfer increased with a higher slope than under the WOS condition. Thus, the conductive contribution appears to be enhanced by larger temperature difference.

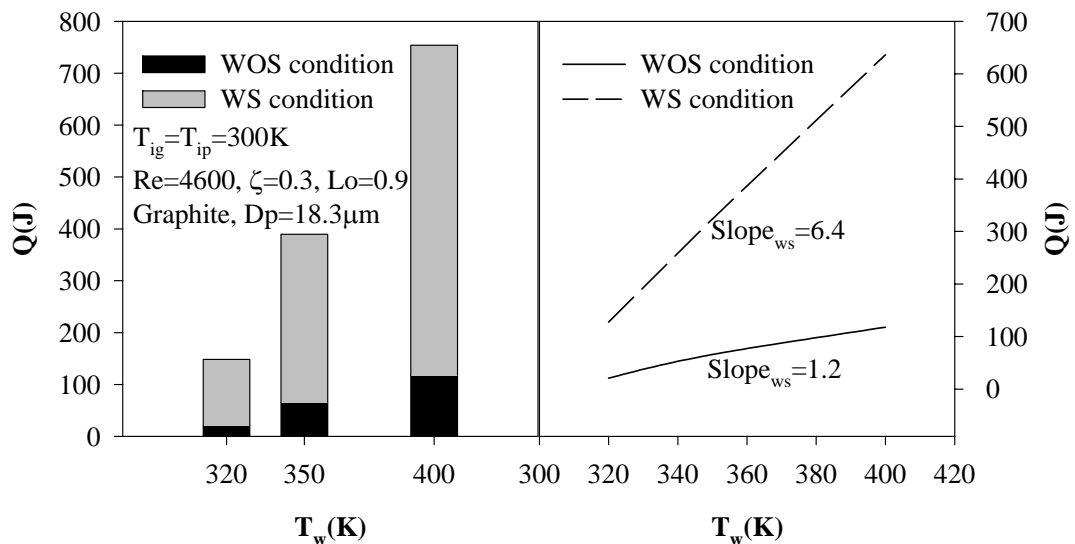


Figure 8.6 Effect of impingement wall temperature on heat transfer

8.2.4 Effects of particle factors on heat transfer

8.2.4.1 Effect of coefficient C and the loading ratio

The heat source (Eq. 3.33) was calculated under the assumptions that the particle-wall collisions were elastic, and the particles were spherical with a fixed diameter. However, these assumptions are not fully valid. So in order to account for inelastic collisions and non-sphericity of the particles, we added a constant coefficient C in

Eq.3.33 to introduce variable weight for the heat source term. First the effects of loading ratio and constant, C , on heat transfer were investigated individually, shown in Figure 8.7 and 8.8, respectively, and then we studied the coupled effects of particle loading ratio and constant C and developed empirical correlations between the average heat transfer rate Q and Lo for two values of C (viz. 1.0 and 1.5) and for both $L/W = 5$ and $L/W = 7$.

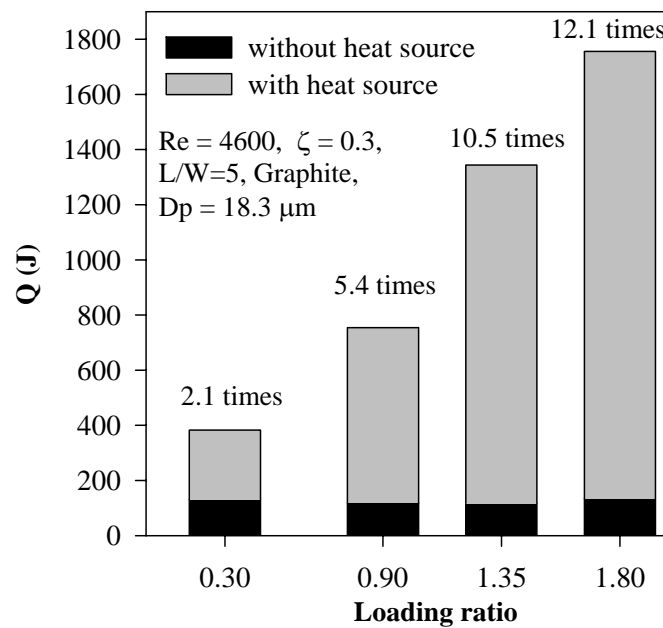


Figure 8.7 Effect of loading ratio on heat transfer for both WOS and WS conditions

From Figure 8.7, we find that when conduction heat transfer is included, the particle loading ratio has a significant effect on heat transfer. On the other hand, as expected, the loading ratio has negligible effect on heat transfer if the heat transfer between particles and wall collisions is neglected. From Figure 8.7, it is noted that the heat transfer rate monotonously increased from 2.1 to 12.1 times when the loading ratio increased from 0.3 to 1.8. The experimental study of Yoshida (1990) of heat transfer of a 2D impinging jet with gas-solid suspensions also showed that the Nusselt number increased with the increase of the particle loading ratio in the range of 0 to 0.8. However, for the gas-particle pipe flow, Avila and Cervantes (1995) found that the

average heat transfer rate increased with the increase of loading ratio when the ratio was greater than 1. When the loading ratio was less than 1, a net reduction of heat transfer rate was produced due to the reduction in turbulence intensity and the suspension heat capacity effect was small. From the monotonically increasing heat transfer rate with the increase of particle loading ratio in impinging jet systems, it can be concluded that the main mechanism of heat transfer enhancement in impinging jet gas-particle system was due to the conduction heat transfer between the particles and the wall.

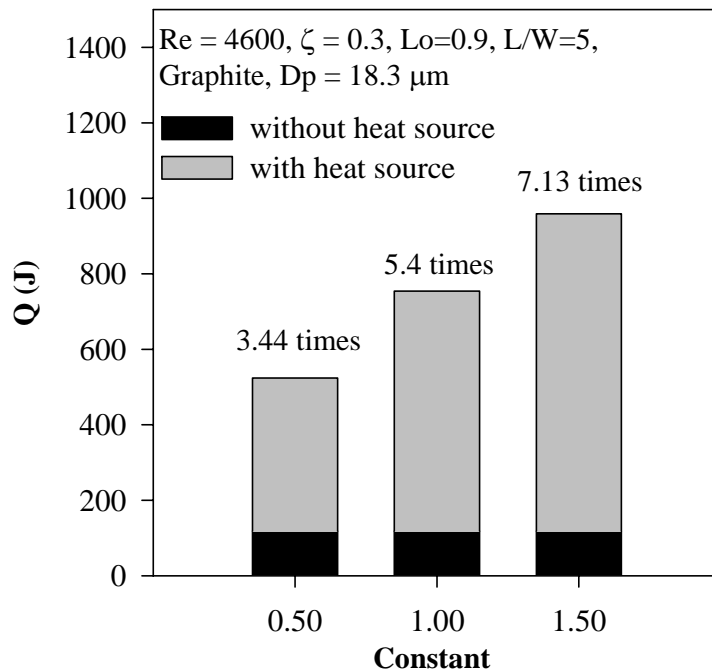


Figure 8.8 Effect of constant C in heat source term on computed heat transfer for both WOS and WS conditions

Figure 8.8 shows the effect of constant, C , in Eq.3.33 on heat transfer rate. The simulations were carried out for three values of C viz. 0.5, 1.0 and 1.5. It was noted that with the increase of the magnitude of C , the total heat transfer, Q , increased. The larger constant results in a larger heat source term; consequently more heat is transferred to the particles from the hotter wall. However, comparing Figures 8.7 and 8.8, it can be seen that the loading ratio has a bigger effect on heat transfer than the

value of C . For example, for a similar rise (1.5 times higher) in C and loading ratio, the effect was 40% greater for loading ratio. From Figure 8.8, it has been seen that the total heat transfer rate is sensitive to the constant in Eq. 3.33. When the constant C increased from 1.0 to 1.5, heat transfer increased by 30%, and these results are in the right range of the experimental data of Yokomine et al. (2002), indicating that the value of C probably lies in the narrow range of 0.5 to 1.5.

Figures 8.9a and 8.9b show the effect of particle loading ratio on heat transfer rate for $C = 1.0$ and $C = 1.5$, respectively. Figures 8.10a and 8.10b are the results for $L/W = 7$. The resulting empirical correlations between the average heat transfer rate Q and Lo for two values of C (viz. 1.0 and 1.5) and for both $L/W = 5$ and $L/W = 7$ are listed in Table 8.3.

Table 8.3 Correlations between heat transfer and loading ratio

C	Correlations ($L/W=5$)	R^2	Correlations ($L/W=7$)	R^2
$C=1.0$	$Q = 815Lo^{1.2}$	0.99	$Q = 1175Lo^{0.62}$	0.99
$C=1.5$	$Q = 771Lo^{1.56}$	0.88	$Q = 1524Lo^{0.76}$	0.99

As expected, Figures 8.9 and 8.10 show that under the WS condition, the particle loading ratio has a significant positive effect on the heat transfer rate as the heat transfer rate increases with increase of the particle loading ratio for both C values, 1.0 and 1.5. On the contrary, the loading ratio has negligible effect on heat transfer if conduction heat transfer is neglected. The dependence of total heat transfer Q on particle loading ratios is described empirically as $Q = aLo^b$. Correlations between particle loading ratio and heat transfer were obtained for both $C = 1.0$ and $C = 1.5$ and both $L/W = 5$ and $L/W = 7$. The regression analysis indicates that the loading ratio had

a higher exponent value for $C = 1.5$ than that for $C = 1.0$ for both L/W values. For a higher value of C , an increase in the source term (Eq. 9) can be expected, which consequently would increase the total heat transfer. However, these correlations are valid only over the parameter ranges examined in this work.

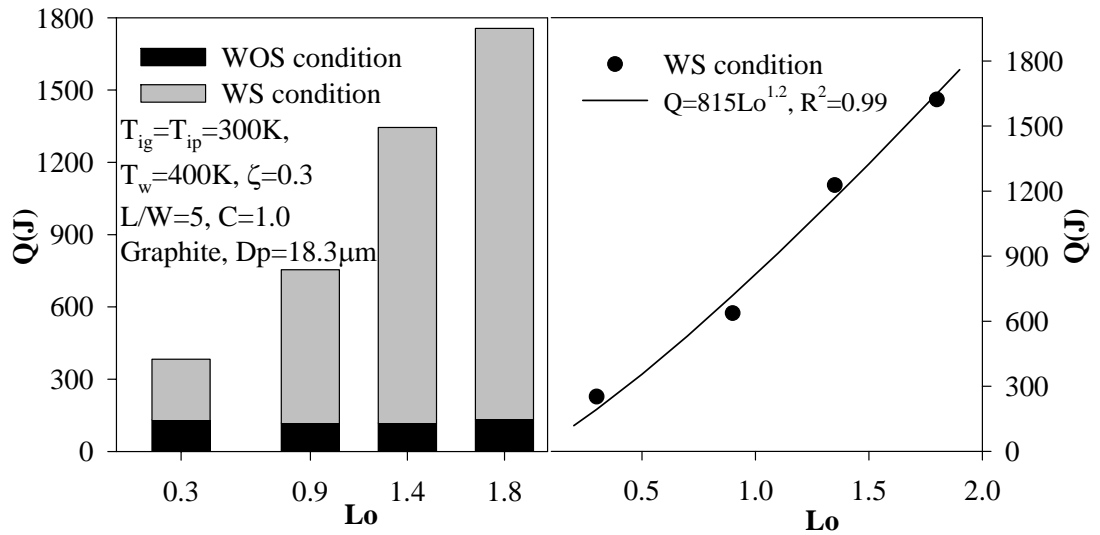


Figure 8.9a Effect of particle loading ratio on heat transfer for $L/W=5$, $C=1.0$

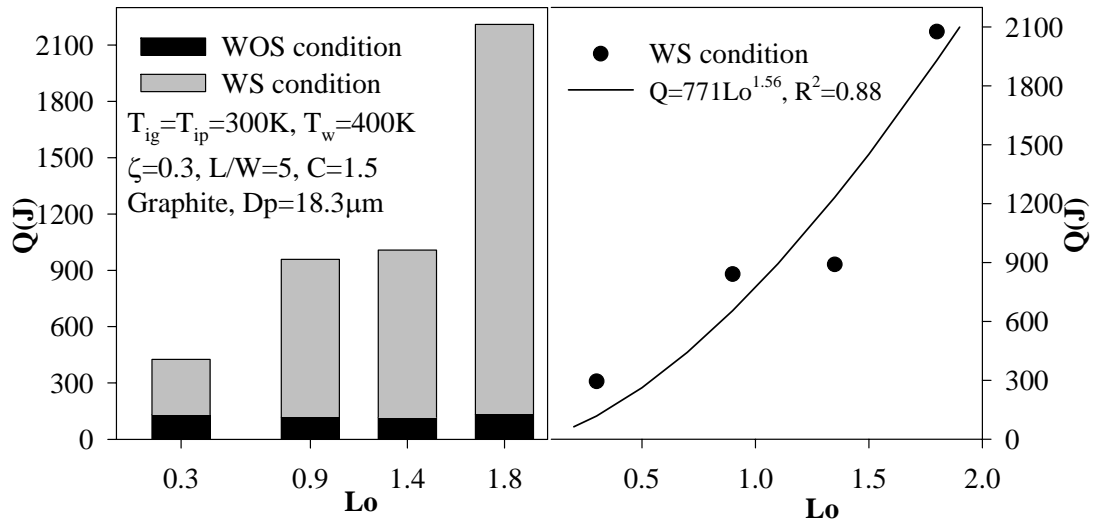


Figure 8.9b Effect of particle loading ratio on heat transfer for $L/W=5$, $C=1.5$

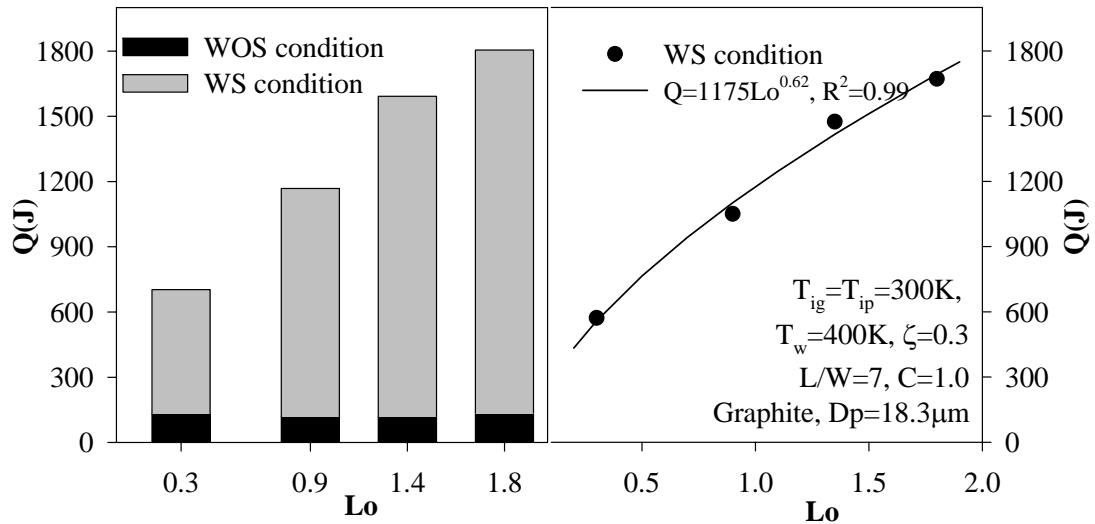


Figure 8.10a Effect of particle loading ratio on heat transfer for $L/W=7$, $C=1.0$

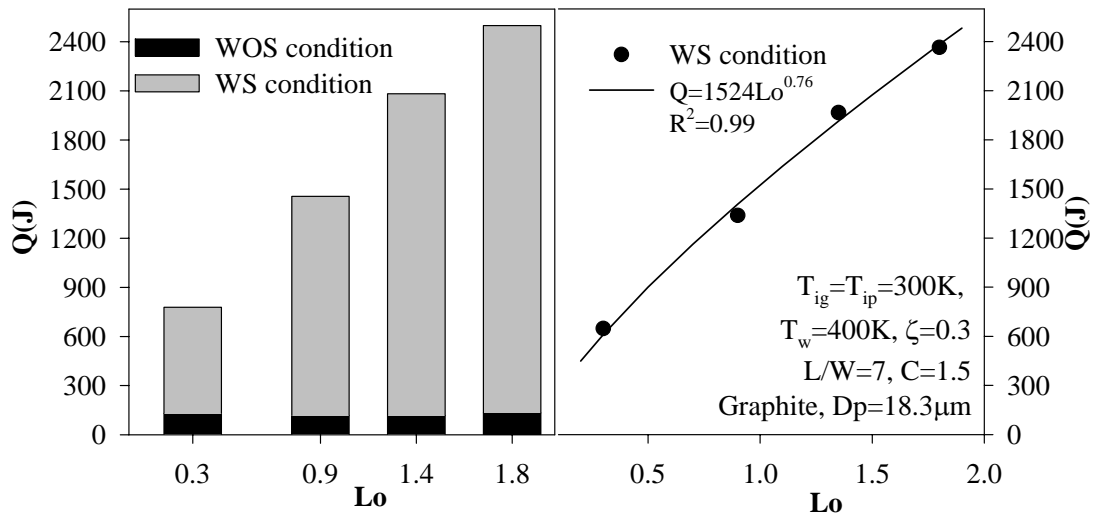


Figure 8.10b Effect of particle loading ratio on heat transfer for $L/W=7$, $C=1.5$

The outlet gas temperature distributions were plotted vs outlet width for both WOS and WS conditions in Figure 8.11. It was noted that under WS condition, the outlet gas temperature distributions increase with the increase of the loading ratio, shown in Figure 8.11. Moreover, the outlet gas temperature distributions for the WS cases are all higher than those for WOS conditions. On the other hand, under WOS condition, the outlet gas temperature distributions decreased with increase of the loading ratio. The gas-particle mixture has a higher thermal-capacity with increase of the particle loading

ratio, therefore, if the heat transfer due to particle-wall collisions is neglected, the outlet gas temperature decreases with the increase of particle loading ratio.

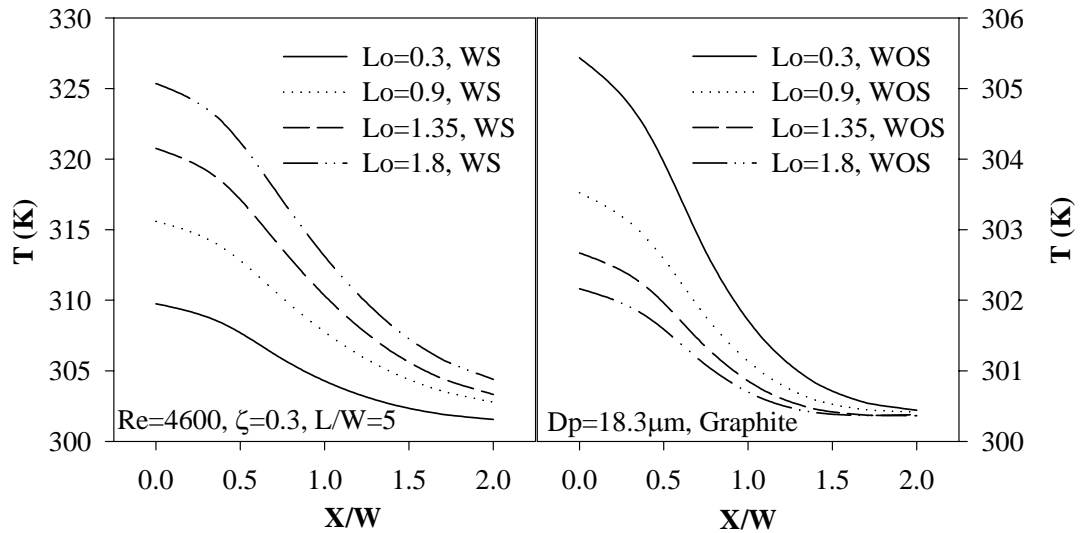


Figure 8.11 Effect of loading ratio on outlet gas temperature distributions for WOS and WS conditions

8.2.4.2 Effect of particle diameter

Figures 8.12 and 8.13 display the effect of particle diameter on the average heat transfer rate for $L/W = 5$ and 7 , respectively. For both values of $L/W = 5$ and 7 , as expected the particle diameter had negligible effect on heat transfer if the particle-wall conduction heat transfer is neglected. By contrast, if the conduction heat transfer between particle and wall is considered, the magnitude of particle diameter had significant effect on heat transfer rate. For example, the smaller the particle diameter, the greater is the heat rate by conduction. Heimann and Schlunder (1986) also reported that the contact heat transfer coefficient from a hot wall to particle is an inverse function of the particle diameter. Their model predicts a heat transfer coefficient that varies approximately as $1/D_p$. In this work, empirical correlations between the heat transfer rate Q and particle diameter D_p were obtained by regression of the numerical results under the WS condition for both $L/W = 5$ and $L/W = 7$. The correlations are

$Q = 2698Dp^{-0.53}$ and $Q = 5873Dp^{-0.61}$, with $R^2=0.97$ and 0.99 for $L/W = 5$ and $L/W = 7$, respectively. It is noted that the exponent values of particle diameter from the regression of numerical data are quite comparable for $L/W = 5$ (-0.5) and $L/W = 7$ (-0.6). The exponent obtained in this work is lower than the Heimann and Schlunder value of approximately -1.0 . However, it may be noted that in their case purely conduction heat transfer was considered while the predicted Q in this work includes both conduction and convection contributions due to the presence of particle in the gas.

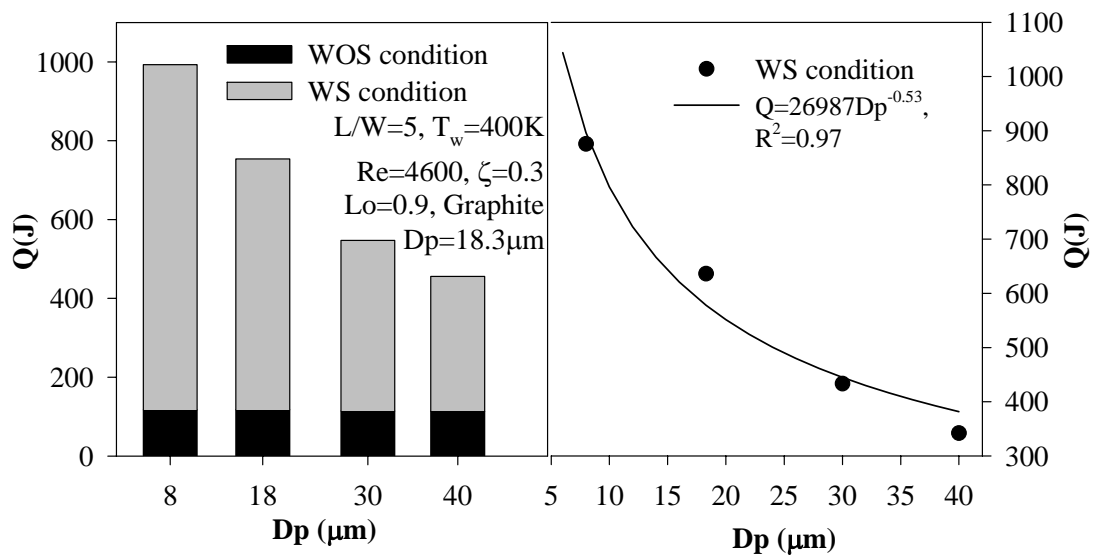


Figure 8.12 Effect of particle diameter on heat transfer for $L/W=5$

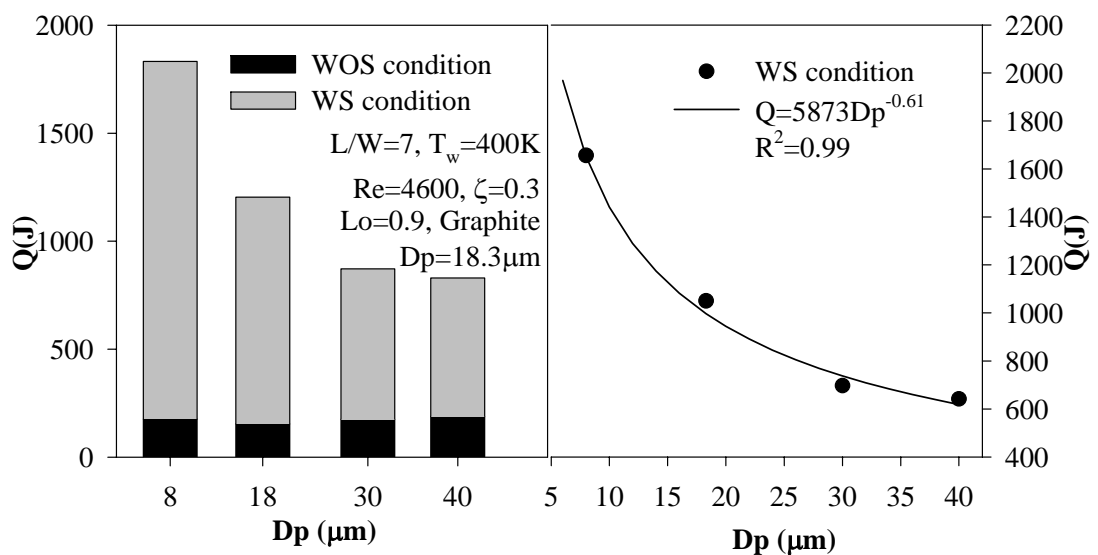


Figure 8.13 Effect of particle diameter on heat transfer for $L/W=7$

8.2.4.3 Effect of particle material

From an analysis of the conduction heat transfer between the particle and wall, it is expected that the particle material properties will have important effects on the conduction heat transfer rate due to particle-wall collisions. Figure 8.14 presents the total heat transfer rates of three particle materials, copper, glass and graphite. The choice of the three materials for the present study was determined by their frequent application in the research work. The properties of the three materials studied in this work are listed in Table 8.2. From Figure 8.14, it is noted that the particle material has no effect on the heat transfer rate under WOS condition since conduction contribution is ignored. On the contrary, if the conduction heat transfer between the particle and wall is included, the particle material has significant effect on the heat transfer rate. In this work, the dependency of the total heat transfer Q on particle properties such as ρ ,

k and C_p can be expressed empirically as $Q = a \left(\frac{\rho}{kC_p} \right)^b$. The correlations between particle properties such as ρ , k , C_p and heat transfer Q were obtained by regression.

The resulting correlation is $Q = 8786 \left(\frac{\rho}{kC_p} \right)^{1.33}$ with R^2 of 0.94 for $L/W = 5$. A similar type of correlation was obtained for $L/W = 7$, but with a poor fit and a low R^2 . The reason is that both the coefficient and exponent are dependent on parameters of the gas, particles as well as the geometry.

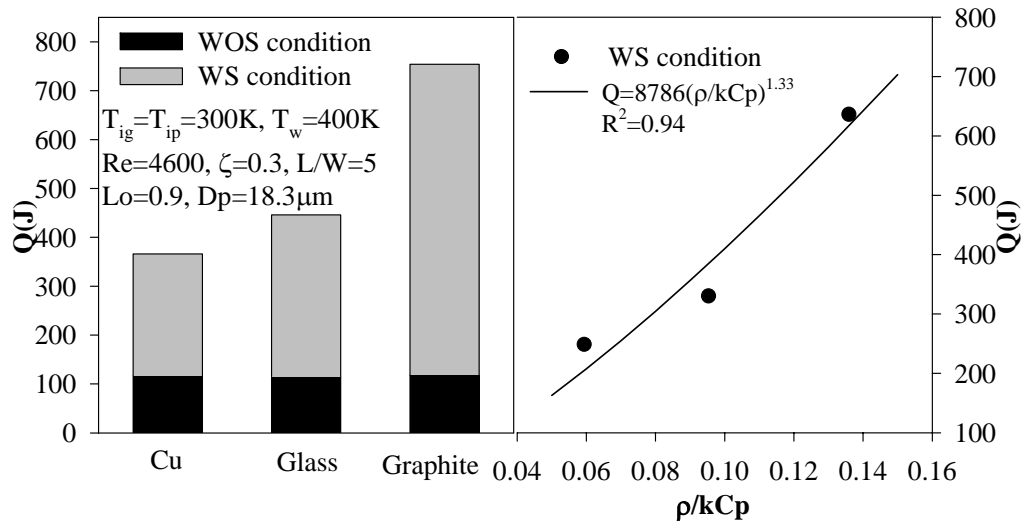


Figure 8.14 Effect of particle materials on heat transfer

8.2.5 Effect of inlet conditions

8.2.5.1 Effect of inlet Reynolds number

Figure 8.15 shows the computed heat transfer rates for three values of the inlet Reynolds number under both WOS and WS conditions. It is noted that the jet Reynolds number has an effect on the heat transfer rate under both WS and WOS conditions. However, it is seen that the inlet Reynolds number has a much greater effect on the heat transfer rate under the WS condition than under the WOS condition. The heat transfer Q increased by four fold when the Reynolds number increased from 2500 to 10,000 under WS condition. The reason is that higher velocities of impact cause shorter contact times of collision, which favors the conduction heat transfer.

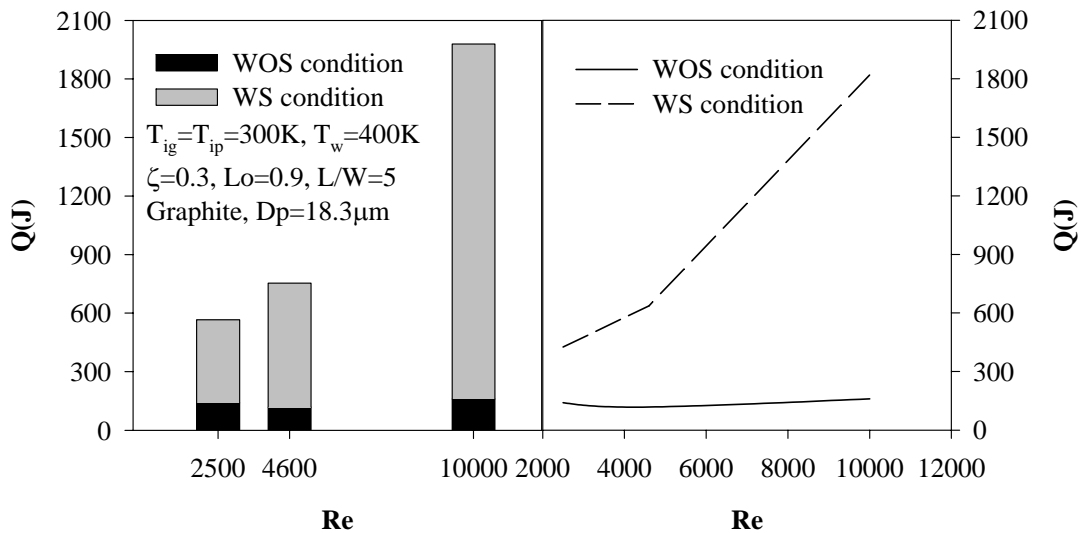


Figure 8.15 Effect of inlet Reynolds number on heat transfer

8.2.5.2 Effect of gravity direction on heat transfer

In our previous section of this work, we compared our numerical data with Yokomine's experimental data (2002). In Yokomine's experiment, the inlet velocities of gas and particles were in the opposite direction of the gravity. Since in some industrial drying applications, the gas and particles are injected in the channel in the same direction as that of the gravity, some simulations were conducted to study the effect of gravity direction on the heat transfer rate. Some typical results are shown in Figure 8.16. From Figure 8.16, we find that under Yokomine's experimental condition, when gravity direction changed to the same direction as that of the inlet gas and particle velocities, a slight increase in the heat transferred from the wall occurs. Under WS condition, slightly more heat is transferred from the wall if the gravity direction is the same as that of the inlet gas and particles velocities as gravity assists the particle motion, and higher velocities of impact are expected resulting in higher heat transfer rate.

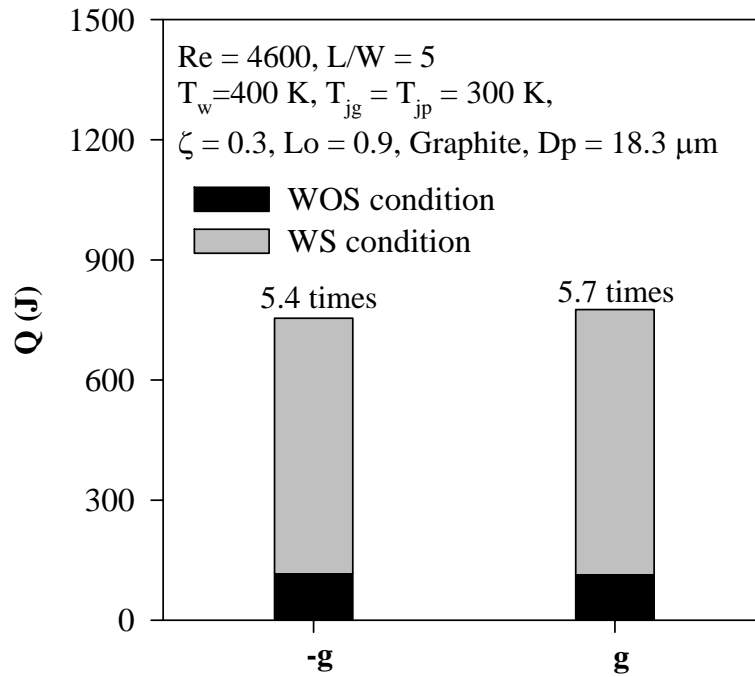


Figure 8.16 Effect of gravity direction on heat transfer

8.3 Conclusions

A new model of heat transfer was developed in this study to predict the heat transfer for multiple turbulent slot impinging jets of dilute gas-particle suspensions by taking into account the conduction heat transfer due to particle-wall collisions in the Eulerian-Lagrangian model. The predicted results approach experimental observations when conduction heat transfer between the particle and wall is included in the model. The effects of different numerical and experimental parameters such as wall factors (properties of wall materials, wall reflection coefficient, and impingement wall temperature), particle factors (particle loading ratios, particle diameter, and particle material properties), and inlet conditions (jet Reynolds number, and direction of the gravitation vector) are discussed. The simulation results indicate that particle diameter; particle material properties and loading ratio have significant effects on the predicted heat transfer rate when the conduction heat transfer between particle and wall is included in the model. Regression analysis was conducted to develop correlations

demonstrating the effects of particle diameter and the particle materials on the heat transfer. The simulation results indicate that with the conduction heat transfer due to particle collision on the wall, the jet Reynolds number and the impingement wall temperature have larger effects on the total heat transfer rate than heat transfer without the particle-wall conduction. It is also found that more heat would be transferred from the wall if the gas and particles were introduced into the impinging jets oriented in the same direction as gravity, and the magnitude of this increase will depend on the size and density of the particles. Thermo-physical properties of the wall material have negligible effect on the heat transfer rate.

Chapter 9

Conclusions

9.1 General conclusions

The flow and heat transfer behavior of turbulent semi-confined impinging slot jets has been simulated using computational fluid dynamics for various configurations, operating parameters and fluid properties. Predictive performance of turbulence models such as the standard k- ϵ and RSM models, and different wall functions such as standard and non-equilibrium wall functions were compared with experimental data. The simulated results compare favorably with the experimental results for large nozzle-to-target spacing (e.g. $H/W = 12$), but the predictions for small nozzle-to-target spacing (e.g. $H/W = 2.6$) call for further improvement.

Different definitions of Nusselt number have been evaluated and the corresponding distributions compared for small and large ΔT s between the jet and the target surface. The local Nusselt number for an isothermal impingement surface can be defined as $Nu_x = \frac{h_x W}{\lambda}$, where λ is the fluid thermal conductivity, $h_x = \frac{q}{\Delta T}$, and ΔT is the temperature difference between the jet and impingement surface. In this work, λ was calculated at jet temperature, film temperature and impingement wall temperature and the corresponding Nusselt numbers were denoted by Nu_j , Nu_f and Nu_w , respectively. Comparison among the three Nusselt definitions shows that small temperature differences (e.g. up to 50°C) show only minor differences in the local Nu_j , Nu_f and Nu_w values. However, large temperature differences (over 100°C) can result in

significant differences among the three types of Nusselt numbers for both heating and cooling. It was shown that the jet Nusselt number, Nu_j , was the best choice among the three Nusselt number definitions to report the heat transfer rate since under large ΔT , the jet Nusselt number spreads the least. The jet Nusselt number definition allows the designer to use previously published correlations, which were obtained at small ΔT . This conclusion is valid regardless of the jet Reynolds number and the nozzle-to-surface spacing.

The effect of fluid Prandtl number on local, stagnation and average heat transfer of semi-confined laminar and turbulent impinging slot jet was investigated over the range of Prandtl number 0.7-71. The variations of Nusselt number for all the tested fluids are similar to those for air. The Nusselt number increases with the increase of fluid Pr number from 0.7 to 71 for both laminar and turbulent flows. Gases with similar Prandtl number exhibit similar values of Nusselt number, but different values of the surface heat transfer coefficient due to their widely different thermal conductivities. Empirical correlations are developed for the stagnation and average Nusselt numbers as a function of the fluid Prandtl number on the basis of extensive numerical experiments for both laminar and turbulent flows.

The flow and heat transfer characteristics of a single semi-confined turbulent slot jet of air impinging normally or obliquely into an imposed air cross-flow of the same or different temperature were simulated using the standard k - ϵ model and Reynolds stress model. The influence of various flow parameters (e.g. jet-to-cross-flow mass ratio) and geometric parameters (e.g. nozzle-to-target spacing and jet angle) were evaluated at a fixed Reynolds number for equal and unequal temperatures of the jet and cross-flow. It

was found that the maximum values of the Nusselt number decreased and shifted downstream as M increased from zero to one. On the other hand, the peak Nusselt number increased and shifted upstream when the jet angle changed from negative 30° to positive 30° . The average Nusselt number decreased with the increase of the cross-flow value with different slopes for different H/W values. Moreover, the temperature difference between the jet and the cross-flow has an effect on the Nusselt number distributions.

Heat transfer in a dilute gas-particle suspension flow through multiple slot impinging jets has been evaluated using a new Eulerian-Lagrangian method, which accounts for the conduction heat transfer due to particle-wall collisions. The numerical results were compared with the experimental data of Yokomine et al. (2002). Good agreement between the experiment and simulation is obtained only if the additional conduction heat transfer due to particle-wall collisions is considered in the model. The effects of particle diameter, particle and wall material properties and particle loading ratios, jet Reynolds number, wall reflection coefficient, impingement wall temperature and direction of the gravitation vector are discussed. The simulation results indicate that particle diameter; particle material properties and loading ratio have significant effects on the predicted heat transfer rate only if the conduction heat transfer between particle and wall was included. With the conduction heat transfer due to particle collision on the wall, the jet Reynolds number and wall temperature have larger effects on the heat transfer rate than under WOS condition. In addition, it is found that more heat would be transferred from the wall if the gas and particles were introduced into the impinging jets oriented in the same direction as gravity.

9.2 Major contributions to knowledge

As a result of the present study, the following contributions have been made to the existing knowledge:

1. In view of the engineering practice, the results provided here can be used by the design engineers to estimate the heat transfer rates and effects of various parameters on impinging jet systems, which were not reported earlier. In addition, simple correlations are developed to use for systems with large temperature difference between the jet and impingement surface, correlations for higher Prandtl number fluids, and impinging jet flow with gas particle suspensions.
2. The numerical results generated in this work provide comparative analysis of relative merits and limitations of commonly used turbulence models in engineering practice. In addition, a new model is proposed which can form the basis of a future effort in developing a model for gas particle heat transfer in turbulent flow.

9.3 Recommendations for future work

This study shows that commercial CFD software such as FLUENT solves the impinging jet problems reasonably well. However, simulated results indicate some deviations from the experimental data near the stagnation point, especially for small nozzle-to-target spacing. Thus, there is thus room for improvement in the simulation. More work is needed to address this issue from two aspects: (i) develop modified turbulence models, and (ii) explore some other existing models such as large-eddy simulation (LES) model and direct numerical simulations (DNS) approach.

The numerical studies for other nozzle geometries, for example, round jet, square jet, are needed under large ΔT . It remains to be shown whether the jet Nusselt number is still a best choice for other jet geometries.

Empirical correlations for stagnation and average Nusselt numbers as a function of the fluid Prandtl number had been obtained. More work is needed to obtain empirical correlations for stagnation and average Nusselt numbers as functions of not only fluid Prandtl number but also the geometric parameters, e.g. Nu_0 (or Nu_{ave}) = $a \text{Pr}^b \left(\frac{H}{W}\right)^c$.

It is shown in this work that the conduction heat transfer between the particle and wall has a significant effect on the heat transfer characteristics of impinging jet flow with dilute particle suspensions. To characterize the effect of gas-particle suspension on heat transfer in impinging jets systems, further fundamental work, both experimental and modeling, is needed to correlate the reflection coefficient with the heat transfer rate.

References

Abdon, A. and B. Sunden. Numerical Investigation of Impingement Heat Transfer Using Linear and Nonlinear Two-Equation Turbulence Models, *Numerical Heat Transfer, Part A*, *40*, pp.563-578. 2001.

Abe, K., T. Kondoh and Y. Nagano. A New Turbulence Model for Predicting Fluid Flow and Heat Transfer in Separating and Reattaching Flows I: Flow Field Calculations, *Int. J. Heat Mass Transfer*, *37*, pp.139-151. 1993.

Abid, R. Evaluation of Two-Equation Turbulence Models for Predicting Transitional Flow, *Int. J. Eng. Sci.*, *31*, pp.831-840. 1993.

Amano, R.S. and H. Brandt. Numerical Study of Turbulent Axisymmetric Jets Impinging on a Flat Plate and Flowing into an Axisymmetric Cavity, *J. Fluids Eng.*, *106*, pp.410-417. 1984.

Arastoopour, H. Review Article, Numerical Simulation and Experimental Analysis of Gas/Solid Flow Systems: 1999 Fluor-Daniel Plenary Lecture, *Powder Technology*, *119*, pp.59-67. 2001.

Arastoopour, H. and S. K. Hae. Numerical Analysis of Dilute Gas Particle Flow Using the Kinetic Theory, *Parallel Computing in Multiphase Flow Systems Simulation ASME*, pp. 27-36. 1994.

References

Ashforth-Frost, S. and K. Jambunathan. Numerical Prediction of Semi-confined Jet Impingement and Comparison with Experimental Data, *Int. J. for Numerical Methods in Fluids*, 23, pp.295-306. 1996.

Ashforth-Frost, S., K. Jambunathan, and C.F. Whitney. Velocity and Turbulence Characteristics of A Semi-confined Orthogonally Impinging Slot Jet, *Exp. Thermal and Fluid Sci.*, 14, pp.60-67. 1997.

Avila, R. and J. Cervantes. Analysis of The Heat Transfer Coefficient in a Turbulent Particle Pipe Flow, *Int. J. Heat Mass Transfer*, 38 (11), pp.1923-1932. 1995.

Baldwin, B.S. and H. Lomax. Thin Layer Approximation and Algebraic Model for Separated Turbulent Flows, *AIAA Paper 78-257*, pp.1-8, 1978.

Barata, J.M.M., D.F.G. Durao, M.V. Heitor and J.J. McGuirk. The Turbulence Characteristics of a Single Impinging Jet through a Crossflow, *Exp. Thermal and Fluid Sci.*, 5, pp.487-498. 1992.

Bart, G.C.J., A.J. van Ijzerloo, L.F.G. Geers, L. Hoek and K. Hanjalic. Heat Transfer of Phase-Locked Modulated Impinging-jet Arrays, *Exp. Thermal and Fluid Sci.*, 26, pp.299-304. 2002.

References

Behnia, M., S. Parneix and P.A. Durbin. Prediction of Heat Transfer in an Axisymmetric Turbulent Jet Impinging on a Flat Plate, *Int. J. Heat Mass Transfer*, *41(12)*, pp.1845-1855. 1998.

Behnia, M., S. Parneix, Y. Shabany, and P.A. Durbin. Numerical Study of Turbulent Heat Transfer in Confined and Unconfined Impinging Jets, *Int. J. Heat Fluid Flow*, *20*, pp.1-9. 1999.

Beitelmal, A.H., M.A. Saad and C.D. Patel. The Effect of Inclination on the Heat Transfer Between a Flat Surface and an Impinging Two-dimensional Air Jet, *Int. J. Heat and Fluid Flow*, *21*, pp.156-163. 2000.

Bejan, A. (ed). *Convection Heat Transfer*. Wiley, New York. 1995.

Bi, Z.Y. Enhancement of Impinging Jet Heat Transfer. M. Eng. Thesis, Chemical Engineering, McGill University. 2001.

Boulet, P., S. Moissette, R. Andreux and B. Oesterlé. Test of an Eulerian-Lagrangian Simulation of Wall Heat Transfer in a Gas-Solid Pipe Flow, *Int. J. Heat Fluid Flow*, *21*, pp.381-387. 2000.

Bourloutski, E.S., A.M. Bubenchikov and A.V. Starchenko. The Comparison of Two Approaches to Numerical Modelling of Gas-Particle Turbulent Flow and Heat Transfer in a Pipe, *Mech. Res. Com.*, *29*, pp.437-445. 2002.

References

Bula, A.J., M.M. Rahman and J.E. Leland. Numerical Modeling of Conjugate Heat Transfer During Impingement of Free Liquid Jet Issuing From a Slot Nozzle, *Numerical Heat Transfer, Part A*, 38, pp.45-66. 2000.

Cadek, F.F. A Fundamental Investigation of Jet Impingement Heat Transfer. Ph. D. Thesis, University of Cincinnati. 1968.

Cao, J. and G. Ahmadi. Gas-particle Two-phase Turbulent Flow in a Vertical Duct, *Int. J. Multiphase Flow*, 21(6), pp.1203-1228. 1995.

Cao, J. and G. Ahmadi. Gas-particle Two-phase Turbulent Flow in Horizontal and Inclined Ducts, *Int. J. Eng. Sci.*, 38, pp.1961-1981. 2000.

Catalano, G.D., K.S. Chang and J.A. Mathis. Investigation of Turbulent Jet Impingement in a Confined Crossflow, *AIAA Journal*, 27, pp.1530-1535. 1989.

Chalupa, R., M. Chen, Y. Modi, and A.C. West. High Schmidt Mass Transfer in a Turbulent Impinging Slot Jet Flow, *Int. J. Heat Mass Transfer*, 44, pp.3775-3785. 2001.

Chatterjee, A., S.C. Dhingra and S.S. Kapur. Laminar Impinging Jet Heat Transfer with a Purely Viscous Inelastic Fluid, *Numerical Heat Transfer, Part A*, 42, pp.193-213. 2002.

Chattopadhyay, H., G. Biswas and N.K. Mitra. Heat Transfer From Moving Surface due to Impinging Jets, *Proc. ASME, Heat Transfer Division*, 1, pp.261-270. 1999.

References

Chattopadhyay, H., S.K. Saha and N.K. Mitra. LES of Heat Transfer From Impinging jets over a Moving Surface. In *Heat and Mass Transfer*, ed by S.P. Msloknath, Venkateshan, B. Basu and V. Prasad, pp. 339-344. Tata McGraw-Hill. 2000.

Chattopadhyay, H. and S.K. Saha. Numerical Investigations of Heat Transfer Over a Moving Surface Due to Impinging Knife-Jets, *Numerical Heat Transfer, Part A*, 39, pp.531-549. 2001.

Chen, M.Y., R. Chalupa, A.C. West and V. Modi. High Schmidt Mass Transfer in a Laminar Impinging Slot Jet Flow, *Int. J. Heat Mass Transfer*, 43, pp.3907-3915. 2000.

Chen, Y.M., W.T. Lee and S.J. Wu. Heat (Mass) Transfer Between an Impinging Jet and a Rotating Disk, *Heat and Mass Transfer*, 34, pp.195-201. 1998.

Chieng, C.C. and B.E. Launder. On the Calculation of Turbulent Heat Transport Downstream from an Abrupt Pipe Expansion, *Numerical Heat Transfer*, 3, pp.189-207, 1980.

Choi, M., H.S. Yoo, G.Y. Yang, J.S. Lee and D.K. Sohn. Measurements of Impinging Jet Flow and Heat Transfer on a Semi-circular Concave Surface, *Int. J. Heat Mass Transfer*, 43, pp.1811-1822. 2000.

References

Chuang S.H., M.H. Chen, S.W. Lii and F.M. Tai. Numerical Simulation of Twin-jet Impingement on a Flat Plate Coupled with Cross-flow, *Int. J. Numerical Methods in Fluids*, *14*, pp.459-475. 1992.

Chung, Y.M., K.H. Luo and N.D. Sandham. Numerical Study of Momentum and Heat Transfer in Unsteady Impinging Jets, *Int. J. Heat Fluid Flow*, *23*, pp.592-600. 2002.

Colucci, D.W. and R. Viskanta. Effect of Nozzle Geometry on Local Convective Heat Transfer to a Confined Impinging Air Jet, *Exp. Thermal Fluid Sci.*, *13*, pp.71-80. 1996.

Cooper, D., D.C. Jackson, B.E. Launder and G.X. Liao. Impinging Jet studies for Turbulence Model Assessment-I. Flow-field Experiments, *Int. J. Heat Mass Transfer*, *36(10)*, pp. 2675-2684. 1993.

Cornaro, C., A.S. Fleischer and R.J. Goldstein. Flow Visualization of a Round Jet Impinging on Cylindrical Surfaces, *Exp. Thermal Fluid Sci.*, *20*, pp.66-78. 1999.

Craft, T.J., L.J.W. Graham and B.E. Launder. Impinging Jet Studies for Turbulence Model Assessment-II. An Examination of The Performance of Four Turbulence Models, *Int. J. Heat Mass Transfer*, *36(10)*, pp.2685-2697. 1993.

Cziesla, T., G. Biswas, H. Chattopadhyay and N.K. Mitra. Large-Eddy Simulation of Flow and Heat Transfer in an Impinging Slot Jet, *Int. J. Heat Fluid Flow*, *22*, pp.500-508, 2001.

References

Das, D. Convective Heat Transfer under a Turbulent Impinging Slot Jet at Large Temperature Differences. M. Eng. Thesis, Chem. Engineering Dept., McGill University. 1982.

Das, D., W.J.M. Douglas and R.H. Crotagino. Convective Heat Transfer under Turbulent Impinging Slot Jet at Large Temperature Differences. In *Drying 85*, ed by A.S. Mujumdar, pp. 354-359. Hemisphere, N.Y. 1985

Dianat, M., M. Fairweather and W.P. Jones. Predictions of Axisymmetric and Two-Dimensional Impinging Turbulent Jets, *Int. J. Heat Fluid Flow*, *17*, pp.530-538. 1996.

Down, S.J. and E.H. James. Jet impingement Heat Transfer-a literature survey, ASME paper no. 87-HT-35, 1987.

Ekkad, S. and D. Kontrovitz. Jet Impingement Heat Transfer on Dimpled Target Surfaces, *Int. J. Heat Fluid Flow*, *23*, pp.22-28. 2002.

Fan, S., B. Lakshminarayana and M. Barnett. A Low-Reynolds Number $k-\epsilon$ Model for Unsteady Turbulent Boundary Layer Flows, *AIAA J.*, *31*, pp.1777-1784. 1993.

Failla, G., E.H. Bishop and J.A. Liburdy. Enhanced Jet Impingement Heat Transfer with Crossflow at Low Reynolds Numbers, *J. Electronics Manufacturing*, *9*(2), pp.167-178. 1999.

References

Fitzgerald, J. and S. Garimella. A Study of The Flow Field of a Confined and Submerged Impinging Jet, *Int. J. Heat Mass Transfer*, *41(8-9)*, pp.1025-1034. 1998.

FLUENT 5.0 User's guide. Volumes 1-4, Fluent Inc. 1998.

FLUENT 6.0 User's guide. Volumes 1-5, Fluent Inc. Dec. 2001.

Fujimoto, H., N. Hatta and R. Viskanta. Numerical Simulation of Convective Heat Transfer to a Radial Free Surface Jet Impinging on a Hot Solid, *Heat and Mass Transfer*, *35*, pp.266-272. 1999.

Gao, S. and P.R. Voke. Large-Eddy Simulation of Turbulent Heat Transport in Enclosed Impinging Jets, *Int. J. Heat and Fluid Flow*, *16*, pp.349-356, 1995.

Gardon, R. and J.C. Akfirat. Heat Transfer Characteristics of Impinging Two-Dimensional Air Jets, *J. Heat transfer*, *88 (1)*, pp.101-108. 1966.

Garimella, S.V. and R.A. Rice. Confined and Submerged Liquid Jet Impingement Heat Transfer, *J. Heat Transfer*, *117*, pp.871-877. 1995.

Garimella, S.V. and B. Nenaydykh. Nozzle Geometry Effects in Liquid Jet Impingement Heat Transfer, *Int. J. Heat Mass Transfer*, *39 (14)*, pp.2915-2923. 1996.

References

Gau, C. and C.M. Chung. Surface Curvature Effect on Slot-Air-Jet Impingement Cooling Flow and Heat Transfer Process, *Transactions of the ASME*, *113*, pp.858-864. 1991.

Gibson, M.M. and B.E. Launder. Ground Effects on Pressures Fluctuations in the Atmospheric Boundary Layer, *J. Fluids Mech.*, *86*, pp.491-511, 1978.

Gibson, M.M. and R.D. Harper. Calculation of Impinging-Jet Heat Transfer with the Low-Reynolds Number q - ξ Turbulence Model, *Int. J. Heat Fluid Flow*, *18*, pp.80-87. 1997.

Goldstein, R.J. and M.E. Franchett. Heat Transfer From a Flat Surface to an Oblique Impinging Jet, *J. Heat Transfer*, *110*, pp.84-90. 1988.

Guo, Y. and D.H. Wood. Measurements in the Vicinity of a Stagnation Point, *Exp. Thermal Fluid Sci.*, *25*, pp.605-614. 2002.

Haneda, Y., Y. Tsuchiya, K. Nakabe and K. Suzuki. Enhancement of Impinging Jet Heat Transfer by Making Use of Mechano-Fluid Interactive Flow Oscillation, *Int. J. Heat Fluid Flow*, *19*, pp.115-124. 1998.

Hansen, L.G. and B.W. Webb. Air Jet Impingement Heat Transfer from Modified Surfaces, *Int. J. Heat Mass Transfer*, *36(4)*, pp.989-997. 1993.

References

Heikkila, P. and N. Milosavljevic. Investigation of Impingement Heat Transfer Coefficient at High temperatures, *Drying Technology*, 20(1), pp.211-222. 2002.

Heimann, F. and E.U. Schlunder. Vacuum Contact Drying of Mechanically Agitated, Coarse Material Wetted with a Binary Mixture. In *Drying 86*, Vol. 1, ed. by A.S. Mujumdar, pp. 238-250. Hemisphere, New York. 1986.

He, G., Y. Guo and A.T. Hsu. The Effect of Schmidt Number on Turbulent Scalar Mixing in a Jet-In-Crossflow, *Int. J. Heat Mass Transfer*, 42, pp.3727-3738. 1999.

Hosseinalipour, S.M. and A.S. Mujumdar. Comparative Evaluation of Different Turbulence Models for Confined Impinging and Opposing Jet Flows, *Numerical Heat Transfer, Part A*, 28, pp.647-666. 1995.

Hosseinalipour, S.M. and A.S. Mujumdar. Flow, Heat Transfer and Particle Drying Characteristics in Confined Opposing Turbulent Jets: A Numerical Study, *Drying Tech.*, 13 (3), pp.753-781. 1995.

Huang, B., Heat Transfer under an Obliquely Impinging Jet on a Moving Surface. Ph.D Thesis, McGill University. 1990.

Huber, A.M. and R. Viskanta. Effect of Jet-Jet Spacing on Convective Heat Transfer to Confined, Impinging Arrays of Axisymmetric Air Jets, *Int. J. Heat Mass Transfer*, 37(18), pp.2859-2869. 1994.

References

Inoue, A., A. Ui, Y. Yamazaki and S. Lee. Studies on Cooling by Two-Dimensional Confined Jet Flow of High Heat Flux Surface in Fusion Reactor, *Nuclear Eng. and Design*, *200*, pp.317-329. 2000.

Jambunathan, K., E. Lai, M.A. Mass and B.L. Button. A Review of Heat Transfer Data for Single Circular Jet Impingement, *Int. J. Heat Fluid Flow*, *13(2)*, pp.106-115. 1992.

Jones, W.P. and B.E. Launder. The Prediction of Laminarization with a Two-equation Model of Turbulence, *Int. J. Heat Mass Transfer*, *15*, pp.301-314. 1972.

Kalita, K., A. Dewan and A.K. Dass. Prediction of Turbulent Jet in Cross-Flow, *Numerical Heat Transfer, Part A*, *41*, pp.101-111. 2002.

Kim, J., P. Moin. Transport of Passive Scalars in a Turbulent Channel Flow. In Proc. 6th Int. Symposium on turbulent Shear Flows, 5.2.1-5.2.6.

Kim, S.W. and T.J. Benson. Calculation of a Circular Jet in Crossflow with a Multiple-Time-Scale Turbulence Model, *Int. J. Heat Mass Transfer*, *35(10)*, pp.2357-2365. 1992.

Knowles, K., Computational Studies of Impinging Jets Using k- ϵ Turbulence Models, *Int. J. Numerical Methods in Fluids*, *22*, pp.799-810, 1996.

References

Knowles, K. and D. Bray. Computation of Normal Impinging Jets in Cross-Flow And Comparison with Experiment, *Int. J. Numerical Methods in Fluids*, *13*, pp.1225-123. 1991.

Lai, Y.G. and R.M.C. So. On Near Wall Modelling of Turbulent Heat Fluxes, *Int. J. Heat Mass Transfer*, *33*, pp. 1429-1440. 1990.

Lain, S., M. Sommerfeld and J. Kussin. Experimental Studies and Modeling of Four-Way Coupling in Particle-Laden Horizontal Channel Flow, *Int. J. Heat Fluid Flow*, *23*, pp.647-656. 2002.

Lam, C.K.G. and K. Bremhorst. A Modified form of the k- ϵ Model for Prediction Wall Turbulence, *J. Fluids Eng.*, *103*, pp.456-460. 1981.

Launder, B.E. and D.B. Spalding. *Lectures in Mathematical Models of Turbulence*. London, England: Academic Press. 1972.

Launder, B.E. and B.I. Sharma. Application of the Energy-Dissipation Model of Turbulence to the Calculation of Flow near a Spinning Disc, *Heat Mass Transfer*, *1*, pp.131-138, 1974.

Launder, B.E. Second-Moment Closure: Pressure....and Future?, *Int. J. Heat Fluid Flow*, *10(4)*, pp.282-300, 1989.

References

Launder, B.E., G.F. Reece and W. Rodi. Progress in the Development of a Reynolds-Stress Turbulence Closure, *J. Fluid Mech.*, 68(3), pp.537-566, 1975.

Lee, D.H., S.Y. Won, Y.T. Kim and Y.S. Chung. Technical Note: Turbulent Heat Transfer From a Flat Surface to a Swirling Round Impinging Jet, *Int. J. Heat Mass Transfer*, 45, pp.223-227. 2002.

Lee, D.H., Y.M. Lee, Y.T. Kim, S.Y. Won and Y.S. Chung. Technical Note: Heat Transfer Enhancement by the Perforated Plate Installed between an Impinging Jet and the Target Plate, *Int. J. Heat Mass Transfer*, 45, pp.213-217. 2002.

Lee, D.H., Y.S. Chung and D.S. Kim. Turbulent Flow and Heat Transfer Measurements on a Curved Surface with a Fully Developed Round Impinging Jet, *Int. J. Heat Fluid Flow*, 18, pp.160-169. 1997.

Lee, D.H., Y.S. Chung and M.G. Kim. Technical Note: Turbulent Heat Transfer from a Convex Hemispherical Surface to a Round Impinging Jet, *Int. J. Heat Mass Transfer*, 42, pp.1147-1156. 1999.

Lee, D.H., Y.S. Chung and S.Y. Won. Technical Note: The Effect of Concave Surface Curvature on Heat Transfer from a Fully Developed Round Impinging Jet, *Int. J. Heat Mass Transfer*, 42, pp.2489-2497. 1999.

References

Lee, J. and S.J. Lee. The Effect of Nozzle Aspect Ratio on Stagnation Region Heat Transfer Characteristics of Elliptic Impinging Jet, *Int. J. Heat Mass Transfer*, *43*, pp.555-575. 2000.

Lee, K., R. Greif, S. Lee and J. Lee. Heat Transfer from a Flat Plate to a Fully Developed Axisymmetric Impinging Jet, *J. Heat Transfer*, *117*, pp.772-776. 1995.

Lee, S.J., J.H. Lee and D.H. Lee. Local Heat Transfer Measurements from an Elliptic Jet Impinging on a Flat Plate Using Liquid Crystal, *Int. J. Heat Mass Transfer*, *37(6)*, pp.967-976. 1994.

Levy, A., T. Mooney, P. Marjanovic and D.J. Mason. A Comparison of Analytical and Numerical Models with Experimental Data for Gas-Solid Flow through a Straight Pipe at Different Inclinations, *Powder Technology*, *93*, pp.253-260. 1997.

Li, C.Y. and S.V. Garimella. Prandtl-Number Effects and Generalized Correlations for Confined and Submerged Jet Impingement, *Int. J. Heat Mass Transfer* *44*, pp.3471-3480. 2001.

Lin, Z.H., Y.J. Chou and Y.H. Hung. Heat Transfer Behaviors of a Confined Slot Jet Impingement, *Int. J. Heat Mass Transfer*, *40(5)*, pp.1095-1107. 1997.

Liu, T and J.P. Sullivan. Heat Transfer and Flow Structures in an Excited Circular Impinging Jet, *Int. J. Heat Mass Transfer*, *39(17)*, pp.3695-3706. 1996.

References

Liu, X, J.H. Lienhard V and J.S. Lombarda. Convective Heat Transfer by Impingement of Circular Liquid Jets, *J. Heat Transfer*, *113*, pp.571-582. 1991.

Lytle, D. and B.W. Webb. Air Jet Impingement Heat Transfer at Low Nozzle-Plate Spacings, *Int. J. Heat Mass Transfer*, *37*, pp.1687-1697. 1994.

Ma, C.F., Q. Zheng, H. Sun, K. Wu, T. Gomi and B.W. Webb. Local Characteristics of Impingement Heat Transfer with Oblique Round Free-Surface Jets of Large Prandtl Number Liquid, *Int. J. Heat Mass Transfer*, *40(10)*, pp.2249-2259. 1997.

Ma, C.F., Q. Zheng, S.C. Lee and T. Gomi. Impingement Heat Transfer and Recovery Effect with Submerged Jets of Large Prandtl Number Liquid-I. Unconfined Circular Jets, *Int. J. Heat Mass Transfer*, *40(6)*, pp.1481-1490. 1997.

Ma, C.F., Y. Zhuang and S.C. Lee and T.Gomi. Impingement Heat Transfer and Recovery Effect with Submerged Jets of Large Prandtl Number Liquid-II. Initially Laminar Confined Slot Jets, *Int. J. Heat Mass Transfer*, *40(6)*, pp.1491-1500. 1997.

Mansoori, Z., M. Saffar-Avval, H.B. Tabrizi and G. Ahmadi. Modeling of Heat Transfer in Turbulent Gas-Solid Flow, *Int. J. Heat Mass Transfer*, *45*, pp.1173-1184. 2002.

Mansoori, Z., M. Saffar-Avval, H.B. Tabrizi, G. Ahmadi and S. Lain. Thermo-Mechanical Modeling of Turbulent Heat Transfer in Gas-solid Flows Including Particle Collisions, *Int. J. Heat Fluid Flow*, *23*, pp.792-806. 2002.

References

Martin, H. Heat and Mass Transfer between Impinging Gas Jets and Solid Surface, *Advances In Heat Transfer*, 13, pp.1-66, 1977.

Mashayek, F. and D.B. Taulbee. A Four-Equation Model for Prediction of Gas-Solid Turbulent Flows, *Numerical Heat Transfer, Part B*, 41, pp.95-116. 2002.

Mashayek, F. and D.B. Taulbee. Turbulent Gas-Solid Flows, Part I: Direct Simulations and Reynolds Stress Closures, *Numerical Heat Transfer, Part B*, 41, pp.1-29. 2002.

Mashayek, F. and D.B. Taulbee. Turbulent Gas-solid Flow, Part II: Explicit Algebraic Models, *Numerical Heat Transfer, Part B* 41, 31-52. 2002.

Moallemi, M.K. and K.S. Jang. Prandtl Number Effects on Laminar Mixed Convection Heat Transfer in a Lid-Driven Cavity, *Int. J. Heat Mass Transfer*, 35(8), pp.1881-1892. 1992.

Mohanty, A.K. and A.A. Tawfek. Heat Transfer Due to a Round Jet Impinging Normal to a Flat Surface, *Int. J. Heat Mass Transfer*, 36, pp.1639-1647. 1993.

Morris, G.K., S.V. Garimella and J.A. Fitzgerald. Flow-Field Prediction in Submerged and Confined Jet Impingement Using the Reynolds Stress Model, *J. Electronic Packaging*, 121, pp.255-262. 1999.

References

Morris, G.K., S.V. Garimella and R.S. Amano. Prediction of Jet Impingement Heat Transfer Using a Hybrid Wall Treatment with Different Turbulent Prandtl Number Functions, *Transactions of the ASME*, *118*, pp.562-569. 1996.

Mujumdar, A.S., P.G. Huang, and W.J.M. Douglas. Prediction of Heat Transfer under a Plane Turbulent Impinging Jet Including Effects of Crossflow and Wall Motion. In *Drying 85*, ed by A.S. Mujumdar, pp. 91-98. Hemisphere, N.Y. 1985.

Mujumdar, A.S. and B. Huang. Impingement Drying. In *Handbook of Industrial Drying*, Chapter 14, ed by A.S. Mujumdar, Marcel Dekker, Inc., 1995.

Murray, D.B. Local Enhancement of Heat Transfer in a Particulate Cross Flow-I and II, *Int. J. Multiphase Flow*, *20*, pp. 493-513, 1994.

Nakabe, K., K. Suzuki, K. Inaoka, A. Higashio, J.S. Acton and W. Chen. Generation of Longitudinal Vortices in Internal Flows with an Inclined Impinging Jet and Enhancement of Target Plate Heat Transfer, *Int. J. Heat Fluid Flow*, *19*, pp.573-581, 1998

Nishino, K., M. Samada, K. Kasuya and K. Torii. Turbulence Statistics in the Stagnation Region of an Axisymmetric Impinging Jet Flow, *Int. J. Heat Fluid Flow*, *17*, pp.193-201. 1996.

Nguyen, A.V. and C.A.J. Fletcher. Particle Interaction with the Wall Surface in Two-Phase Gas-Solid Flow, *Int. J. Multiphase Flow*, *25*, pp.139-154. 1999.

References

Nguyen, A.V., C.A.J. Fletcher and J.Y. Tu. CFD Study of the Heat Transfer between a Dilute Gas Particle Suspension Flow and an Obstruction, *Numerical Heat Transfer, Part A*, 35, pp.537 -551. 1999.

Park, T.S. and H.J. Sung. Development of a Near-Wall Turbulence Model and Application to Jet Impingement Heat Transfer, *Int. J. Heat Fluid Flow*, 22, pp.10-18. 2001.

Patankar, S.V. *Numerical Heat Transfer and Fluid Flow*. Hemisphere Publishing Co.: Washington, D.C, 1980.

Patel, V.C., R. Wolfgang and J. Scheuerer. Turbulence Models for Near-Wall and Low-Reynolds-Number Flows: A Review, *AIAA J*, 23(9), pp.1308-1319. 1985.

Phares, D.J. and G.T. Smedley. The Inviscid Impingement of a Jet with Arbitrary Velocity Profile, *Physics of Fluids*, 12(8), pp.2046-2055. 2000.

Polat, S., B. Huang, A.S. Mujumdar and W.J.M. Douglas. Numerical Flow and Heat Transfer under Impinging Jets. In *Annual Review of Numerical Fluid Mechanics and Heat Transfer*, Vol, 2, ed. by C.L. Tien and T.C. Chawla, pp. 157-196. New York: Hemisphere. 1989.

Polat, S. Heat And Mass Transfer In Impingement Drying, *Drying Technology*, 11(6), pp. 1147-1176. 1993.

References

Polat, S., A.S. Mujumdar and W.J.M. Douglas. Heat Transfer Distribution under a Turbulent Impinging Jet- A Numerical Study, *Drying Technology*, 3(1), pp.15-38. 1985.

Polat, S., A.S. Mujumdar and W.J.M. Douglas. Impingement Heat Transfer under a Confined Slot Jet. Part I: Effect of Surface Throughflow, *Canadian J. of Chem. Engrn.*, 69, pp.266-273. 1991.

Polat, S., A.S. Mujumdar and W.J.M. Douglas. Impingement Heat Transfer under A Confined Slot Jet. Part II: Effect of Surface Motion and Throughflow, *Canadian J. of Chem. Engrn.*, 69, pp.274-280. 1991.

Prakash, M., O.F. Turan, Y. Li, J. Mahoney and G.R. Thorpe. Impinging Round Jet Studies in a Cylindrical Enclosure with and without a Porous Layer: Part I-Flow Visualizations And Simulations, *Chemical Eng. Sci.*, 56, pp.3879-3892. 2001.

Prakash, M., O.F. Turan, Y. Li, J. Mahoney and G.R. Thorpe. Impinging Round Jet Studies in a Cylindrical Enclosure with and without a Porous Layer: Part II-LDV Measurements and Simulations, *Chemical Eng. Sci.*, 56, pp.3855-3878. 2001.

Rahman, M.M., A.J. Bula and J.E. Leland. Conjugate Heat Transfer during Free Jet Impingement of a High Prandtl Number Fluid, *Numerical Heat Transfer, Part B*, 36, pp.139-162. 1999.

References

Roy, S., K. Nasr, P. Patel and B. AbdulNour. An Experimental and Numerical Study of Heat Transfer off an Inclined Surface Subject to an Impinging Airflow, *Int. J. Heat Mass Transfer*, *45*, pp.1615-1629. 2002.

Rozenblit, R., M. Simkhis, G. Hetsroni, D. Barnea and Y. Taitel. Heat Transfer in Horizontal Solid-Liquid Pipe Flow, *Int. J. Multiphase Flow*, *26*, pp.1235-1246. 2000.

Saad, N.R., Flow and Heat Transfer for Multiple Turbulent Impinging Slot Jets. Ph.D. Thesis, McGill University. 1981.

Saad, N.R., S. Polat and W.J.M. Douglas. Confined Multiple Impinging Slot Jets without Crossflow Effects, *Int. J. Heat Fluid Flow*, *13*, pp.2-14, 1992.

Sailor, D., D.J. Rohli and Q. Fu. Effect of Variable Duty Cycle Flow Pulsations on Heat Transfer Enhancement for an Impinging Air Jet, *Int. J. Heat Fluid Flow*, *20*, pp.574-580. 1999.

San, J.Y., C.H. Huang and M.H. Shu. Impingement Cooling of a Confined Circular Air Jet, *Int. J. Heat Mass Transfer*, *40(6)*, pp.1355-1364. 1997.

Sarkar, S. and T.K. Bose. Comparison of Different Turbulence Models for Prediction of Slot-Film Cooling: Flow and Temperature Field, *Numerical Heat Transfer, Part B*, *28*, pp.217-238. 1995.

References

Satake, S.I. and T. Kunugi. Direct Numerical Simulation of an Impinging Jet into Parallel Disks, *Int. J. Numerical Methods for Heat & Fluid Flow*, 8(7), pp.768-780. 1998.

Sato, Y., H. Kishizawa, K. Hishida and M. Maeda. Particle-Laden Turbulent Flow with Transverse Magnetic Field in a Vertical Channel. In *Experimental and Computational Aspects of Validation of Multiphase Flow CFD Codes*, ed by I. Celik, Y. Hassan, D. Huges, R. Johnson and M. Sommerfeld, pp. 93-100. 1994.

Sato, Y., K. Hishida and M. Maeda, Effect of Dispersed Phase on Modification of Turbulent Flow in a Wall Jet, *J. Fluids Engineering*, 118, pp.307-315, 1996.

Sato, Y., E. Deutsch and O. Simonin. Direct Numerical Simulations of Heat Transfer by Solid Particles Suspended in Homogeneous Isotropic Turbulence, *Int. J. Heat and Fluid Flow*, 19, pp.187-192. 1998.

Schiewe, T., K.E. Wirth, O. Moderus, K. Tuzla, A.K. Sharma and J.C. Chen. Measurements of Solid Concentration in A Downward Vertical Gas-Solid Flow, *Particle Technology and Fluidization*, *AIChE Journal*, 45(5), pp. 949-955. 1999.

Seyedein, S.H., M. Hasan and A.S. Mujumdar. Modeling of a Single Confined Turbulent Slot Jet Impingement Using Various k- ϵ Turbulence Models, *Appl. Mach. Modeling*, 18, pp.526-537. 1994.

References

Seyedein, S.H., M. Hasan and A.S. Mujumdar. Turbulent Flow and Heat Transfer from Confined Multiple Impinging Slot Jets, *Numerical Heat Transfer, Part A*, 27, pp.35-51. 1995.

Sharma, K.R. Relative Contributions from Particle Conduction and Gas Convection to the Heat Transfer Coefficient between Dense Gas-Solid Fluidized Beds and Surfaces, *Powder Technology*, 91, pp.75-80. 1997.

Shi, YL., M.B. Ray and A.S. Mujumdar. Computational Study of Impingement Heat Transfer under a Turbulent Slot Jet, *Ind. Eng. Chem. Res.*, 41(18), pp.4643-4651. 2002.

Shi, YL., M.B. Ray and A.S. Mujumdar. Effect of Large Temperature Differences on Local Nusselt Number under Turbulent Slot Impingement Jet, *Drying Technology*, 20(9), pp.1803-1825. 2002.

Shiravi, A.H., A.S. Mujumdar and G.J. Kubes. Numerical Study of Heat Transfer and Fluid Flow in Multiple Turbulent Impinging Jets, *Drying Technology*, 13(5-7), pp.1359-1375. 1995.

Shuja, S.Z., B.S. Yilbas and M.O. Budair. Gas Jet Impingement on a Surface Having a Limited Constant Heat Flux Area: Various Turbulence Models, *Numerical Heat Transfer, Part A*, 36, pp.171-200. 1999.

References

Sommerfeld, M. and N. Huber. Experimental Analysis and Modeling of Particle-Wall Collisions, *Int. J. Multiphase Flow*, 25, pp.1457-1489. 1999.

Stevens, J. and B.W. Webb. The Effect of Inclination on Local Heat Transfer under an Axisymmetric Free Liquid Jet, *Int. J. Heat Mass Transfer*, 34(4/5), pp.1227-1236. 1991.

Sun, J. and M.M. Chen. A Theoretical Analysis of Heat Transfer due to Particle Impact, *Int. J. Heat Mass Transfer*, 31(5), pp.969-975. 1988.

Tan, S.M. Correlations for Heat Transfer Coefficients in Low Viscosity Liquids Using CFD. M. Eng Thesis, National University of Singapore, 2001.

Taulbee, D.B., F. Mashayek and C. Barre. Simulation and Reynolds Stress Modeling of Particle-Laden Turbulent Shear Flows, *Int. J. Heat Fluid Flow*, 20, pp.368-373. 1999.

Tawfek, A.A. Heat Transfer Studies of the Oblique Impingement of Round Jets upon a Curved Surface, *Heat and Mass Transfer*, 38, pp.467-475. 2002.

Thakre, S.S. and J.B. Joshi. CFD Modelling of Heat Transfer in Turbulent Pipe Flow, *AIChE Journal*, 46(9), pp.1798-1811. 2000.

Triesch, O. and M. Bohnet. Measurement and CFD Prediction of Velocity and Concentration Profiles in a Decelerated Gas-Solids Flow, *Powder Technology*, 115, pp.101-113. 2001.

References

Tzeng, P.Y., C.Y. Soong and C.D. Hsieh. Numerical Investigation of Heat Transfer under Confined Impinging Turbulent Slot Jets, *Numerical Heat Transfer, Part A*, 35, pp.903-924. 1999.

van Heiningen, A.R.P. Heat Transfer under an Impinging Slot Jet. Ph. D. Thesis, McGill University. 1982.

Viskanta, R. Heat Transfer to Impinging Isothermal Gas and Flame Jets, *Exp. Thermal and Fluid Sci.*, 6, pp.111-134. 1993.

Voke, P.R. and S. Gao. Numerical Study of Heat Transfer from an Impinging Jet, *Int. J. Heat Mass Transfer*, 41(4-5), pp.671-680. 1998.

Ward, J., M.T. Oladiran and G.P. Hammond. Effect of Nozzle Inclination on Jet-Impingement Heat Transfer in a Confined Cross Flow. *ASME*. 91(181), pp.25-31. 1991.

Webb, B.W. and C-F. Ma. Single-Phase Liquid Jet Impingement Heat Transfer, *Advance in Heat Transfer*, 26, pp.105-217. 1995.

Yan, X.J. and N. Saniei. Heat Transfer from an Obliquely Impinging Circular Air Jet to a Flat Plate, *Int. J. Heat and Fluid Flow*, 18, pp.591-599. 1997.

References

Yang, G.Y., M. Choi and J.S. Lee. An Experimental Study of Slot Jet Impingement Cooling on Concave Surface: Effects of Nozzle Configuration and Curvature, *Int. J. Heat Mass Transfer*, *42*, pp.2199-2209. 1999.

Yapici, S., S. Kuslu, C. Ozmetin, H. Ersahan and T. Pekdemir. Surface Shear Stress for a Submerged Jet Impingement Using Electrochemical Technique, *J. Applied Electrochemistry*, *29*, pp.185-190. 1999.

Yokomine, T., A. Shimizu and A. Saitoh. Heat Transfer of Multiple Impinging Jets with Gas-Solid Suspensions, *Exp. Thermal Fluid Sci.*, *26(6-7)*, pp.617-626. 2002.

Yoshida, H., K. Suenaga and R. Echigo. Turbulence Structure and Heat Transfer of a Two-Dimensional Impinging Jet with Gas-Solid Suspensions, *Int. J. Heat Mass Transfer*, *33(5)*, pp.859-867. 1990.

Zhao, Y and R.S. Brodkey, Particle Paths in Three-Dimensional Flow Fields as a Means of Study: Opposing Jet Mixing System, *Powder Technology*, *100*, pp.161-165. 1998.

Zhe, J and V. Modi. Near Wall Measurements for a Turbulent Impinging Slot Jet, *Transactions of the ASME*, *123*, pp.112-120. 2001.

Publications

Shi, YL., M.B. Ray and A.S. Mujumdar. Computational Study of Impingement Heat Transfer under a Turbulent Slot Jet, *Industrial and Engineering Chemistry Research*, *41(18)*, 2002, pp. 4643-4651.

Shi, YL., M.B. Ray and A.S. Mujumdar. A Parametric Study of Impingement Heat Transfer under a Slot Jet Using CFD, The 2nd Asian-Oceania Drying Conference, Pulau Pinang, Malaysia, pp. 65-76, 2001.

Shi, YL., M.B. Ray and A.S. Mujumdar. Effect of Temperature Differences on Local Nusselt number Under Turbulent Slot Jets, in *Proceeding of the 13th International Drying Symposium*, Beijing, P. R. China, pp. 128-134, August 2002.

Shi, YL., M.B. Ray and A.S. Mujumdar. Effect of Large Temperature Differences on Local Nusselt Number Under Turbulent Slot Impingement Jet, *Drying Tech.* *20(9)*, pp. 1803-1825, 2002.

Shi, YL., M.B. Ray and A.S. Mujumdar. Effects of Prandtl Number on Impinging Jet Heat Transfer Under a Semi-Confined Turbulent Slot Jet, in *Proceeding of the 9th APCCHE Congress and CHEMECA 2002*, Christchurch, New Zealand, 2002.

Shi, YL., M.B. Ray and A.S. Mujumdar. Effect of Cross-Flow on Turbulent Flow and Heat Transfer Characteristics Under Normal and Oblique Semi-Confined Impinging Slot

Jets, in Proceeding of the 9th APCCChE Congress and CHEMECA 2002, Christchurch, New Zealand, 2002.

Shi, YL., M.B. Ray and A.S. Mujumdar. Effect of Prandtl Number on Impinging Jet Heat Transfer Under a Semi-Confined Turbulent Slot Jet, *International Communications in Heat and Mass Transfer*, 29(7), pp. 929-938. 2002.

Shi, YL., M.B. Ray and A.S. Mujumdar. Effect of Prandtl Number on Impinging Jet Heat Transfer Under a Semi-Confined Laminar Slot Jet, *International Communications in Heat and Mass Transfer*, 30(4), 2003, pp. 455-464.

Shi, YL., M.B. Ray and A.S. Mujumdar. Numerical Study of Effect of Cross Flow on Turbulent Flow and Heat Transfer Characteristics under Normal and Oblique Semi-confined Impinging Slots Jets, *Drying Technology*, 21(10), 2003, pp. 1923-1939.

Shi, YL., A.S. Mujumdar and M.B. Ray. Heat transfer under two dimensional multiple turbulent slot impinging jets of gas-particle suspensions, submitted to *Numerical Heat Transfer, Part A*, February, 2004

Shi, YL., A.S. Mujumdar and M.B. Ray. Parametric Study of Heat Transfer in Turbulent Gas-Solid Flow in Multiple Impinging Jets, *Industrial and Engineering Chemistry Research*, 42, 2003, pp. 6223-6231.

Publications

Shi, YL., A.S. Mujumdar and M.B. Ray. Effect of Large Temperature Difference on Impingement Heat Transfer Under a Round Turbulent Jet, *International Communications in Heat and Mass Transfer*, 31(2), 2004, pp. 251-260.